CHARACTERIZATION OF EARLY-TIME PERFORMANCE OF A WELL WITH A VERTICAL FRACTURE PRODUCING AT A CONSTANT PRESSURE

A Thesis

by

NICHOLAS EDWARD WIEWIOROWSKI

Submitted to the Office of Graduate and Professional Studies of
Texas A&M University
in partial fulfillment of the requirements for the degree of

MASTER OF SCIENCE

Chair of Committee,	Thomas A. Blasingame
Committee Members,	Maria A. Barrufet
	Walter Ayers
Head of Department,	A. Daniel Hill

August 2016

Major Subject: Petroleum Engineering

ABSTRACT

The flowback performance of multi-fractured horizontal wells completed in an ultra-low permeability (shale) reservoir often includes an anomalous flowrate feature at early times prior to the development of a characteristic reservoir flow regime (*i.e.,* linear or bilinear flow). This flowrate feature is evident in all of the flow phases (gas, oil, water, and total fluid) and is caused by the "unloading" of the well (essentially the "clean-up" behavior following well stimulation). Our concept is that this flowrate feature is caused by decaying skin effects, a changing wellbore storage effect, or a combination of both a decaying skin effects and changing wellbore storage effects. For simplicity — and as a proof-of-concept, this research considers only the case of a vertical well with a single vertical fracture, but the concept and relations developed in this work can be directly extended to the solution for a multi-fractured horizontal well.

As noted, the goal of this research is to develop series of time-dependent skin and wellbore storage models to characterize the early-time flowrate behavior observed in practice, under the constraint of a constant wellbore flowing pressure. Our procedure is to couple case of time-dependent wellbore storage and skin effects with a set of reservoir flow models (*i.e.,* power-law, bilinear and formation linear flow) and by applying the convolution integral to the constant pressure condition, we generate various scenarios of production performance.

Specifically, in this work we provide derivations of the development of each constant pressure solution, where all work is performed Laplace domain and the Stehfest Algorithm is used to numerically invert each case to the real domain. A graphical illustration of the performance of each model is provided and a generalized workflow is presented (we note that this workflow can easily be extended to more complex fracture structures — *i.e.,* the multi-fractured horizontal well case).

Although these models represent different physical phenomena, we observe that all of the proposed models provide some mechanism for representing early-time variations in flowrates. We demonstrate the relevance of these models, which are based on empirical time-dependent models for wellbore storage and skin effects, as proxies that can be used to represent early-time flowrate behavior. In short, we demonstrate that each time-dependent model has unique characteristics which could theoretically allow for characterization of fracture behavior prior to the onset of an undistorted "reservoir" flow regime (*i.e.,* formation linear or bilinear flow).

DEDICATION

To my family.

Each One Should Use Whatever Gift He Has Received To Serve Others, Faithfully

— 1 Peter 4:10

ACKNOWLEDGEMENTS

I would like to thank:

Dr. Blasingame. For all of your support, dedication and tough love, I give my whole-hearted gratitude. Thank you for pushing me to reach further than I would have gone alone.

My advisory committee members, Dr. Barrufet and Dr. Ayers, for their support during my Masters studies.

Mr. Alex Valdes, for all of your help, patience, guidance and most importantly, friendship.

Mr. Mark Ostapenko, the best friend a guy could have.

To the Blasingame Research Group: I thank everyone who has gone through and currently is going through the gauntlet of this advisory group, for the support and camaraderie you have shown me through this process.

TABLE OF CONTENTS

LIST OF FIGURES

LIST OF TABLES

CHAPTER I

INTRODUCTION

1.1 Motivation

The motivation of this work originates from the lack of information available during flowback testing until the development of a characteristic reservoir flow regime (*i.e.,* linear or bilinear flow) from which we can diagnose reservoir behavior. Empirical analysis of field data, specifically the observation of an anomalous flowrate feature at early times (often a "hump" in the flowrate profile), leads to the hypothesis that reservoir behavior may not be uniquely identified nor quantified from flowback production performance. The goal of this present work is to utilize empirical and/or semi-analytical models to capture the anomalous behavior observed in flowback production performance as a means of possibly "diagnosing" causes of this behavior. At present, we do not provide any mechanisms to use such models to estimate reservoir (or well) properties or to "uncouple" wellbore and reservoir flow behavior — such topics will be left to subsequent research.

1.2 Objectives

The main objectives of the work are:

- To *provide* a constant pressure model for describing the early-time rate transient effects of a vertically fractured well including time-dependent wellbore storage and time-dependent wellbore skin effects.
- To *provide* diagnostic understanding of the behavior of the various time-dependent models.
- To *provide* a workflow of methodology to apply this technique to other applications.
- To *generate* dimensionless flowrate type-curves suitable for visualizing these flow phenomena.

1.3 Workflow for Model Development

In this section, we present a workflow which demonstrates the steps taken to develop our constant pressure solution, presented in **Fig. 1.1.** This workflow incorporates each historical flow regime and each of the time-dependent models presented in this proposal, and the major steps required to combine these models and presents a final solution in the Laplace domain.

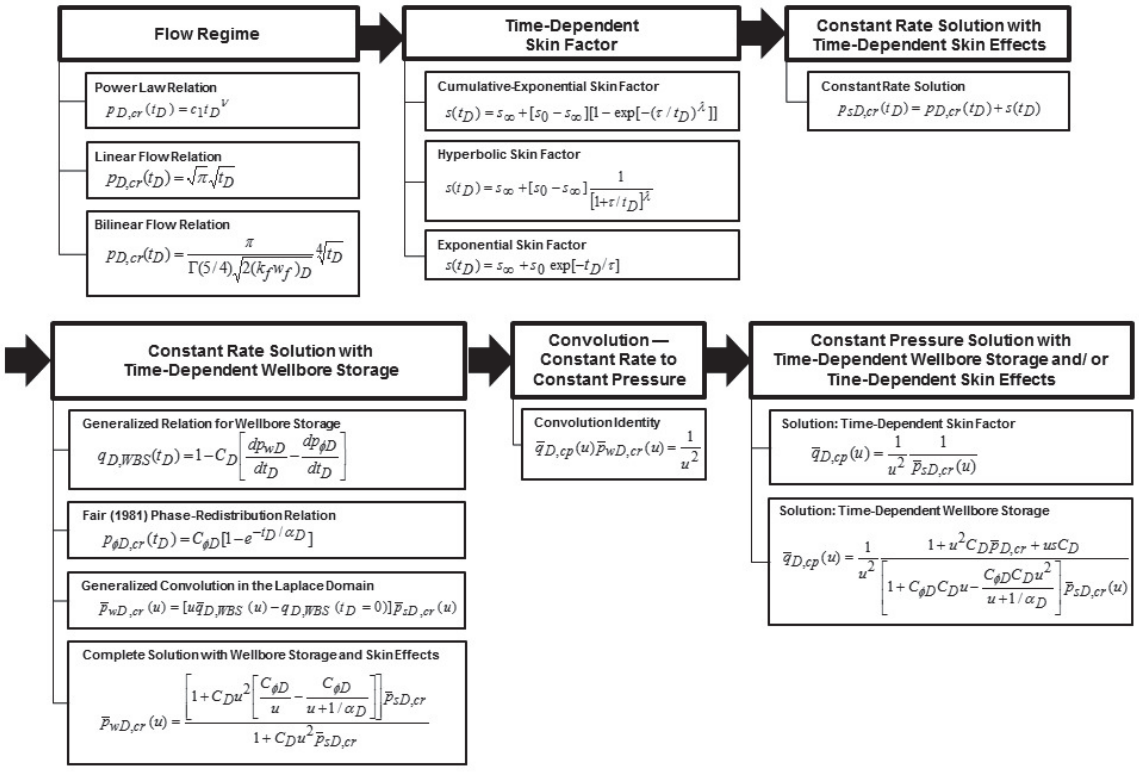

Figure 1.1 — Workflow for pressure and rate prediction with time-dependent wellbore storage and skin effects.

1.4 Basic Concepts

The development of the constant pressure solution for a vertically fractured well requires the understanding of basic concepts which are defined in this chapter and applied throughout the derivation of the proposed model.

Wellbore Storage is the phenomena that accounts for the difference between surface and bottomhole flowrates due primarily to the compressibility of the fluid within the wellbore. Occurring immediately after any change in the flowrate, the expansion or compression of the fluid causes a delay in the measured rates of the fluid. Wellbore storage is of significant interest due to its nature to mask reservoir behavior, at early-time, typically during well tests (*e.g.*, shut-in tests), but also during early flowback operations. Incorporation of the wellbore storage behavior is essential to development of the constant pressure model in this work.

Two types of wellbore storage are commonly examined (Lee, Rollins and Spivey, 2003), that of the single phase liquid filled wellbore, as illustrated by **Fig. 1.2**, and that of the two phase, gas-liquid filled wellbore

with rising or falling interface. Derivation of the wellbore storage effect is performed using a mass balance approach assuming a constant wellbore volume and fluid density. Although pressure differences within the wellbore could potentially lead to overall density changes in a two phase system, for practical applications, this assumption has been shown to be valid (Ramey, 1970). The generalized rate relation, in dimensionless form, for the wellbore storage effect is described by:

$$q_D = 1 - C_D\left[\frac{dp_{wD}}{dt_D} - \frac{dp_{tD}}{dt_D}\right]. \quad \text{.....(1.1)}$$

The dimensionless wellbore storage coefficient (C_D) is a function of reservoir properties and fracture properties including formation porosity, height of the fracture, total system compressibility, fracture half-length and the wellbore storage coefficient as defined by:

$$C_D = \frac{1}{0.00372}\frac{24C_S}{\phi h c_t x_f{}^2}, \quad \text{.....(1.2)}$$

where field units are used. The wellbore storage coefficient, C_S, is dependent on the type of wellbore storage case (*i.e.,* single-phase slightly compressible fluid or two-phase rising liquid interphase) examined (Lee, Rollins and Spivey, 2003).

Solving Eq. 1.1 yields the generalized constant pressure solution, an identity utilized throughout this work. The solution of the generalized rate relation (Eq. 1.1) is performed in the Laplace domain. *Assuming that the tubing pressure remains constant for all times*, (Blasingame, 1994) we solve for the dimensionless wellbore flowing pressure using the convolution integral (in the Laplace domain) to provide a relationship between the dimensionless wellbore flowrate and the dimension wellbore flowing pressure, as shown in Eq. 1.3 below:

$$\bar{p}_{wD}(u) = \frac{1}{\dfrac{1}{\bar{p}_{sD}(u)} + u^2 C_D}, \quad \text{.....(1.3)}$$

where $p_{wD}(u)$ is the dimensionless wellbore pressure inclusive of wellbore storage and skin effects, $p_{sD}(u)$ is the dimensionless wellbore pressure which only includes skin effects, and u is the Laplace transform parameter.

Agarwal, Hussainy and Ramey (1970) provided a number of observations which should be considered during the analysis and interpretation of well test data.

- The duration of the wellbore storage effect can be estimated primarily from the wellbore volume, the formation permeability and fluid compressibility.

- During the time of wellbore storage, the formation permeability and skin factor cannot be estimated; however, the wellbore storage coefficient can be determined.
- A transition period occurs after the wellbore storage period ends and is characterized by a change from unit slope to the characteristic signature of the flow regime of the reservoir, on a diagnostic plot.

Graphically, on a log-log diagnostic plot, the effects of wellbore storage will appear as a unit slope line at early times. It should be noted that wellbore storage is often mistaken (conceptually, not practically) with late time flow regimes such as boundary-dominated flow, therefore, understanding of the reservoir system is crucial for accurate diagnosis of reservoir behavior. Due to the significant impact wellbore storage has on pressure and rate transient analysis, extensive literature is available for the curious reader.

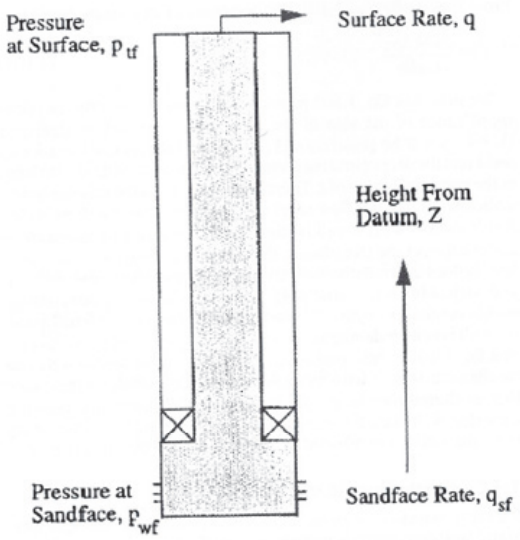

Figure 1.2 — Wellbore diagram for a well producing a single-phase fluid (Lee, Rollins and Spivey, 2003)

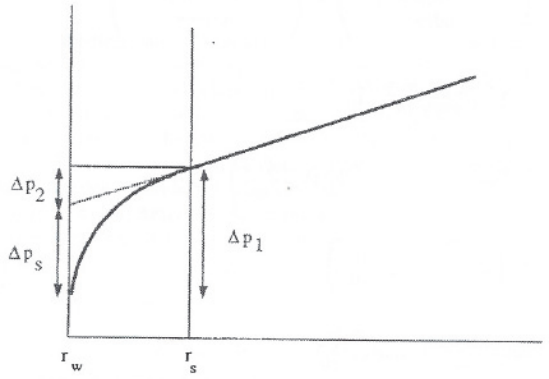

Figure 1.3 — Effect of near wellbore altered permeability (skin effect) on wellbore pressure (reproduced from Lee et al. 2003)

Wellbore Skin is the additional pressure drop (Van Everdingen, 1953) near the wellbore due to formation damage from adverse drilling and completion conditions creating a zone of reduced permeability. Hawkins (Lee et al. 2003), as demonstrated from **Fig. 1.3**, presented a definition of skin relating it to the wellbore flowing pressure and reservoir properties. This classic definition is developed from a radial model assuming two concentric zones around the wellbore. The inner region, as demonstrated by **Fig. 1.4**, is the zone of altered permeability while the outer zone maintains the original reservoir properties. From this work, the skin factor is defined by:

$$s = \left[\frac{k}{k_s} - 1\right] \ln\left[\frac{r_s}{r_w}\right], \quad \text{.....(1.4)}$$

which is a function of the ratio between reservoir and skin permeability, and the logarithmic ratio of the radius of the damaged zone to the wellbore radius. In terms of reservoir parameters, this can be further expressed by:

$$s = \frac{kh}{141.2qB\mu}(p - p_{wf}), \quad \text{.....(1.5)}$$

where the derivation assumes constant rate production, and constant reservoir parameters.

The skin factor has been demonstrated to be an additive function to the wellbore pressure response for the constant rate solution (Lee et al. 2003). In dimensionless form, the near wellbore pressure inclusive of skin effects is:

$$p_{sD}(t_D) = p_D(t_D) + s, \quad \text{.....(1.6)}$$

where $p_{sD}(t_D)$ is the dimensionless wellbore pressure which only includes skin effects, and $p_D(t_D)$ is the dimensionless wellbore pressure without any skin effects. In the Laplace domain, Eq. 1.6 is expressed as:

$$\overline{p}_{sD}(u) = \overline{p}_D(u) + \frac{s}{u}, \quad \text{.....(1.7)}$$

where u is the Laplace parameter. As an additive function, the inclusion of the skin factor into the constant rate pressure solution generates a simple algebraic expression, pertinent to the completion of this work.

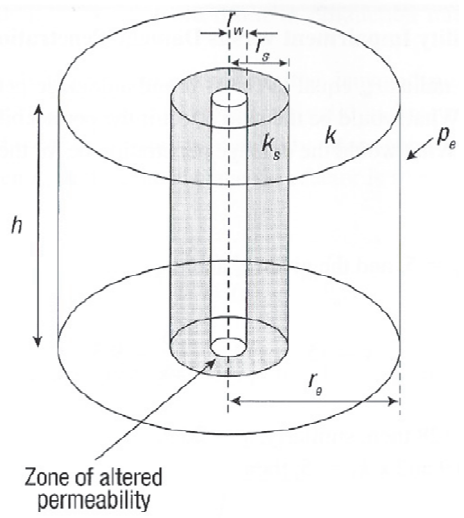

Figure 1.4 —Near wellbore zone of altered permeability (reproduced from Economides, Hill Ehlig-Ecomomides et. al., 2013)

Fracture Face Skin, was proposed by Cinco and Samaniego (1977) as an alternative type of skin effect which occurs during hydraulic fracture stimulation. Fracture face skin, different from the classic Hawkins skin developed for radial flow as demonstrated above, is physically described by the process of fluid leak-off from the fracture into the formation during well stimulation. The fracture is considered to contain a zone of altered permeability, as depicted by **Fig. 1.5**, which creates an additional pressure drop which the fluid must overcome when flowing from the reservoir into the fracture. This skin zone is defined as:

$$s_f = \frac{\pi}{2}\frac{w_s}{x_f}\left[\frac{k}{k_s}-1\right], \quad \text{.....(1.8)}$$

Where w_s is the width of the damaged zone (b_s in **Fig. 1.5**) and x_f is the fracture half length. The fracture face skin, in a similar respect to wellbore skin, is a function of the ratio of original reservoir permeability and fracture skin permeability. In dimensionless form, the pressure drop relation due to the fracture face skin is expressed as:

$$\Delta p_{sD} = \frac{kh}{141.2qB\mu}\Delta p_s, \quad \text{.....(1.9)}$$

where the flowrate is assumed constant and the pressure drop due to skin is described by:

$$\Delta p_s = \frac{443.6qw_s}{hk}\left[\frac{k}{k_s}-1\right] \quad \text{.....(1.10)}$$

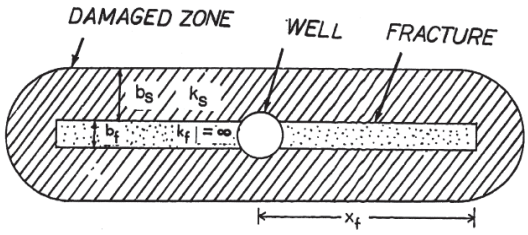

Figure 1.5 — Infinite conductivity fracture with fracture face skin damage (reproduced from Cinco and Samaniego 1981b)

Valdes et al. (2011) has performed further work on this subject introducing a Transient Interporosity Transfer model to describe the bilinear flow relation between the rock matrix and fracture with an additional skin between the two different porous structures.

Choked Fracture Skin as discussed by Cinco and Samaniego (1981b) proposes a second variation of fracture damage due to completions in a fractured well. Choked fracture skin occurs due to crushed proppant, or proppant lost or embedded in a fracture near the wellbore, as shown in **Fig. 1.6**. The reduced permeability of this near wellbore damage will cause an increased pressure drop which the fluid must overcome when flowing from the fracture to the wellbore.

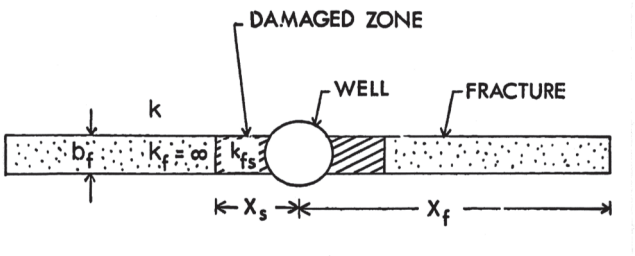

Figure 1.6 — Infinite conductivity fracture with choked fracture skin damage (reproduced from Cinco and Samaniego 1981b)

This skin zone is defined as:

$$s_{f,ch} = \frac{\pi x_s k_f}{w_f k_{fs}}, \quad \text{.....(1.11)}$$

where w_f is the width of the damaged zone (b_f in **Fig. 1.6**) and x_s is the length of damage along the fracture. The choked fracture skin is a function of the ratio of original fracture permeability to the damaged fracture permeability.

Convolution Integral allows for the overlap of one function as it is shifted over another function, or a "blending" of two functions together (Wolfram, 2007). In well test analysis, convolution was introduced by van Everdingen and Hurst (1949) to provide a mechanism in which to combine the constant rate solution with the constant pressure solution. The convolution integral, defined for a continuously changing flowrate, is expressed as:

$$p_{wD}(t_D) = \int_0^{t_D} q_D(\tau) p_{sD}(t_D - \tau) d\tau \; . \quad (1.12)$$

where $p_{sD}(t_D)$ is described by Eq. 1.6. In the Laplace domain, Eq. 1.12 reduces to:

$$\overline{p}_{wD}(u) = u\overline{q}_D(u)\overline{p}_{sD}(u) \; , \quad (1.13)$$

where $q_D(u)$ is the constant-pressure sand-face flowrate in the Laplace domain and $p_{sD}(u)$ is the constant-rate wellbore pressure inclusive of skin effects, in the Laplace domain. Eq. 1.13 provides an identity in which the constant rate solution, which has been a focus of significant well test research, may be transformed into the constant pressure solution (Van Everdingen & Hurst, 1949). This identity is fundamental to the completion of this work.

Numerical Laplace Inversion

Analytical inversion of a function into the real domain from the Laplace domain is commonly performed through the use of "look-up tables" (Roberts and Kaufman, 1966). However, when analytical inversion is either impossible or so cumbersome that it becomes impractical to use, numerical inversion techniques are applied. The Gaver-Stehfest algorithm is utilized in this work for all numerical inversion.

Gaver-Stehfest Algorithm is arguably the most common numerical inversion algorithm used in petroleum engineering due to its simplicity, accuracy and speed of performance in most applications. Originally proposed by Gaver in the late 1960's, with Stehfest providing a variation of the original Gaver work allowing for faster computation and accuracy, the Gaver-Stehfest algorithm is described as:

$$f_{GS}(n,t) = \frac{\ln(2)}{t} \sum_{i=1}^{n} V_i \overline{F}\left[\frac{\ln(2)}{t} i\right], \quad (1.14)$$

where Stehfest provided extrapolation coefficients given as:

$$V_i = (-1)^{\frac{n}{2}+i} \sum_{k=\left\lfloor \frac{i+1}{2} \right\rfloor}^{Min\left[i, \frac{n}{2}\right]} \frac{k^{\frac{n}{2}}(2k)!}{\left[\frac{n}{2} - k\right]! k!(k-1)!(i-k)!(2k-i)!} \quad (1.15)$$

Theoretically, the larger the Stehfest number (n) the more accurate the approximation to the real solution. However, it has been demonstrated repeatedly in literature (Cheng et al, 1994) that at very large values of n the solution begins to diverge from the real solution. Therefore, $8 \leq n \leq 20$ is considered appropriate for most applications.

Valkó and Abate (2004) developed code for use in Mathematica based on the acceleration scheme by Gaver-Wynn-Rho (GWR) algorithm. The code controls the precision of numerical inversion based upon a user-defined requirement (n). This code was employed for all numerical inversion requirements with a minimum precision level of n=32 (which is not to be confused with the number of terms of summation from Eq. 1.15).

The author notes, that although highly applicable for most transient flow problems, the Gaver-Stehfest numerical inversion algorithm has been demonstrated to be inadequate for oscillatory and discontinuous functions. Initial research led to the examination of other numerical inversion techniques, returning to the GWR algorithm as the most suitable for this research.

CHAPTER II

LITERATURE REVIEW

This chapter presents a summary of notable milestones achieved in the study of well test analysis for fractured wells as is directly relevant to the content of this paper. For further reference, Cinco (1982) provides a thorough evaluation of all major contributions to the evaluation of hydraulic fractures for pressure transient analysis through 1982. This chapter further examines notable works by authors upon which the fundamentals of the constant pressure solution presented in this paper are built.

2.1 History of Short Term Well Test Analysis for Fractured Wells

Short-term well testing developed primarily in response to the high cost of performing very long duration tests used to evaluate radial flow and average reservoir pressure. The lost revenue due to extended well shut-ins drove engineers to examine other methods to interpret the nature and behavior of the reservoir. With the widespread application of well stimulation, notably through hydraulic fracturing, further work was performed as it was recognized that classic radial flow theory did not apply to fractured wells.

Muskat (1937) first examined infinite conductivity vertical fractures in a steady-state analytical model. Initial studies, mostly at steady-state, focused on the improved productivity gained through fracturing wells.

Russell and Truitt (1964) worked with transient pressure behavior for infinite conductivity fractures, calculating wellbore pressure as a function of time depending on fracture half-length.

Linear flow theory, in unsteady-state analysis, was first applied by Clark (1968) and Millheim and Cichowicz (1968) noticing the straight line relationship between the wellbore pressure against the square root of time.

Transient flow behavior was reexamined by Gringarten, Ramey and Raghavan (1975) and three different models were developed. These being: the case of an infinite conductivity vertical fracture, the uniform flux vertical fracture, and the uniform flux horizontal fracture. In all three cases, linear flow periods were demonstrated before the occurrence of pseudo-radial flow. **Fig. 2.1** demonstrates the flow regimes associated with vertically fractured wells. "Type curve analysis" was used to graphically diagnose flow regimes and determine formation and fracture properties.

Wellbore storage was first introduced in literature by van Everdingen and Hurst (1949). They expressed the phenomena in terms of a drawdown test where the unloading of the annulus is corrected to include the effects of the fluid column hydrostatic head as shown:

$$q(\Delta T) = C_s \frac{d\Delta p}{dT} \quad \text{.....(2.1)}$$

where C_S is the volume of fluid unloaded from the annulus per unit bottomhole pressure per thickness of the reservoir.

Agarwal, Hussainy and Ramey (1970) examined analytically the effect of wellbore storage and skin on short time transient flow behavior.

In a radial system, Gringarten, Ramey and Raghavan (1975) applied this theory for fractured wells, further adding to the list of type curves available for well test analysis at the time.

Cinco, Samaniego and Dominguez (1978) demonstrated that the infinite conductivity fracture is not valid for all cases, developing the finite conductivity vertical fracture model. Further, this system was shown not to exhibit linear flow, and new analysis methods would be required. Cinco, Samaniego and Dominguez (1978) presented a solution for the two-dimensional diffusivity equation through the use of Greens functions and source function, applying the Newman product method as discussed by Gringarten, Ramey and Raghavan (1973). The solution presented by the authors (Cinco, Samaniego and Dominguez, 1978) uses a discretization of the fracture (*i.e.,* assuming fracture flux has a stepwise distribution in both time and space). Due to the complexity of this solution, the authors re-cast the problem using the Laplace transform.

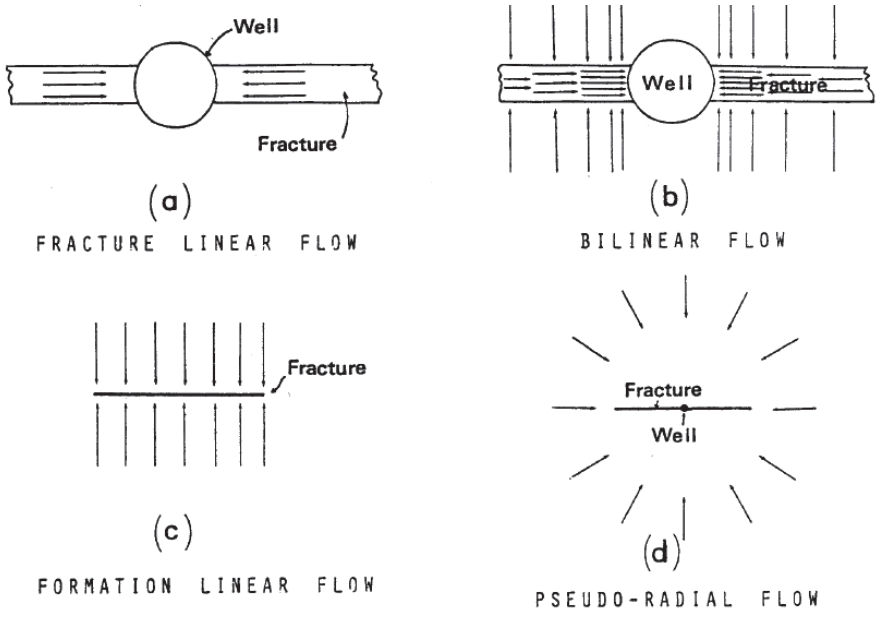

Figure 2.1 —Flow periods for a vertically fractured well (reproduced from Cinco and Samaniego, 1981a)

Building on the work performed in 1978, Cinco and Samaniego (1981a) introduced the bilinear flow regime**, Fig. 2.1b**, for a fracture which exhibits "finite-conductivity" fracture behavior. They developed semi-log analysis for wellbore pressure to demonstrate this behavior. Approximations for fracture linear flow and bilinear flow regimes are presented as:

$$p_{wD} = \frac{2}{(k_f w_f)_D}\sqrt{\pi \eta_{fD} t_D} \qquad \text{(formation linear flow)} \qquad (2.3)$$

$$p_{D,cr}(t_D)\frac{\pi}{\Gamma(5/4)\sqrt{2(k_f w_f)_D}}\sqrt[4]{t_D} \qquad \text{(bilinear flow).} \qquad (2.4)$$

Type curves were developed to diagnose transitions between flow regimes and to estimate reservoir and fracture parameters. The constant rate solutions presented by Cinco and Samaniego (1981a) are fundamental to the efforts in this thesis, and a full derivation of their work may be found in **Appendix B**.

2.2 Transient Flow Behavior for Constant Pressure Production

Understanding the practical difficulty in holding rate constant during production, Guppy, Cinco and Ramey (1981) examined the constant pressure solution for the vertical fracture with finite conductivity. Assuming the pressure response in the fracture varies only with distance along the fracture (fluid flowrate varies with both distance and time) the pressure gradient is expressed as a function of formation constants and the integration of rate along the fracture, as shown by:

$$p_{fD}(0,t_D) - p_{fD}(x_{D_j},t_D) = \frac{2\pi q_D}{(k_f w_f)_D}\int_0^{x_{D_j}} q_{cD}\, dx'_D \qquad (2.5)$$

The pressure response in the formation, solved in a similar manner, includes integral rates with respect to time and distance from the fracture, and exponential functions as shown in Eq. 2.6:

$$p_D(x_D = 0, t_{Dx_f}) = \int_0^{t_{Dx_f}} \frac{q_D(\tau)}{4}\int_0^1 \frac{q_{fD}(x',\tau)}{t_D - \tau}\left[e^{-\frac{(x_D - x')^2}{4(t_D-\tau)}} + e^{-\frac{(x_D + x')^2}{4(t_D-\tau)}}\right] \qquad (2.6)$$

The full solution requires the coupling of Eq. 2.5 and Eq. 2.6 equating the pressure drop in the fracture. The final solution requires a discretization of the fracture length and a relationship between formation flow and fracture flow. The authors suggested utilizing convolution as a method of solution, however, the full analytic solution would not be of any practical value. Therefore, the authors preferred to present approximations based upon the conductivity of the fracture, shown as:

$$\frac{1}{q_D(t_D)} = \frac{\pi\Gamma(3/4)}{\sqrt{2k_{fD}w_{fD}}} t_D^{1/4} \quad \text{(low conductivity fracture).} \quad (2.7)$$

$$q_D(t_D) = 2\sqrt{\frac{t_D}{\pi^3}} \quad \text{(high conductivity fracture).} \quad (2.8)$$

Equations 2.7 and 2.8 display the same behavioral characteristics of bilinear flow and linear flow regimes, respectively, as demonstrated by Cinco and Samaniego (1981a).

In the formulation of the high and low conductivity fracture behavior, Eqs. 2.7 and 2.8 respectively, Guppy et al. (1981) proposed significant assumptions. For the low conductivity case, the effect of the fracture tips were considered negligible, resulting in a fracture flow differential equation that does not vary with time. For high conductivity fractures, the pressure drop within the fracture was assumed negligible.

Although the assumptions made by Guppy et al. (1981) are valid for very short times in the formulation of the approximate solutions, this author suggests, specifically for the low conductivity fracture case, a more rigorous approach. We assumed that the pressure response in the fracture varies with both time and distance along the fracture, which was incorporated into our full diffusivity equation, shown in **Appendix B**.

2.3 Variable Skin in Well Test Analysis

Early-time cleanup effects in drawdown data can, when improperly analyzed, can provide the impression of additional pressure support by the reservoir leading to an inflated flow capacity (Larsen and Kviljo, 1990). Assuming a constant production rate, due to small transients in pressure, a limited zone of damage in radial coordinates, Larsen and Kviljo (1990) proposed a (time-dependent) variable skin model to account for the pressure increase caused by near-well cleanup. Based on empirical data, Larsen and Kviljo (1990) proposed a "hyperbolic" relation of the skin factor with time as demonstrated by:

$$s(t) = \frac{a}{b+t} + c\,, \quad (2.9)$$

where c is the value of skin that the system would achieve if cleanup continued to fruition. The parameters a and b are determined from drawdown data and are unique to each well (and perhaps to each producing scenario). Larsen et al. (1990) demonstrated that cleanup effects can be modeled using a hyperbolic expression of skin as a function of time, substituting a variable skin into constant skin drawdown solutions providing a reliable estimation of the flow capability of the system.

2.4 Pressure Buildup Analysis with Wellbore Phase Redistribution

Wellbore phase redistribution is a wellbore storage phenomena occurring when both liquid and gas flow through the tubing. After shut-in, gravity will cause a separation of fluids, with liquid falling and gas rising to surface. In the closed system, as liquid fills the tubing, the inability of gas to expand may cause, at early-times, a temporary increase in pressure above the formation pressure coined "gas-humping." Eventually pressure equilibrium is restored with the formation (Stegmeier and Matthews, 1958).

Fair (1981) expanded on the general work of Stegmeier and Matthews (1958) and Earlougher (1977) by performing a rigorous analysis of wellbore phase redistribution incorporating the additional wellbore storage effect into the diffusivity equation. Starting from van Everdingen and Hurst (1949) definition for the effect on wellbore pressure with time due to wellbore storage, Fair (1981) added a term for phase distribution as shown by:

$$q_D(t_D) = 1 - C_D\left[\frac{dp_{wD}}{d_{tD}} - \frac{dp_{\phi D}}{d_{tD}}\right], \quad (2.10)$$

where $p_{\phi D}$ is the pressure caused by phase redistribution. Based on a single laboratory test, and theoretical postulation, Fair (1981) defined the pressure caused by wellbore phase redistribution as:

$$p_{\phi D}(t_D) = C_{\phi D}[1 - e^{-t_D/\alpha_D}], \quad (2.11)$$

where C_D is the dimensionless phase redistribution constant and α_D is the time in which 63% of the total change has occurred. Fair (1981) defines each dimensionless term as:

$$p_{\phi D} = \frac{khp_{\phi}}{141.2qB_o\mu} \quad (2.12a)$$

$$C_{\phi D} = \frac{khC_{\phi}}{141.2qB\mu} \quad (2.12b)$$

$$t_D = \frac{0.00264kt}{\phi\mu c_t {r_w}^2} \quad (2.12c)$$

$$\alpha_D = \frac{0.00264k\alpha}{\phi\mu c_t {r_w}^2} \quad (2.12d)$$

where all values are listed in field units. Fair (1981) uses the well-known diffusivity equation in radial coordinates:

$$\frac{\partial^2 p_D}{{dr_D}^2} + \frac{1}{r_D}\frac{\partial p_D}{dr_D} = \frac{\partial p_D}{dt_D}. \quad (2.13)$$

With initial and boundary conditions which incorporate the phase redistribution and near wellbore skin:

$$p_D(r_D,0)=0 \qquad \text{(initial condition)} \qquad (2.14)$$

$$\lim_{r_D\to\infty} p_D(r_D,t_D)=0 \qquad \text{(outer boundary condition)} \qquad (2.15)$$

$$-\left[\frac{\partial p_D}{\partial r_D}\right]_{r_D=1}=1-C_D\left[\frac{dp_{wD}}{dt_D}-\frac{dp_{\phi D}}{dt_D}\right] \qquad \text{(inner boundary condition)} \qquad (2.16)$$

$$p_{wD}=\left[p_D-s\left[\frac{dp_D}{dr_D}\right]\right] \qquad (2.17)$$

Fair (1981) solved the diffusivity equation in Laplace domain providing solutions for cylindrical and line source wells. The wellbore pressure solutions, in Laplace domain are:

$$\overline{p}_{wD}(u)=\frac{\left[\frac{K_0\sqrt{u}}{uK_1\sqrt{u}}+s\right]\left[1+C_DC_{\phi D}u^2\left[\frac{1}{u}-\frac{1}{u+1/\alpha_D}\right]\right]}{u\left[1+C_Du\left[\frac{K_0\sqrt{u}}{uK_1\sqrt{u}}+s\right]\right]} \qquad \text{(Cylindrical Source Well)} \qquad (2.17)$$

$$\overline{p}_{wD}(u)=\frac{\left[K_0\sqrt{u}+s\right]\left[1+C_DC_{\phi D}u^2\left[\frac{1}{u}-\frac{1}{u+1/\alpha_D}\right]\right]}{u[1+C_Du[K_0\sqrt{u}+s]]} \qquad \text{(Line Source Well),} \qquad (2.18)$$

Where K_0 and K_1 are modified Bessel functions. Fair generated type curves for various values of the dimensionless wellbore storage constant and dimensionless wellbore phase distribution constant. As a demonstration (Fair, 1981), field data obtained from a gas-lift well were matched very well using the Fair model (Eq. 2.11).

Extension of the phase redistribution concept to model the behavior of flowback data is logical, particularly for cases of gas condensate and volatile oils, but this concept alone may not be sufficient to capture uniquely the behavior of early-time flowback data as we believe that a time-dependent skin function will also be required to capture the effect of stimulation fluid "clean-up" which occurs during flowback operations.

CHAPTER III

PROPOSED MODELS

Examining the reservoir flow behavior of a hydraulically fractured vertical well, we assume that time-dependent wellbore storage and skin effects dominate the "early-time" classically observed flow regimes (*i.e.,* linear and bilinear flow) for a vertical fracture. Our proposed time-dependent wellbore storage and skin effect models are coupled with each classical flow regime (linear flow, bilinear flow, and a general power-law model) in the Laplace domain. Application of the convolution integral provides the mechanism to evaluate the constant pressure (rate) solution. This chapter contains a summary of each of the proposed time-dependent models which could theoretically allow for diagnosis of reservoir behavior prior to the onset of "late-time" (*i.e.,* linear or bilinear) reservoir flow regimes.

3.1 Assumptions

The following specific assumptions are made in this work:

- A vertical well with a single vertical fracture penetrates the entire thickness of the reservoir.
- The reservoir thickness is uniform (constant).
- The reservoir is initially at pressure, p_i.
- The reservoir is infinite in size.
- The well produces from a constant flowrate.
- The rock properties are constant.
- The fracture has finite conductivity.
- The fracture is infinite in length.
- Flow to the wellbore occurs only through the vertical fracture.
- The system contains a "slightly-compressible" fluid.
- The effects of gravity are negligible.
- The pressure gradients are small.
- The system obeys Darcy's Law.

A schematic of the proposed model is shown in **Fig. 3.1.**

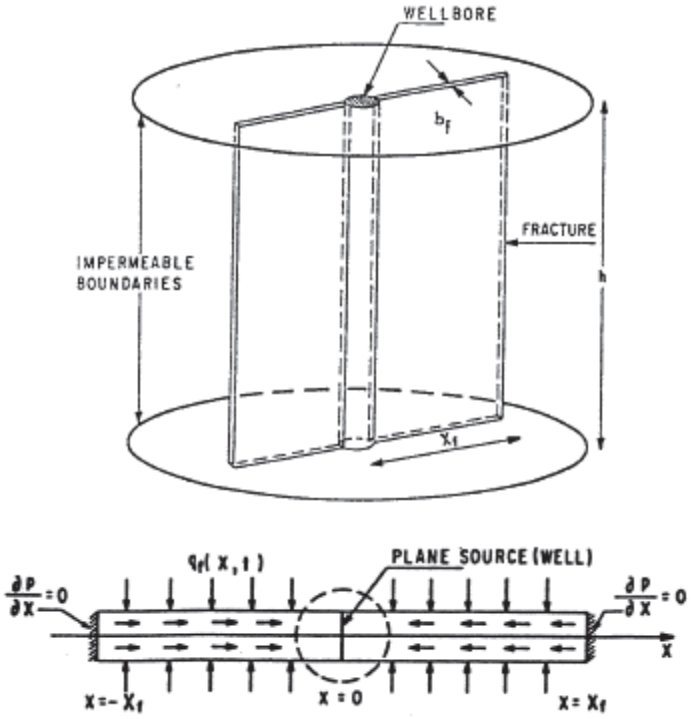

Figure 3.1 — Schematic representation of the proposed model (reproduced from Cinco and Samaniego, 1978)

3.2 Flow Regime Development

Cinco and Samaniego (1981a) described four flow regimes, classically considered to describe reservoir behavior for hydraulically fractured vertical wells. These models are summarized as:

- Fracture Linear Flow
- Formation Linear Flow
- Bilinear Flow
- Pseudo-Radial Flow

Fracture linear flow, in practice, occurs too early in the unloading of the system to (ever) be observed through conventional means. Further, in an ultra-low permeability reservoir, the time required to attain pseudo-radial flow far exceeds the "early-time" parameters of this work. For these reasons, the "fracture linear" and "pseudo-radial" flow regimes will not be considered in this work.

Formation Linear Flow Relation

Formation linear flow was described by Gringarten, Ramey and Raghavan (1974) derived from the continuous line-source solution originally presented by Carslaw and Jaeger (1946). Fully derived in **Appendix A**, the formation linear flow derivation begins with a statement of the continuous line source solution:

$$\Delta p_{cls}(x,y,t) = \frac{1}{4\pi\eta_f}\int_0^t q_{cls}(\tau)\exp\left[-\frac{(x-x_w)^2+(y-y_w)^2}{4\eta_f(t-\tau)}\right]\frac{d\tau}{t-\tau} \quad \text{.....(3.1)}$$

Integration through substitution and non-dimensionalizing, the system yields a formulation consisting of error functions and exponential integrals as shown by Eq. 3.2: (constant rate formulation)

$$p_{D,cr}(x_D,t_D) = \frac{\sqrt{\pi t_D}}{2}\left[erf\left[\frac{1+x_D}{2\sqrt{t_D}}\right]+erf\left[\frac{1-x_D}{2\sqrt{t_D}}\right]\right]+ \left[\frac{1-x_D}{4}\right]E_i\left[\frac{[1-x_D]^2}{4t_D}\right]+\left[\frac{1+x_D}{4}\right]E_i\left[\frac{[1+x_D]^2}{4t_D}\right]$$

.....(3.2)

At very early-times, Eq. 3.2, evaluating at x_D=0, may be approximated by:

$$p_{D,cr}(x_D=0,t_D) = \sqrt{\pi}\sqrt{t_D} \quad \text{.....(3.3)}$$

which is the approximation linear flow. The authors further simplified Eq. 3.2 for late-time pseudo-radial flow — however, this result is not applicable to this work. Use of the convolution integral in the Laplace domain provides a mechanism to re-cast this formulation as a constant pressure solution. Taking the Laplace transform of Eq. 3.3 yields:

$$\overline{p}_{D,cr}(u) = \sqrt{\pi}\frac{\Gamma(3/2)}{u^{3/2}} \quad \text{.....(3.4)}$$

Where u is the Laplace transform parameter. Eq. 3.4 is to be combined with time-dependent wellbore storage and skin effects in an attempt to model the "early-time" (flowback) production performance.

Bilinear Flow Relation

Bilinear Flow was originally proposed by Cinco and Samaniego (1981) for "finite-conductivity" fractures, where the pressure drop across the fracture is not negligible and must be considered when evaluating reservoir performance. Derivation of the bilinear flow regime is provided in complete detail in **Appendix B**. The differential equation, coupling fracture flow with formation flow is given as:

$$\frac{\partial^2 p_{fD,cr}}{\partial {x_D}^2} + \frac{2}{(k_f w_f)_D} \left.\frac{\partial p_D}{\partial y_D}\right|_{y_D=0} = \frac{1}{\eta_{fD}} \frac{\partial p_{fD,cr}}{\partial t_D} \quad (0 < x_D < \infty) \qquad (3.5)$$

The proposed method of solution takes the formulation given by Eq. 3.5 into the Laplace domain, and is solved using traditional methods for a second-order, ordinary differential equation. The result, in the Laplace domain, is a function which describes both fracture linear flow and bilinear flow behavior. Eq. 3.6 describes the combined formulation for a finite-conductivity vertical fracture:

$$\bar{p}_{D,cr}(u) = \frac{\pi}{(k_f w_f)_D} \frac{1}{u\left[\frac{u}{\eta_{fD}} + \frac{2\sqrt{u}}{(k_f w_f)_D}\right]^{1/2}} \qquad (3.6)$$

As fracture linear flow is not relevant to this work, we examine when Eq. 3.6 tends to long times (u tends towards zero in the Laplace domain) which results in the following late-time approximation:

$$\bar{p}_{D,cr}(u) = \frac{\pi}{\sqrt{2(k_f w_f)_D}} \frac{1}{u^{5/4}} \qquad (3.7)$$

Inversion from the Laplace domain yields:

$$p_{D,cr}(t_D) = \frac{\pi}{\Gamma(5/4)\sqrt{2(k_f w_f)_D}} \sqrt[4]{t_D} \qquad (3.8)$$

which is the bilinear flow approximation that we will use in this work.

Power-Law Flow Relation

We have included a third model, the general power-law formulaiton which provides the potential to describe additional reservoir behavior. Proposed as a general power-law relation, Eq. 3.9 describes any flow regime which produces a straight line on a log-log plot, shown as:

$$p_{D,cr}(t_D) = c_1 t_D{}^{\nu} \qquad \text{(power-law flow)} \qquad (3.9)$$

where c_1 is a problem-dependent constant, likened to the dimensionless fracture conductivity term in the bilinear flow case, and ν may be any value between zero and one.

3.3 Time-Dependent Skin Effects

Larsen and Kviljo (1990) examined the effects of wellbore cleanup and proposed a hyperbolic time-dependent skin factor to account for the overestimation of a wells flow capacity. The original formulation given by Larsen and Kviljo (1990) is presented as:

$$s = \frac{a}{b+t} + c \qquad (3.10)$$

where c is the theoretical minimum skin a system would reach assuming continuous cleanup.

Using Eq. 3.10 as a basis for our formulations, we postulated the following time-dependent skin factor models for the work in this thesis:

$$s(t_D) = s_\infty + [s_0 - s_\infty][1 - \exp[-(\tau / t_D)^{\lambda}]] \qquad \text{(cumulative-exponential, } s(t)\text{)} \qquad (3.11)$$

$$s(t_D) = s_\infty + s_0 \exp[-(t_D / \tau)] \qquad \text{(exponential, } s(t)\text{)} \qquad (3.12)$$

$$s(t_D) = s_\infty + [s_0 - s_\infty]\frac{1}{[1+\tau / t_D]^{\lambda}} \qquad \text{(hyperbolic, } s(t)\text{)} \qquad (3.13)$$

To demonstrate the behavior of each model, we provide a graphical representation of each model in **Fig. 3.2** shown below.

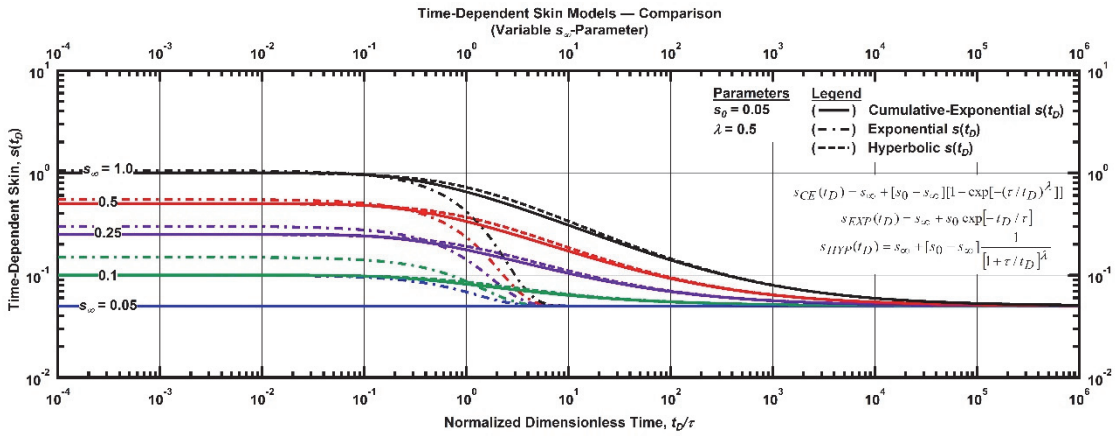

Figure 3.2 —Log-log plot of time-dependent skin factor models for select values of s_∞-parameter.

Each time-dependent skin model was provided with an upper and lower boundary for the skin values, in the forms of the s_0- and s_∞-parameters. These formulations provide a mechanism to maintain a positive value of the skin factor for each model.

It has been demonstrated that the skin factor is an additive dimensionless pressure term: (Lee, Rollins and Spivey, 2003)

$$p_{sD,cr}(t_D) = p_{D,cr}(t_D) + s(t_D) \quad \text{.....(3.14)}$$

Where the constant-rate dimensionless pressure inclusive of skin ($p_{sD,cr}(t_D)$) is equal to the constant-rate dimensionless pressure ($p_{D,cr}(t_D)$) plus a time-dependent skin factor ($s(t_D)$).

The generalized constant pressure solution in the Laplace domain, presented below for reference, utilizes the convolution integral to provide a direct relationship between the constant rate and constant pressure solutions.

$$\bar{q}_{D,cp}(u) = \frac{1}{u^2}\frac{1}{\bar{p}_{sD,cr}(u)} \quad \text{.....(3.15)}$$

Inverting the three different flow regimes, along with the three different time-dependent skin factors, into the Laplace domain, and combining with Eq. 3.14 yields nine different models to be evaluated in this thesis.

A full derivation of the generalized constant rate-solution is provided in **Appendix C**. As a point of importance, we note that during the formulation of the generalized constant-rate solution for the constant

wellbore storage case, the constant pressure result does not exist due to mathematical condition that the pressure cannot be constant at both the sandface and the surface at the same time. Specifically, the Roberts and Kaufman reference [Roberts and Kaufman (1966, pg. 202, Eq.172)] demonstrate that the inverse Laplace transform of a constant yields the Dirac delta, $\delta(t)$, an impulse function which has no meaning for our cases. As the Laplace Transform Operator is a linear operator (Spiegel, 1971), we know that the wellbore storage constant will either be zero, or infinity for the constant pressure solution in the real domain.

As the constant wellbore storage case is not relevant for our work, we will utilize the time-dependent wellbore storage (or wellbore phase redistribution) model proposed by Fair (1981) as our primary means of representing wellbore flow effects (discussed in the next section). Our approach is to combine the Fair (1981) time-dependent wellbore storage model with the prescribed constant rate models (*i.e.,* the linear, bilinear, or general power-law cases) in the Laplace domain to obtain the constant pressure (rate) solution for each case. The inverse Laplace transformation (*i.e.,* the real domain) solutions are generated numerically through the use of the Stehfest algorithm.

For the cases of time-dependent skin effects (only), the following summary is presented for reference:

Power Law Flow:

- $\bar{q}_{D,cp}(u) = \dfrac{1}{c_1 u^{(1-\nu)}\Gamma(1+\nu) + s_\infty u + u\Gamma(1+\lambda)U(\lambda,0,u\tau)[s_0 - s_\infty]}$ ..... (hyperbolic $s(t)$)

- $\bar{q}_{D,cp}(u) = \dfrac{1}{c_1 u^{(1-\nu)}\Gamma(1+\nu) + us_\infty + \dfrac{u^2 s_0}{u+1/\tau}}$ .....(exponential $s(t)$)

- $\bar{q}_{D,cp}(u) = \dfrac{1}{c_1 u^{(1-\nu)}\Gamma(1+\nu) + us_0 - \dfrac{2u^2 K_1\left[\dfrac{2}{\sqrt{1/u\lambda\tau}}\right][s_0 - s_\infty]}{\sqrt{u/\lambda\tau}}}$ .....(cumulative-exponential $s(t)$)

Linear Flow:

- $\bar{q}_{D,cp}(u) = \dfrac{1}{\sqrt{\pi}\sqrt{u}\Gamma(3/2) + s_\infty u + u\Gamma(1+\lambda)U(\lambda,0,u\tau)[s_0 - s_\infty]}$ ..... (hyperbolic $s(t)$)

- $\bar{q}_{D,cp}(u) = \dfrac{1}{\sqrt{\pi}\sqrt{u}\Gamma(3/2) + us_\infty + \dfrac{u^2 s_0}{u+1/\tau}}$ .....(exponential $s(t)$)

- $\bar{q}_{D,cp}(u) = \dfrac{1}{\sqrt{\pi}\sqrt{u}\Gamma(3/2) + us_0 - \dfrac{2u^2 K_1\left[\dfrac{2}{\sqrt{1/u\lambda\tau}}\right][s_0 - s_\infty]}{\sqrt{u/\lambda\tau}}}$ .....(cumulative-exponential $s(t)$)

Bilinear Flow:

- $$\bar{q}_{D,cp}(u) = \frac{1}{\frac{\pi \exp[5/4]}{\sqrt{2(k_f w_f)_D}} \frac{\Gamma(5/4)}{u^{3/4}} + s_\infty u + u\Gamma(1+\lambda) U(\lambda, 0, u\tau)[s_0 - s_\infty]}$$ ..... (hyperbolic $s(t)$)

- $$\bar{q}_{D,cp}(u) = \frac{1}{\frac{\pi \exp[5/4]}{\sqrt{2(k_f w_f)_D}} \frac{\Gamma(5/4)}{u^{3/4}} + u s_\infty + \frac{u^2 s_0}{u + 1/\tau}}$$ .....(exponential $s(t)$)

- $$\bar{q}_{D,cp}(u) = \frac{1}{\frac{\pi \exp[5/4]}{\sqrt{2(k_f w_f)_D}} \frac{\Gamma(5/4)}{u^{3/4}} + u s_0 - \frac{2u^2 K_1\left[\frac{2}{\sqrt{1/u\lambda\tau}}\right][s_0 - s_\infty]}{\sqrt{u/\lambda\tau}}}$$ ...(cumulative-exponential $s(t)$)

3.4 Time-Dependent Wellbore Storage

In a two phase (gas-liquid) system, when a well is shut-in at the surface, gravity effects cause phase separation and due to the incompressibility of liquid relative to gas, may cause an increase in surface pressure before system equilibrium is attained. Evaluating these anomalous pressure readings, Fair (1981) proposed the incorporation of a wellbore phase redistribution pressure term into the solution of the radial flow diffusivity equation. From empirical evidence and a single laboratory test given by another author, Fair (1981) postulated an exponential pressure function as shown by Eq. 3.16:

$$p_{\phi D}(t_D) = C_{\phi D}(1 - e^{-t_D/\alpha_D}) \quad \text{.....(3.16)}$$

Fully derived in **Appendix E**, the fluid flowrate due to changing sandface and wellbore phase redistribution pressures was described by Fair (1981) as:

$$q_D(t_D) = 1 - C_D\left[\frac{dp_{wD}}{d_{tD}} - \frac{dp_{\phi D}}{d_{tD}}\right] \quad \text{.....(3.17)}$$

Transforming Eq. 3.17 into the Laplace domain, and solving for the wellbore flowing pressure yields:

$$\bar{p}_{wD,cr}(u) = \frac{[1 + C_D u^2 \bar{p}_{\phi D}(u)]\bar{p}_{sD}(u)}{1 + C_D u^2 \bar{p}_{sD}(u)} \quad \text{.....(3.18)}$$

Which is the generalized constant rate dimensionless pressure solution in the Laplace domain, as a function of the wellbore phase redistribution pressure ($p_{\phi D}(u)$), the sandface flowing pressure inclusive of skin ($p_{sD}(u)$), the Laplace parameter (u) and the wellbore storage constant (C_D). For this formulation, we assume that the skin effect is constant.

In order to find a constant pressure solution, we return to the convolution integral in Laplace domain for a constant flowrate defined as:

$$\overline{q}_{D,cp}(u)\overline{p}_{wD,cr}(u) = \frac{1}{u^2} \quad \text{.....(3.19)}$$

Substituting Eq. 3.18 into Eq. 3.19 and solving for the constant pressure (rate) solution yields:

$$\overline{q}_{D,cp}(u) = \frac{1}{u^2}\frac{1+C_D u^2 \overline{p}_{sD}(u)}{[1+C_D u^2 \overline{p}_{\phi D}(u)]\overline{p}_{sD}(u)} \quad \text{.....(3.20)}$$

We recall our pressure solutions, presented in the Laplace domain, as:

$$\overline{p}_{\phi D}(u) = \frac{C_{\phi D}}{u} - \frac{C_{\phi D}}{u+1/\alpha_D}, \quad \text{.....(3.21)}$$

$$\overline{p}_{sD,cr}(u) = \overline{p}_{D,cr}(u) + \frac{s}{u} \quad \text{.....(3.22)}$$

Substitution of Eq. 3.21 and Eq. 3.22 into Eq. 3.20 yields a generalized time-dependent wellbore storage solution, in the Laplace domain, as shown:

$$\overline{q}_{D,cp}(u) = \frac{1}{u^2}\frac{1+C_D u^2\left[\overline{p}_{D,cr}(u)+\frac{s}{u}\right]}{\left[1+C_{\phi D}C_D u + \frac{C_{\phi D}C_{\phi D}u^2}{u+1/\alpha_D}\right]\left[\overline{p}_{D,cr}(u)+\frac{s}{u}\right]} \quad \text{.....(3.23)}$$

Incorporation of each flow relation into the generalized constant-pressure solution (Eq. 3.23) inclusive of time-dependent wellbore storage is provided below:

- $$\overline{q}_{D,cp}(u) = \frac{1}{u^2}\frac{1+u^2 C_D c_1 \frac{\Gamma(1+\nu)}{u^{1+\nu}} + usC_D}{\left[1+C_{\phi D}C_D u - \frac{C_{\phi D}C_D u^2}{u+1/\alpha_D}\right]\left[c_1\frac{\Gamma(1+\nu)}{u^{1+\nu}}+\frac{s}{u}\right]}$$ .....(general power-law flow)

- $$\overline{q}_{D,cp}(u) = \frac{1}{u^2}\frac{1+u^2 C_D \sqrt{\pi}\frac{\Gamma(3/2)}{u^{3/2}} + usC_D}{\left[1+C_{\phi D}C_D u - \frac{C_{\phi D}C_D u^2}{u+1/\alpha_D}\right]\left[\sqrt{\pi}\frac{\Gamma(3/2)}{u^{3/2}}+\frac{s}{u}\right]}$$ ..... (linear flow)

- $$\bar{q}_{D,cp}(u) = \frac{1}{u^2} \frac{1 + u^2 C_D \dfrac{\pi \exp[5/4]}{\sqrt{2(k_f w_f)_D}} \dfrac{\Gamma(5/4)}{u^{5/4}} + usC_D}{\left[1 + C_{\phi D} C_D u - \dfrac{C_{\phi D} C_D u^2}{u + 1/\alpha_D}\right]\left[\dfrac{\pi \exp[5/4]}{\sqrt{2(k_f w_f)_D}} \dfrac{\Gamma(5/4)}{u^{5/4}} + \dfrac{s}{u}\right]}$$ ..... (bilinear flow)

3.5 Time-Dependent Wellbore Storage and Skin Effects

The validation of the proposed (early-time) time-dependent models for wellbore storage and skin effects is likely to be very challenging, if not impossible to achieve in practice. However, the logical progression of this work is to integrate the combined effects of time-dependent wellbore storage with a time-dependent skin factor. As a simplification, we have chosen only a single example for this evaluation, due to the unlikeliness of a practical application, our goal is a "demonstration" of what such an integrated model could provide. *Specifically, we have chosen to combine the cumulative-exponential time-dependent skin factor model with time-dependent wellbore storage for the case of the linear flow regime.*

To develop this model, we have taken the time-dependent wellbore storage formulation, derived in **Appendix E**, and substituted the time-dependent cumulative-exponential skin model. We recall the cumulative-exponential time-dependent skin below.

$$s(t_D) = s_\infty + [s_0 - s_\infty][1 - \exp[-(\tau / t_D)^\lambda]] \qquad \text{(cumulative-exponential } s(t)\text{)} \qquad (3.11)$$

Returning to the constant pressure time-dependent wellbore storage model, we substitute in a time-dependent skin factor for the constant skin in the original formulation, as shown by Eq. 3.24.

$$\bar{q}_{D,cp}(u) = \frac{1}{u^2} \frac{1 + u^2 C_D \sqrt{\pi} \dfrac{\Gamma(3/2)}{u^{3/2}} + usC_D}{\left[1 + C_{\phi D} C_D u - \dfrac{C_{\phi D} C_D u^2}{u + 1/\alpha_D}\right]\left[\sqrt{\pi} \dfrac{\Gamma(3/2)}{u^{3/2}} + \dfrac{s}{u}\right]} \qquad (3.24)$$

Substituting in Eq. 3.11 into Eq. 3.24 yields a constant pressure (rate) model with time-dependent wellbore storage and cumulative-exponential skin effects, as shown below:

$$\bar{q}_{D,cr}(u) = \frac{1}{u^2} \frac{1 + u^2 C_D \sqrt{\pi} \dfrac{\Gamma(3/2)}{u^{3/2}} + u[s_\infty + [s_0 - s_\infty][1 - \exp[-(\tau / t_D)^\lambda] C_D}{\left[1 + C_{\phi D} C_D u - \dfrac{C_{\phi D} C_D u^2}{u + 1/\alpha_D}\right]\left[\sqrt{\pi} \dfrac{(3/2)}{u^{3/2}} + \dfrac{[s_\infty + [s_0 - s_\infty][1 - \exp[-(\tau / t_D)^\lambda]]}{u}\right]}, \qquad (3.25)$$

which is the full constant pressure (rate) solution inclusive of time-dependent wellbore storage and the cumulative-exponential skin factor.

CHAPTER IV

SOLUTIONS AND RESULTS

In this section, we demonstrate the viability of this work through numerous illustrations of the proposed models, with plots chosen to represent significant features from each model. Variations in each parameter for all time-dependent wellbore storage or skin factor models, for each flow relation are documented in **Appendix F** of this thesis.

4.1 Power-Law Flow Relation

The power-law flow regime proposed in Chapter 3 is a generalized relation that allows for any "power-law" flow regime, theoretical or observed, to be represented during "early-time" performance. We have chosen an arbitrary flow relation where the flowrate is proportional to the 3/4 root time (*i.e.,* 3:4 slope) in order to illustrate the applicability of our time-dependent model. In future sections we evaluate the classical linear and bilinear flow models (1/2 and 1/4 root time models, respectively). The generalized power-law flow relation is displayed below for reference:

$$p_{D,cr}(t_D) = c_1 t_D{}^{\nu}, \quad \text{.....(4.1)}$$

Where c_1 represents an arbitrary constant for a given system (*i.e.,* fracture conductivity), and ν may represent any positive value less than one describing a flow regime (*i.e.,* linear flow (1/2 root time) or bilinear flow (1/4 root time)). The following sections examine the time-dependent models using the generalized power-law flow relation (recall that we have selected 3/4 root time as our general case).

4.2 Power-Law Flow Relation with Cumulative-Exponential Time-Dependent Skin Effects

The cumulative-exponential time-dependent skin effect is proposed based on empirical observations of reservoir performance for ultra-low permeability reservoirs. In **Appendix D** we provide the derivation of the constant pressure solution in the Laplace domain for the case of the cumulative-exponential, time-dependent skin effect model applied to the power-law flow regime.

Certain unique trends have been observed in flowrate data taken from field operations. In order to validate the applicability of our model, we need to demonstrate that our model(s) exhibits the features observed in the field — and while we do not have a practical diagnostic approach, we can vary each parameter within the model to generate possible field scenarios. The range of each parameter is defined by either mathematical or field limitations (*e.g.*, skin values will be limited to cases observed in practice, and/or from physical limitations (*e.g.*, skin factors for fractured wells should not be negative)).

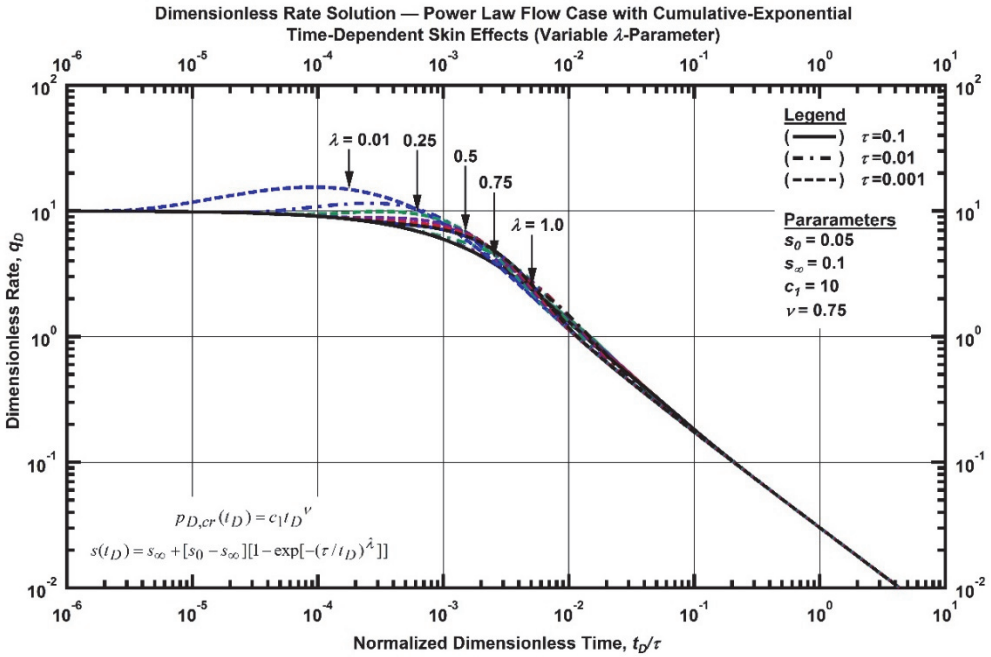

Figure 4.1 —Log-log plot (constant pressure dimensionless rate solution) for the power-law flow model combined with the cumulative-exponential time-dependent skin factor model for select values of the λ-parameter.

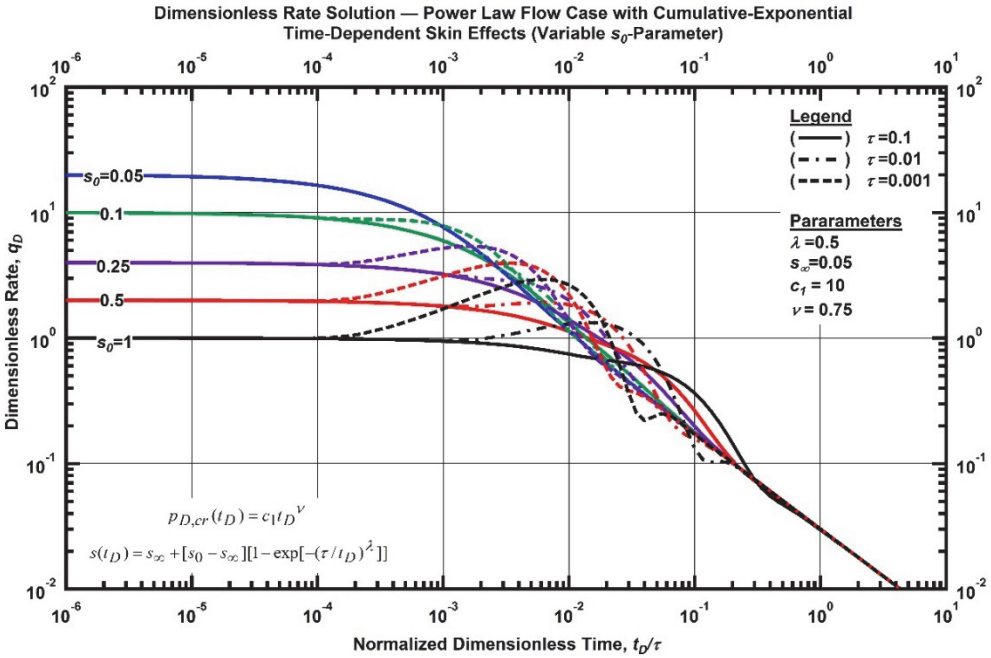

Figure 4.2 —Log-log plot (constant pressure dimensionless rate solution) for the power-law flow model combined with the cumulative-exponential time-dependent skin factor model for select values of the s_0-parameter.

As shown in **Fig. 4.1,** the λ-parameter imposes little impact on the dimensionless flowrate, except for the potential for a slight increase during the transition between early-time and late-time power-law flow. In this application, the λ-parameter is bounded between zero and one. In **Fig. 4.2** we observe that the s_0-parameter affects the initial flowrate — the higher the value of the s_0 -parameter (a proxy for the maximum skin available to the system), the lower the initial flowrate. The minimum skin factor for a given case is established through the s_∞-parameter as shown in **Fig. 4.3**. The greater the difference between the s_0-and s_∞-parameters, the larger the rate "hump" observed during the transition to late-time. Validation of this model is achieved as the s_∞- and s_0-parameters approach zero — *i.e.,* the time-dependent skin effects become negligible which yields the power-law flow regime.

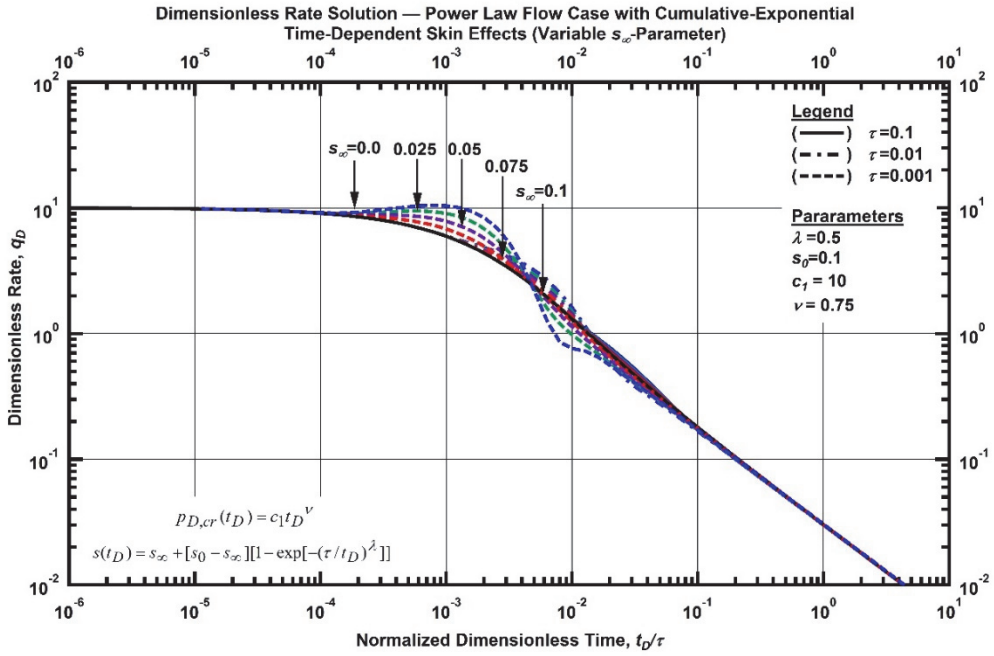

Figure 4.3 —Log-log plot (constant pressure dimensionless rate solution) for the power-law flow model combined with the cumulative-exponential time-dependent skin factor model for select values of the s_∞-parameter.

As shown in **Fig. 4.4**, the c_1-parameter illustrates flow transitions from early-time distorted flow behavior to late-time power-law flow behavior. We note that the higher the value of the c_1-parameter, the earlier that late-time flow behavior occurs. As the power-law flow regime is a generalization for all potential flow regimes, the c_1-paramter may be correlated to other constants such as (inverse) fracture conductivity seen in bilinear flow. This similarity will be demonstrated in future sections.

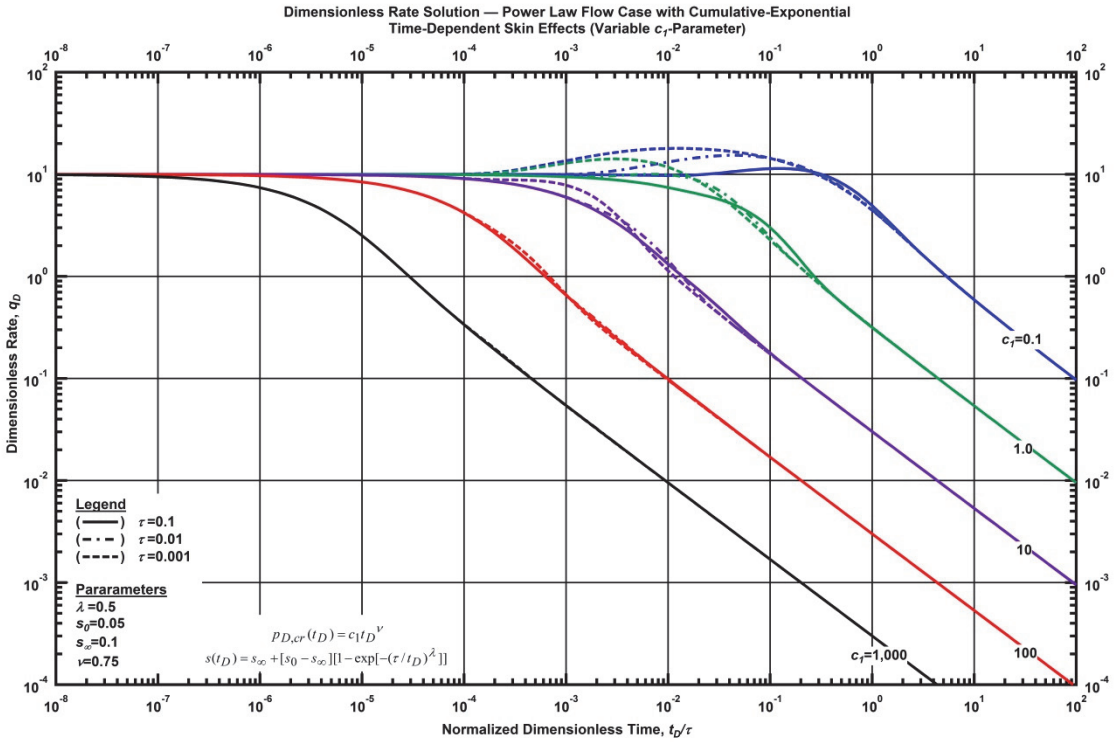

Figure 4.4 — Log-log plot (constant pressure dimensionless rate solution) for the power-law flow model combined with the cumulative-exponential time-dependent skin factor model for select values of the c_1-parameter.

Variations in the ν-parameter are shown in **Fig. 4.5** and we note that the ν-parameter is a proxy for the system flow regime. We observe variations in the late-time slope with all flowrates crossing at approximately the same coordinate. As we will demonstrate with the constant rate solution (in the next section), this inflection point is based on the mathematics of the power-law flow relation.

As shown in the previous examples (**Fig. 4.1** -**Fig. 4.5**) a time-dependent skin factor function is used to represent rate features observed from field data — including the "hockey-stick" shape, where the dimensionless flowrate shows an flat or gently increasing (derivative is positive) rate at early-times, followed by a rollover (*i.e.,* transition) feature, which is then followed by a decline into a late-time flow regime, in this case we have specified the 3/4 root time relation.

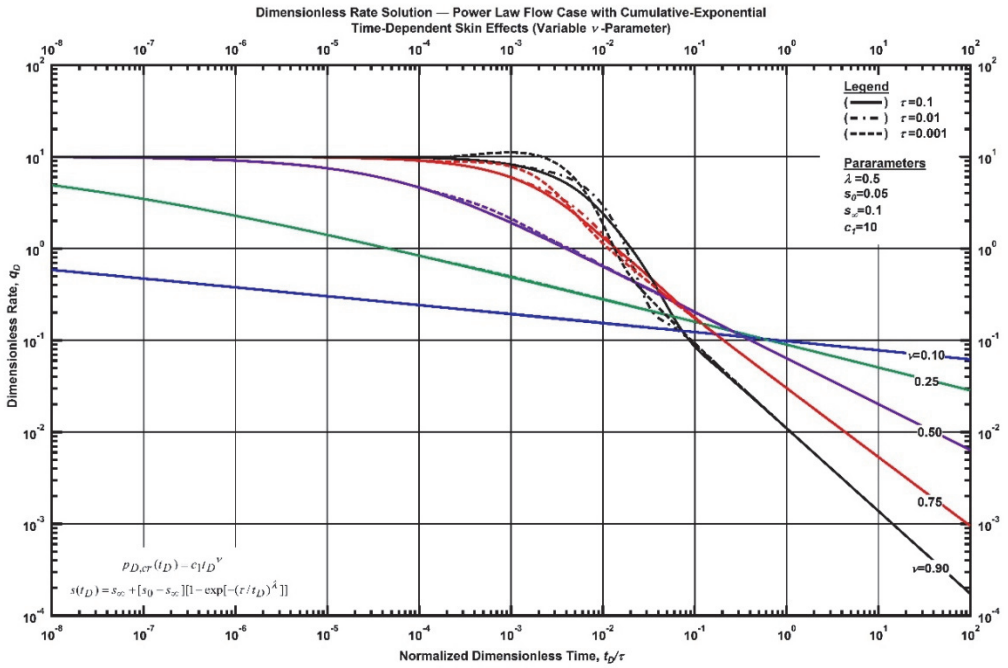

Figure 4.5 — Log-log plot (constant pressure dimensionless rate solution) for the power-law flow model combined with the cumulative-exponential time-dependent skin factor model for select values of the ν-parameter.

Supplementing the constant pressure solution, we have provided additional diagnostic material to support the validation of this time-dependent model — specifically, we provide examples of the rate derivative, the cumulative production, and the time-normalized cumulative production performance. Not all parameters will be evaluated in this section, however, all combinations and permutations of parameters may be found in **Appendix F**.

The flowrate derivative plot has significant diagnostic potential in its ability to enhance subtle changes in flowrate performance for qualitative behavioral (and eventually qualitative) evaluation. As shown in **Fig. 4.6,** the rate increase exhibited by the s_0-parameter results in the rate derivative approaching zero. Our time-dependent skin effect assumes, within limiting boundaries, that the skin factor will decrease for a period of time due to cleanup effects, increasing the fluid flowrate. The greater the difference between the s_0- and s_∞-parameter, the greater potential for clean-up; therefore, the greater the potential flowrate increase.

The rate derivative for the various cases of the s_∞-parameter are shown in **Fig. 4.7**. This performance highlights the small rate increase exhibited within the dimensionless flowrate (which is also plotted). However, the unique "double hump" shown in the derivative has potential for diagnostic capabilities. This author notes, that unless otherwise states, the τ-parameter always maintains a value of 0.01 for all presented examples.

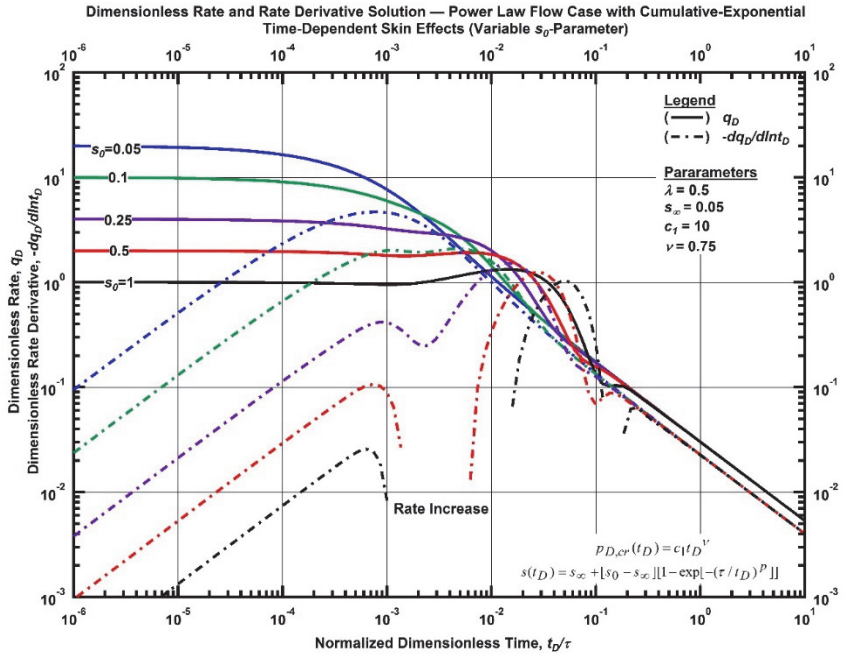

Figure 4.6 —Log-log plot (constant pressure dimensionless rate derivative solution) for the power-law flow model combined with the cumulative-exponential time-dependent skin factor model for select values of the s_0-parameter.

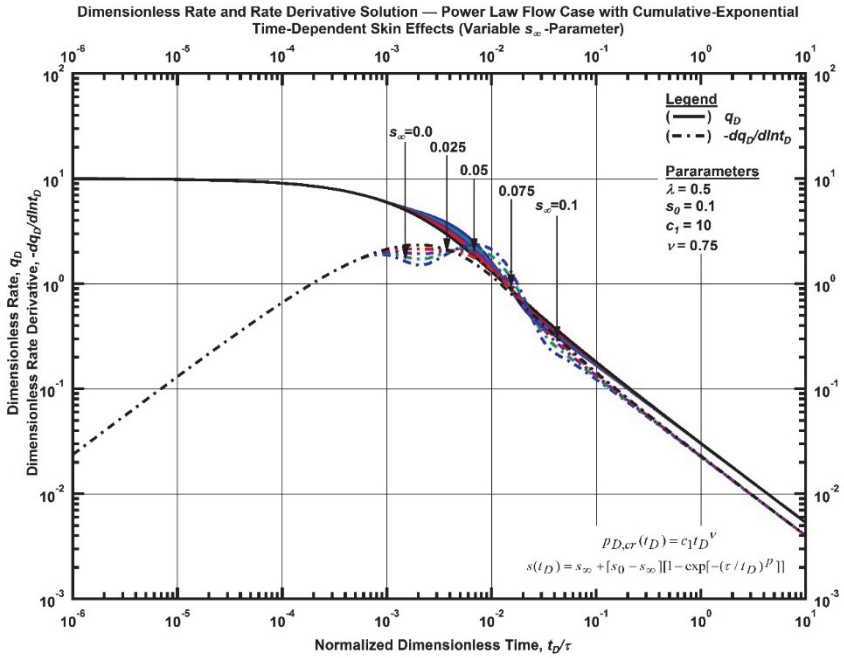

Figure 4.7 —Log-log plot (constant pressure dimensionless rate derivative solution) for the power-law flow model combined with the cumulative-exponential time-dependent skin factor model for select values of the s_∞-parameter.

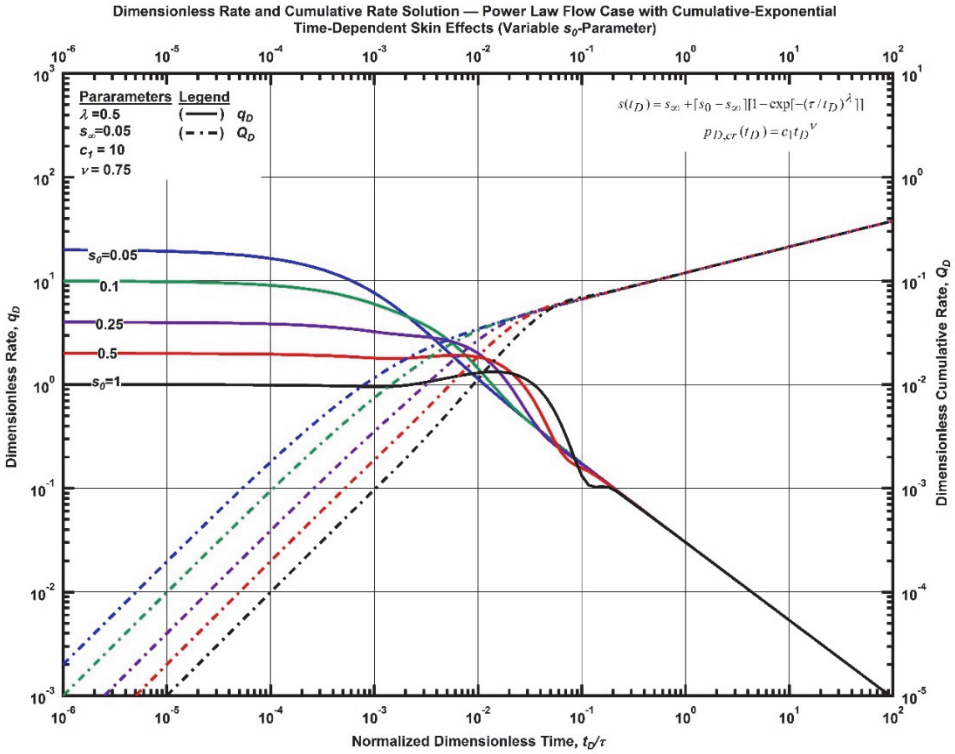

Figure 4.8 —Log-log plot (constant pressure dimensionless cumulative production solution) for the power-law flow model combined with the cumulative-exponential time-dependent skin factor model for select values of the s_0-parameter.

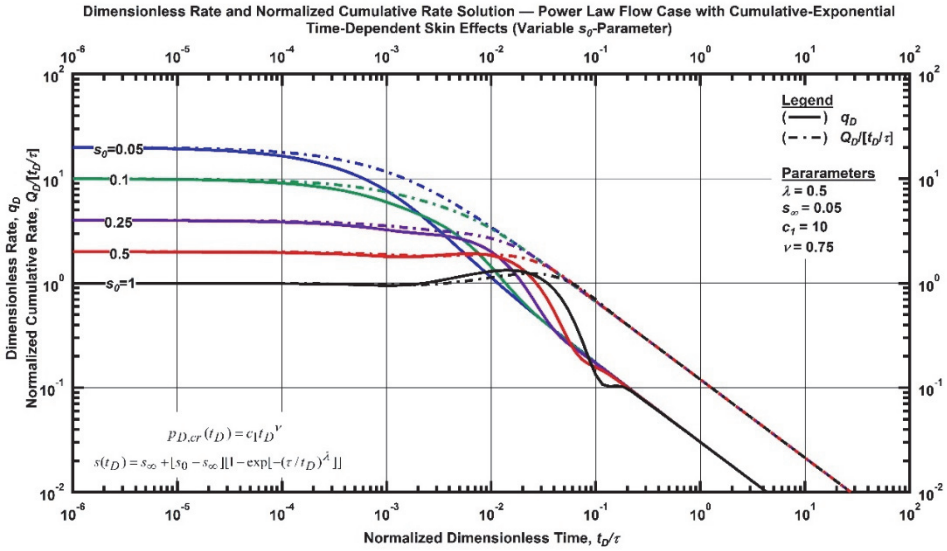

Figure 4.9 —Log-log plot (constant pressure time-normalized dimensionless cumulative production solution) for the power-law flow model combined with the cumulative-exponential time-dependent skin factor model for select values of the s_0-parameter.

In **Fig. 4.8** we introduce the dimensionless cumulative production function and we plot this function with the dimensionless rate function to illustrate the "smooth" nature of the dimensionless cumulative production. In **Fig. 4.9** we present the time-normalized dimensionless cumulative production function and we again plot this function with the dimensionless rate function. We immediately note that the time-normalized dimensionless cumulative production function does not have same "hump" features as in the dimensionless rate function, but this behavior is somewhat expected due to the smoothing inherent in the cumulative production. As a comment, we note that the higher values of the s_0-parameter yields more extreme character in the rate functions. While this work is "theoretical" rather than "practical," we can see from **Figs. 4.6-4.9** that the effect of the time-dependent factor is both unique for some functions, and less so for others, but taken as a part of a diagnostic workflow, we believe that such "type curves" will help guide understanding of flowback performance in unconventional reservoirs.

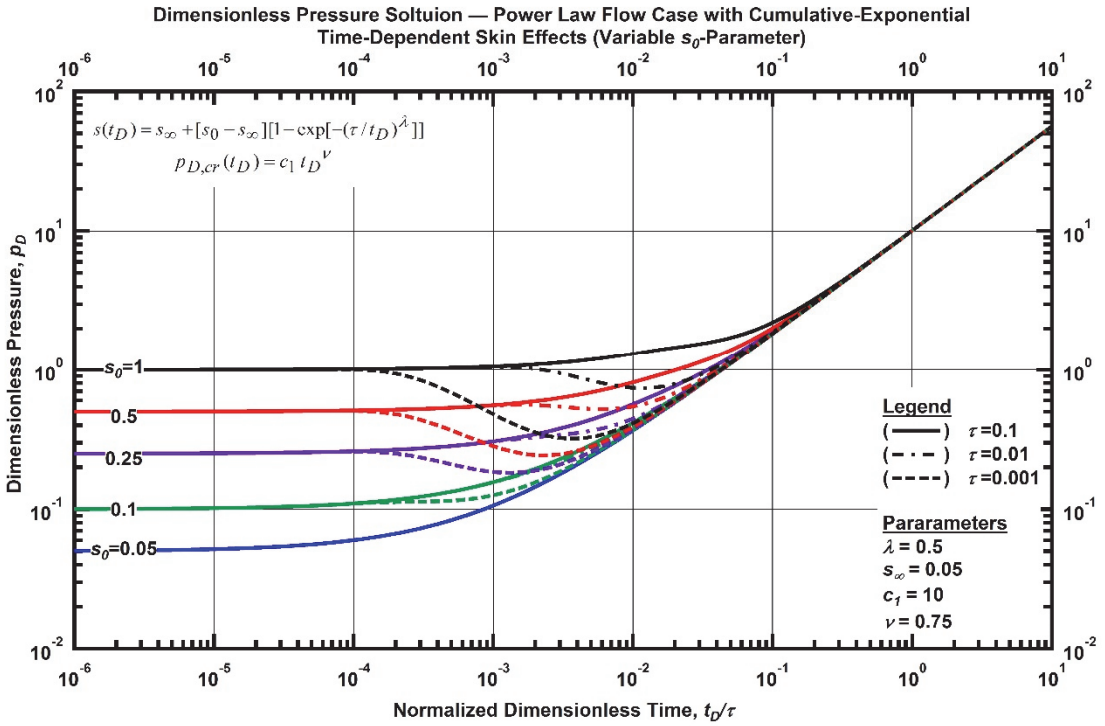

Figure 4.10 — Log-log plot (constant rate dimensionless pressure solution) for the power-law flow model combined with the cumulative-exponential time-dependent skin factor model for select values of the s_0-parameter.

In order to thoroughly examine the behavior of the cumulative-exponential time-dependent skin effect model, we have created additional plots for the constant rate dimensionless pressure and the constant rate

derivative pressure functions for each parameter considered for this model. In some aspects, the diagnostic features are similar to those for the constant pressure solution functions. For reference, an exhaustive evaluation of all parameters considered for the cumulative-exponential time-dependent skin effects model coupled with the generalized power-law flow regime can be found in **Appendix F**.

As shown in **Fig. 4.10**, the constant rate dimensionless pressure solution is a sort of "mirror image" of the constant pressure solution (trends increase to the right, as opposed to decreasing). In this particular case we are varying the ν-parameter (ν = 0.1, 0.25, 0.5, 0.75, and 0.9), and the skin factor parameters (s_0 and s_∞) are constant. The s_∞-parameter (s_∞ = 0.1) controls the performance at early times (several cases are constant at $p_D(t_D)$ = 0.1 until the power-law portion of the solution dominates).

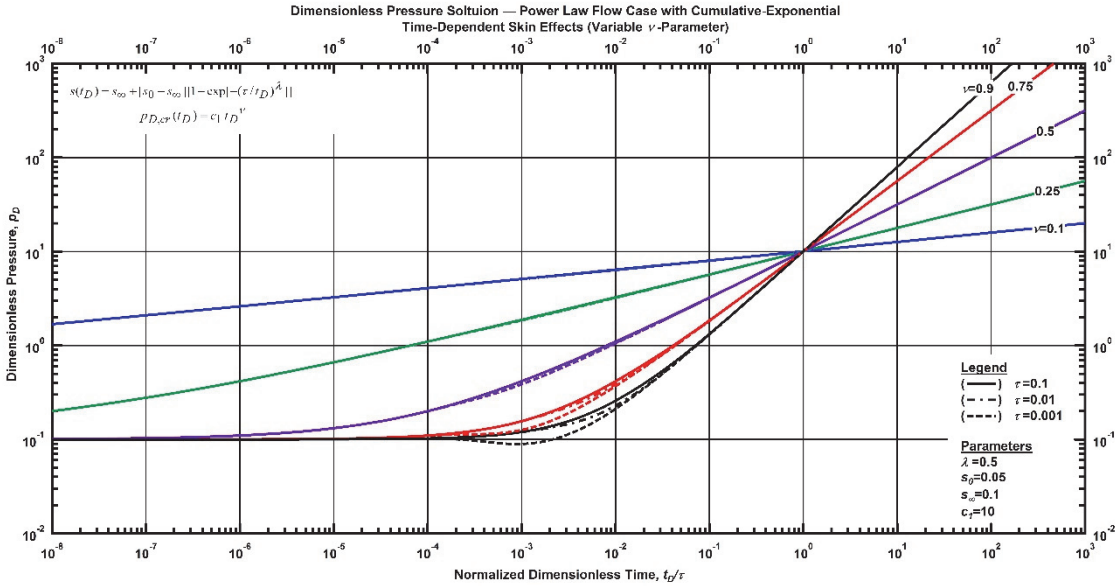

Figure 4.11 — Log-log plot (constant rate dimensionless pressure solution) for the power-law flow model combined with the cumulative-exponential time-dependent skin factor model for select values of the ν-parameter.

We observe an inflection point, shown in **Fig. 4.11,** as the ν-parameter is varied. The power-law flow regime formulation states that when the dimensionless time is one, all flow regimes will intersect at a pressure influenced notably by the c_1-parameter, which is this point of intersection (*i.e.,* c_1 = 10).

In summary, the behavior of the cumulative-exponential time-dependent skin effect model appears to be unique and relevant for representing the behavior of early-time rate "flowback" (see **Fig. 4.2 -Fig. 4.11**). In a practical sense, there appears to be significant potential in the diagnostic capabilities of the

cumulative-exponential time-dependent skin effects model, where the rate and pressure performance functions include: the dimensionless rate, the dimensionless rate derivative, the dimensionless cumulative production, time-normalized dimensionless cumulative production, dimensionless pressure, and dimensionless pressure derivative functions.

4.3 Power-Law Flow Relation with Exponential Time-Dependent Skin Effects

The exponential time-dependent skin effect model is proposed as a "more simple" alternative to the cumulative-exponential time-dependent skin effect model. In **Appendix D** we provide the derivation of the constant pressure solution in the Laplace domain for the exponential time-dependent skin effect model couple with the model for the generalized power law flow regime.

The exponential time-dependent skin effect model is very similar in function to the cumulative-exponential skin effects model. As we examine each parameter for the exponential time-dependent skin model, provide comparison to the previous function and provide evidence as to the validity of our time-dependent relation as a diagnostic tool for observed features from field data.

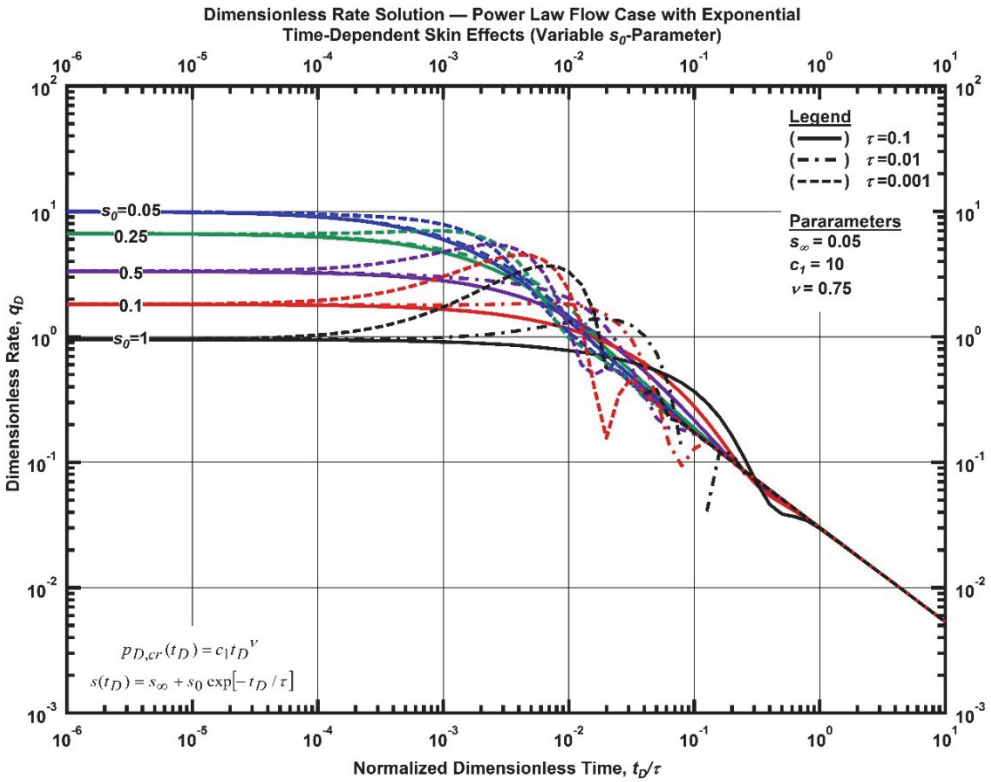

Figure 4.12 — Log-log plot (constant pressure dimensionless rate solution) for the power-law flow model combined with the exponential time-dependent skin factor model for select values of the s_0-parameter.

In **Fig. 4.12** we note the effect of the s_0-parameter on the dimensionless rate trends, where these values were chosen to represent a range of skin factor values expected to be observed in practice. We do note a bit of instability in the $\tau = 0.001$ cases, and as comment, we did try to address this with higher precision specifications in the Gaver-Stehfest algorithm, but these instabilities remain. Examining the rate derivative solution shown in **Fig. 4.13**, we note (as expected) that the "rate hump" causes an negative rate derivative function (recall that the derivative is make negative because we assume a declining flowrate function, if the rate increase, the definition of the rate derivative becomes negative. Regardless, we can comment that the dimensionless rate derivative function has more "character" than the dimensionless rate function, and that this observed character could be useful as a "diagnostic" function.

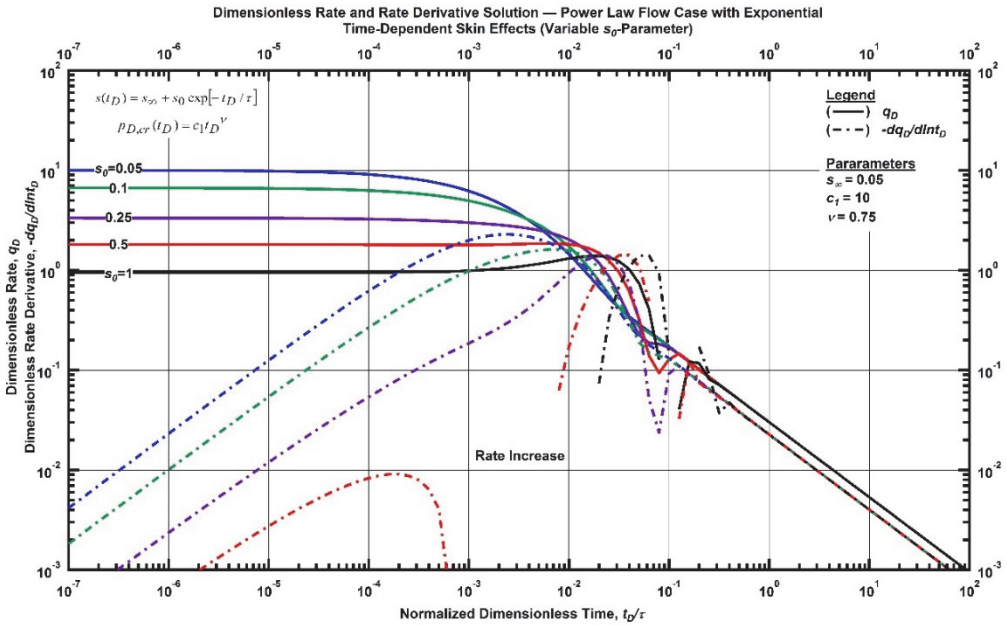

Figure 4.13 — Log-log plot (constant pressure dimensionless rate derivative solution) for the power-law flow model combined with the exponential time-dependent skin factor model for select values of the s_0-parameter.

In **Fig. 4.14** we observe the influence of the s_∞-parameter, in particular, on the initial flowrate. We again observe a stability issue with regard to the cases where $\tau = 0.001$, and we again note that these instabilities could not be resolved in a computational sense. The behavior of the dimensionless rate functions shown in **Fig. 4.14** do resemble expected performance in the field, and due to the relative simplicity of this skin factor model, this case may be preferred for diagnostics in practice.

In **Fig. 4.15** we observe the influence of the c_1-parameter, and again we note the instabilities for the $\tau =$ 0.001 cases. The influence of the c_1-parameter is essentially just a "displacement" in time of the various

trend functions. We note, that for very large values of the c_1-parameter (a possible proxy for inverse fracture conductivity) the time-dependent choked fracture skin has essentially no impact on the dimensionless flowrate function.

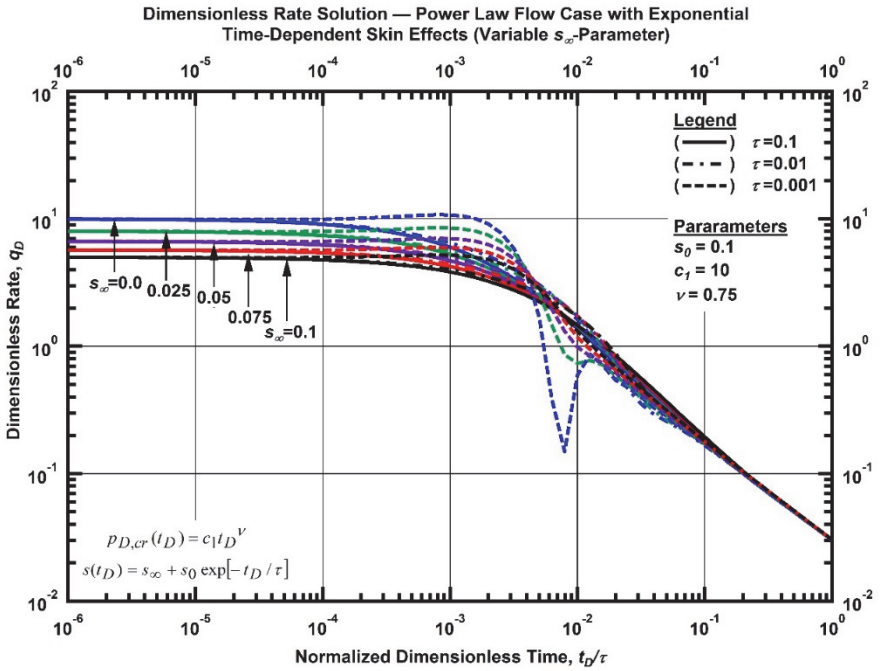

Figure 4.14 — Log-log plot (constant pressure dimensionless rate solution) for the power-law flow model combined with the exponential time-dependent skin factor model for select values of the s_∞-parameter.

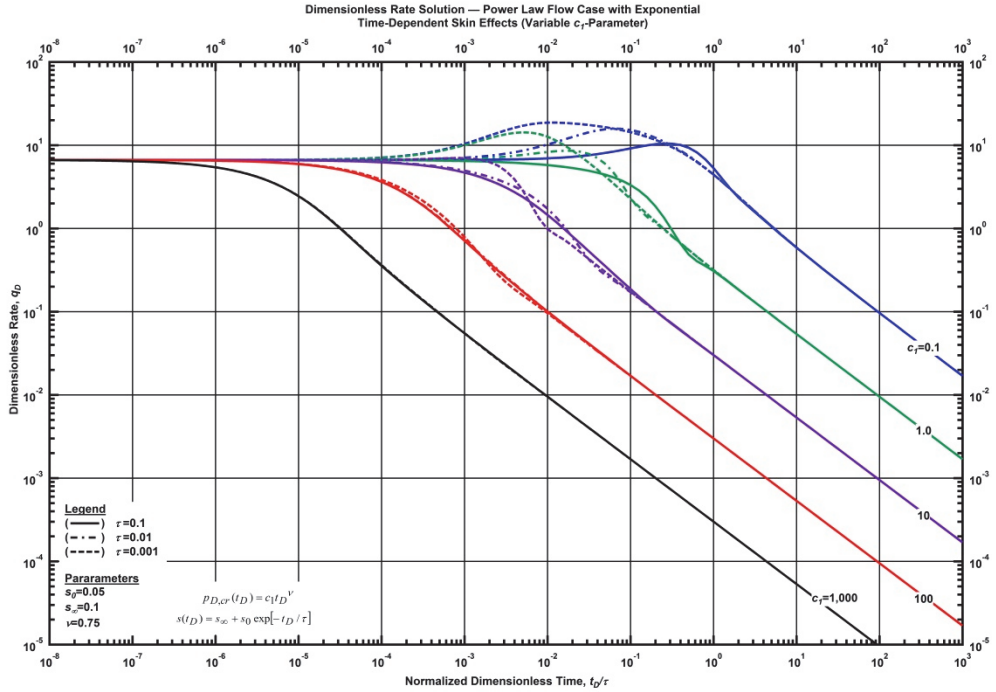

Figure 4.15 — Log-log plot (constant pressure dimensionless rate solution) for the power-law flow model combined with the exponential time-dependent skin factor model for select values of the c_1-parameter.

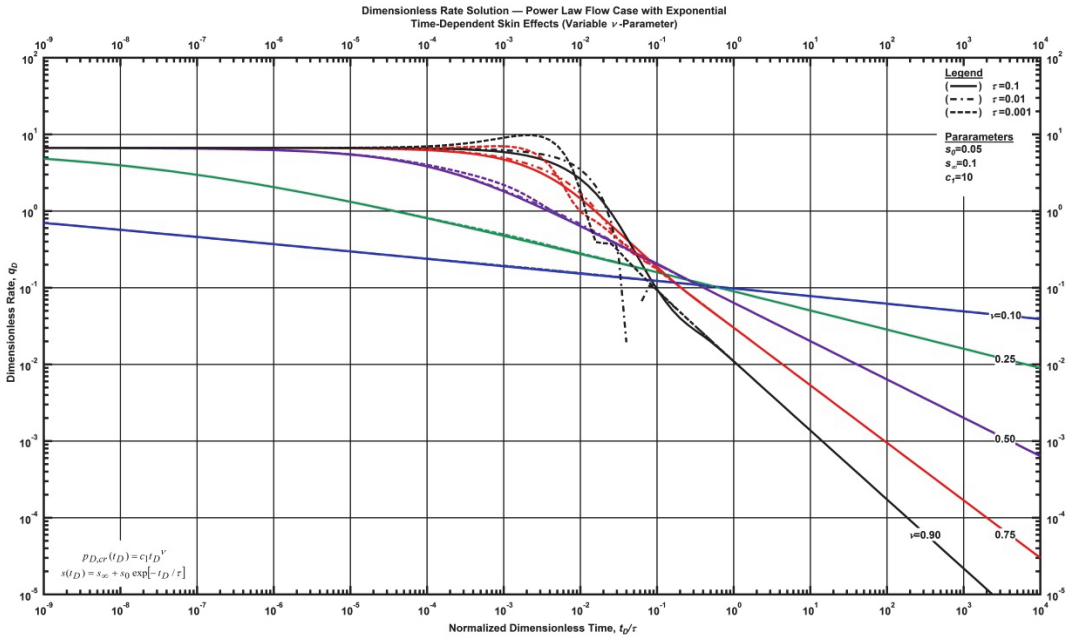

Figure 4.16 — Log-log plot (constant pressure dimensionless rate solution) for the power-law flow model combined with the exponential time-dependent skin factor model for select values of the ν-parameter.

As shown in **Fig. 4.16**, the influence of the ν-parameter is observe, and we can comment that the lowest values of the ν-parameter are the least affected by the prescribed exponential time-dependent skin factor model. This is likely due to the fact that the lower ν-parameter cases represent a lesser decline in time and hence are less affected by the skin factor.

As has been demonstrated in the previous example (**Fig. 4.12** — **Fig. 4.16**), a second time dependent skin factor is used to represent rate features from field data. Features are very similar to those of the cumulative-exponential time-dependent skin effect — including the desired "hockey-stick" profile, a rollover (*i.e.,* transition) feature dissipating into late-time reservoir characteristic power-law flow. Early-time behavior is generally flat or gently increasing, with a potential for a flowrate increase during the transition period as the time-dependent skin effects are imposed on the system.

A number of additional diagnostic plots have been included to validate the exponential time-dependent skin factor for implementation in field data. All available plots may be found in **Appendix F**.

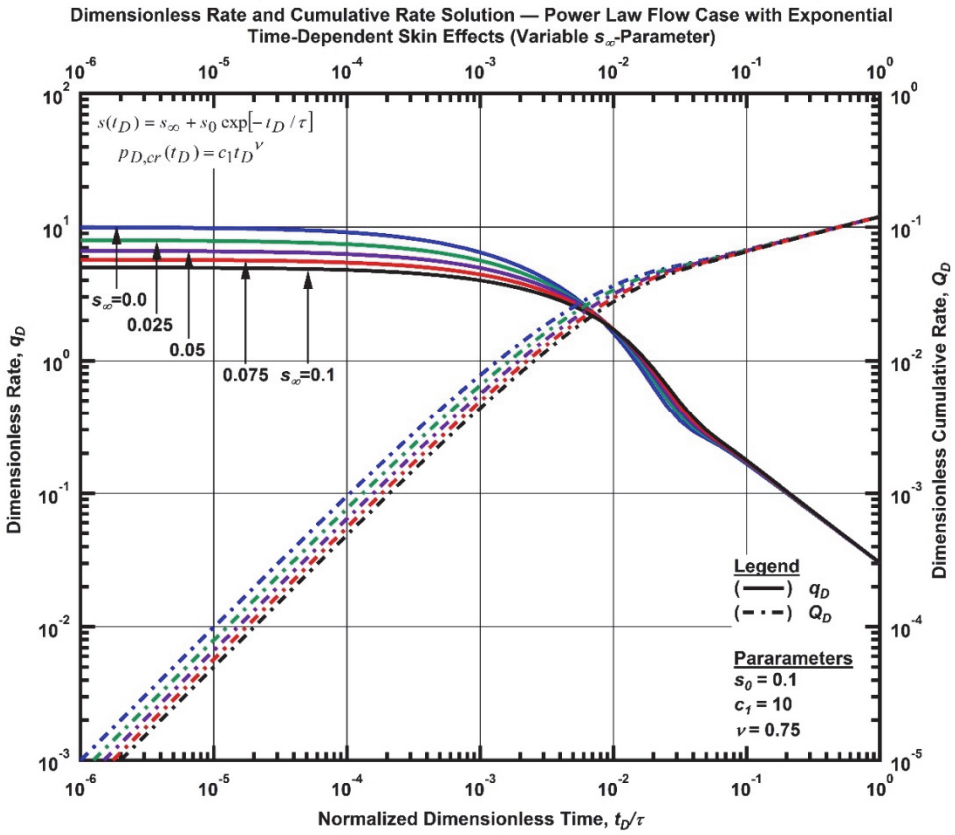

Figure 4.17 — Log-log plot (constant pressure dimensionless cumulative production solution) for the power-law flow model combined with the exponential time-dependent skin factor model for select values of the s_∞-parameter.

As shown in **Fig. 4.17** and **Fig. 4.18** the dimensionless cumulative production and time-normalized dimensionless cumulative rate provide further diagnostic measures to evaluate the behavior and performance of early-time transient production of ultra-low permeability reservoirs.

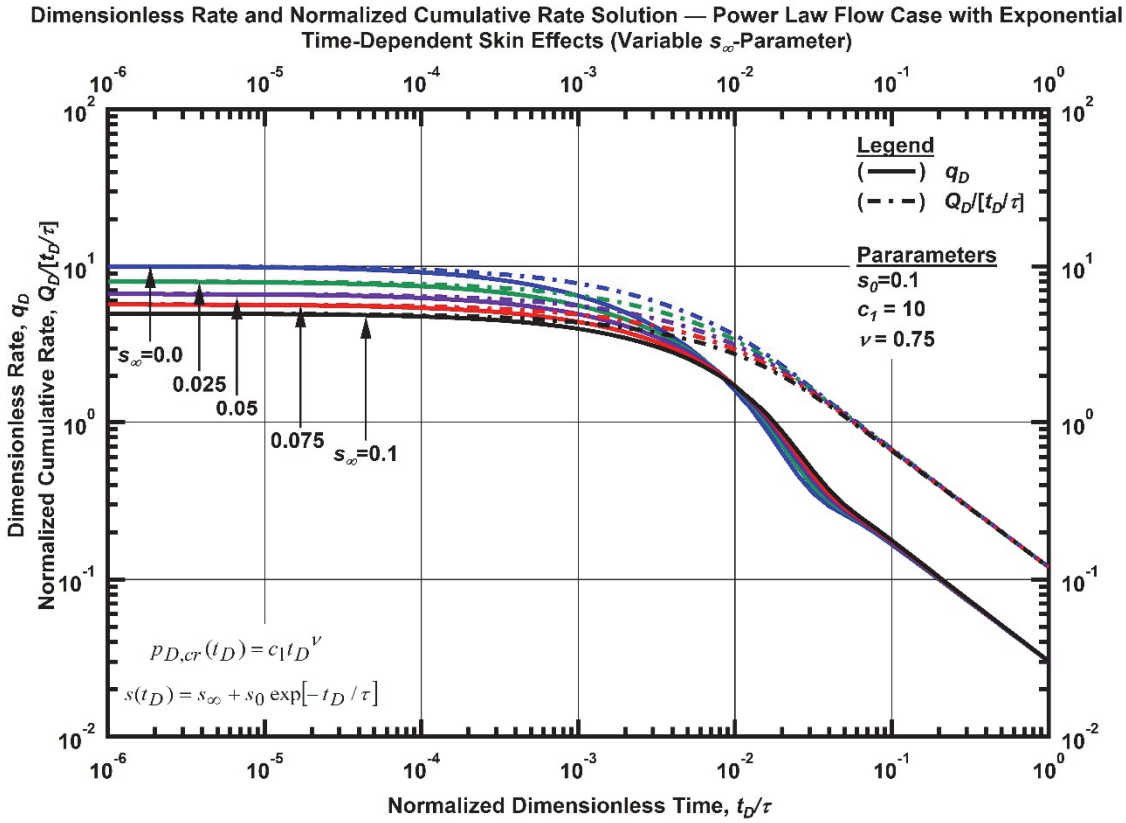

Figure 4.18 —Log-log plot (constant pressure time-normalized dimensionless cumulative rate solution) for the power-law flow model combined with the exponential time-dependent skin factor model for select values of the s_∞-parameter.

Through the evaluation of the exponential time-dependent skin factor with power-law flow regime, some diagnostic capabilities are demonstrated in **Fig. 4.12** through **Fig. 4.18** representing rate features observed in field data. The variety of diagnostic plots available provide additional measures to ensure evaluation of the reservoir performance.

4.4 Power-Law Flow Relation with Hyperbolic Time-Dependent Skin Effects

The hyperbolic time-dependent skin effect is proposed as an alternative model to the cumulative-exponential and exponential time-dependent skin models to further characterize reservoir performance for ultra-low permeability reservoirs. **Appendix D** provides a derivation of the constant pressure solution in the Laplace domain with hyperbolic time-dependent skin effects and the power law flow regime.

Following, we examine the effect of each parameter of the constant pressure solution through a number of diagnostic plots providing support to validate the applicability of the hyperbolic time-dependent skin model for field implementation.

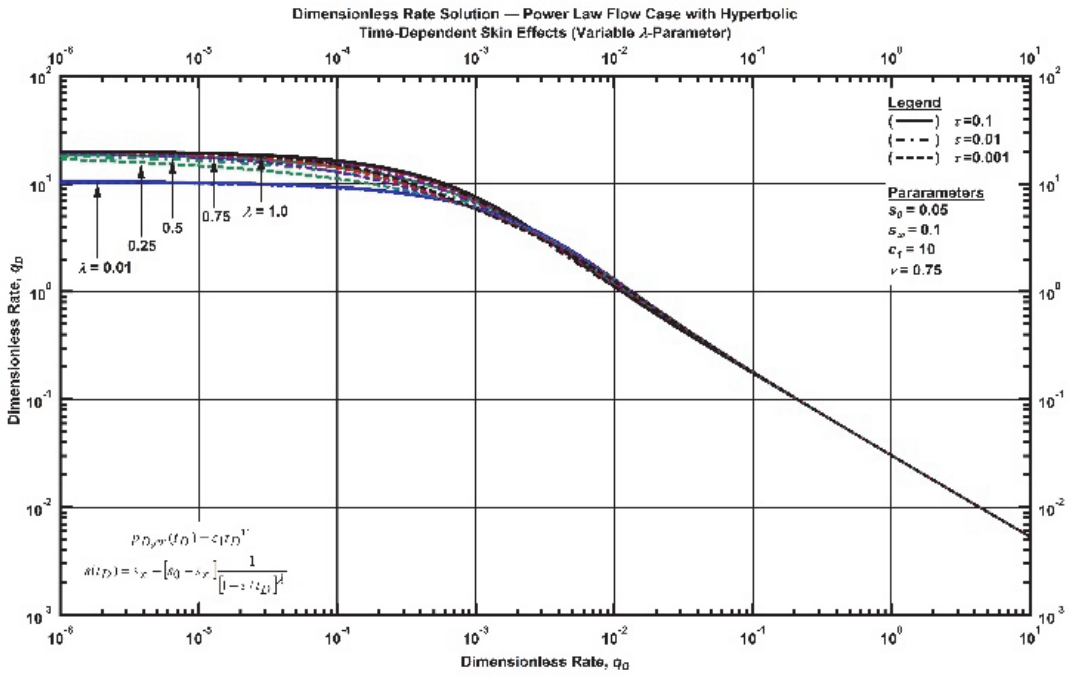

Figure 4.19 — Log-log plot (constant pressure dimensionless rate solution) for the power-law flow model combined with the hyperbolic time-dependent skin factor model for select values of the λ-parameter.

For the limited range considered, the λ-parameter, shown in **Fig. 4.19,** imposes little impact on the constant pressure solution. The derivative, shown in **Fig. 4.20**, has much stronger features than the rate function, and although this may be difficult to assess in practice, its behavior is noted for possible use as a diagnostic characteristic.

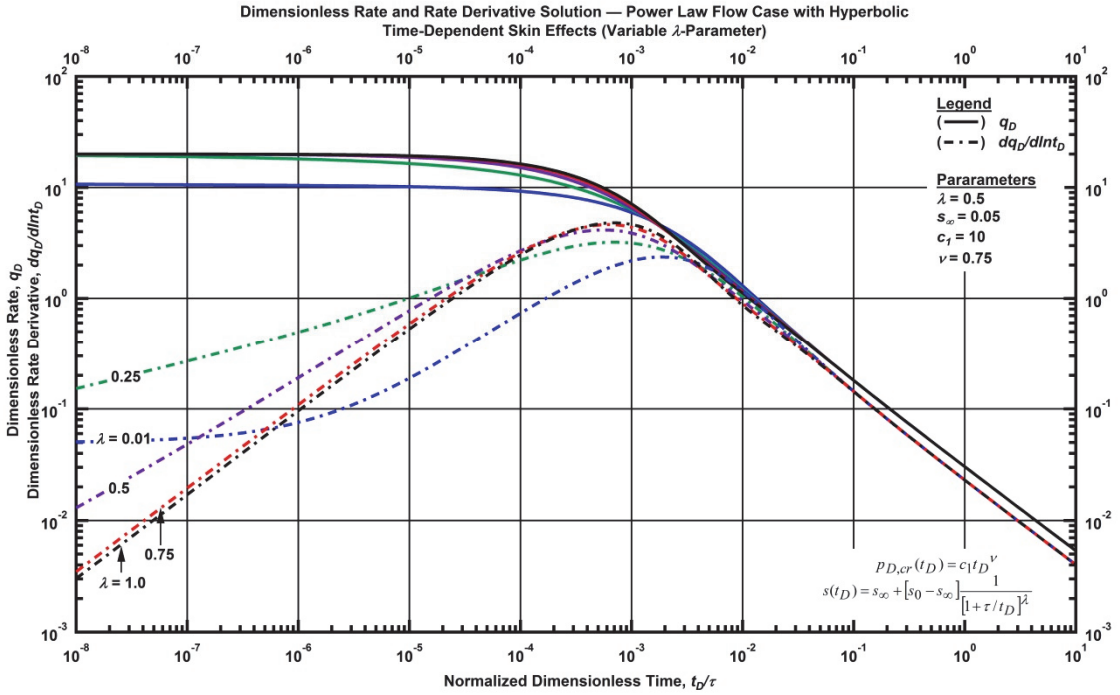

Figure 4.20 — Log-log plot (constant pressure dimensionless rate derivative solution) for the power-law flow model combined with the hyperbolic time-dependent skin factor model for select values of the λ-parameter ($\tau = 0.01$).

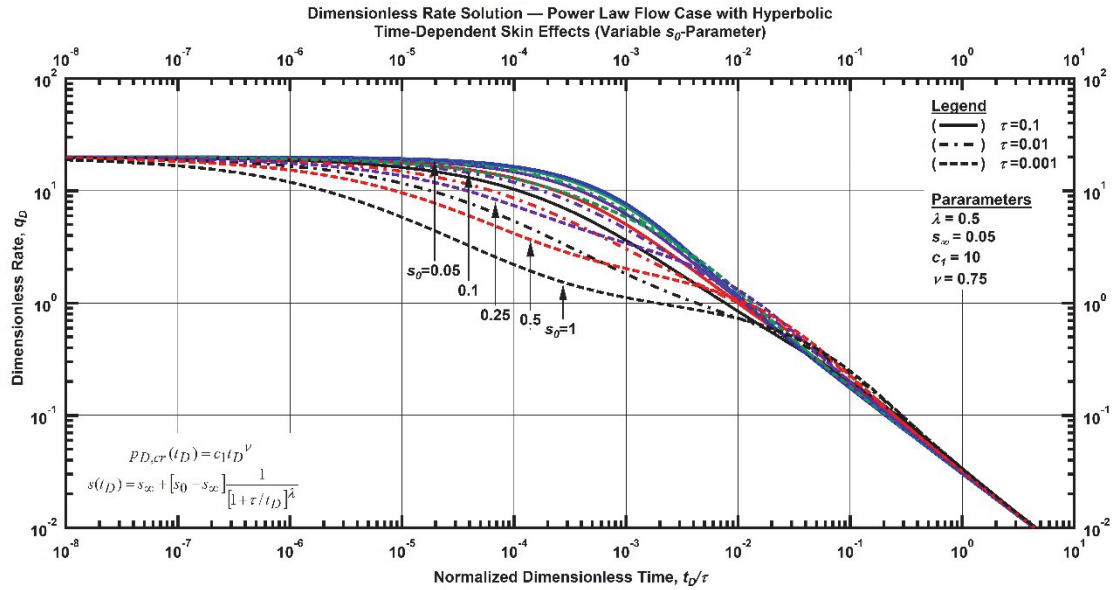

Figure 4.21 — Log-log plot (constant pressure dimensionless rate solution) for the power-law flow model combined with the hyperbolic time-dependent skin factor model for select values of the s_0-parameter.

As a proxy for the maximum skin of the system, the s_0-parameter, shown in **Fig. 4.21**, impacts the rate at which the system reaches late-time power-law flow. The higher the s_0-parameter, the lower the dimensionless flowrate, and the longer the system required to attain late-time flow. The lower boundary for the skin factor, the s_∞-parameter, shown in **Fig. 4.22**, influences the initial rate of the system. The higher the s_∞-parameter, the lower the initial flowrate. Validation of this model is achieved as the s_∞- and s_0-parameters approach zero — *i.e.,* the time-dependent skin effects become negligible which yield the power law flow regime.

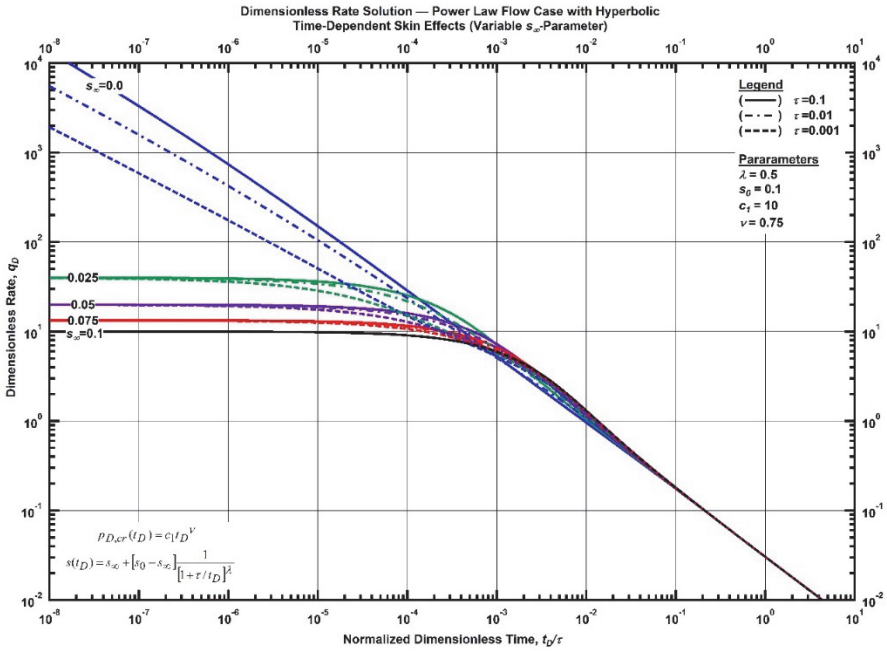

Figure 4.22 — Log-log plot (constant pressure dimensionless rate solution) for the power-law flow model combined with the hyperbolic time-dependent skin factor model for select values of the s_∞-parameter.

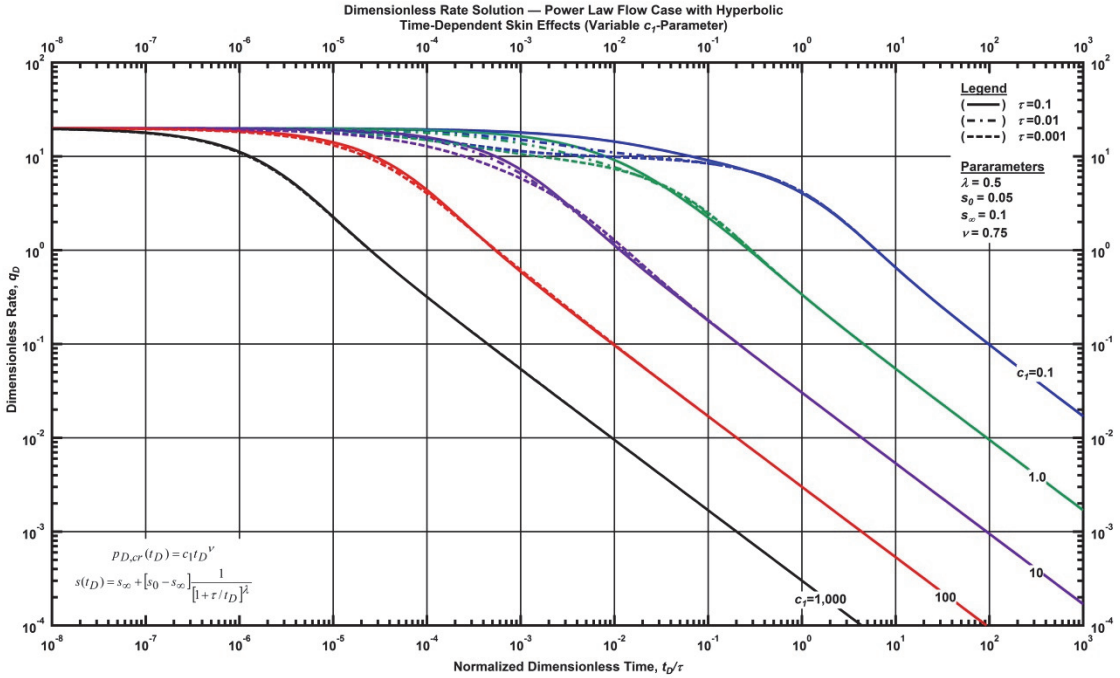

Figure 4.23 — Log-log plot (constant pressure dimensionless rate solution) for the power-law flow model combined with the hyperbolic time-dependent skin factor model for select values of the c_1-parameter.

The c_1-parameter affects the time until transition into late-time flow regimes, as shown in **Fig. 4.23**. This plays a significant role in the cumulative rate of the system, shown in **Fig. 4.24**. The larger the c_1-parameter, the faster late-time flow is reached and the smaller cumulative production achieved. As the power-law flow regime is a generalization for all potential flow relations, the c_1-parameter is a proxy for any parameter appropriate to a particular flow relation (*e.g.,* fracture conductivity for bilinear flow regime).

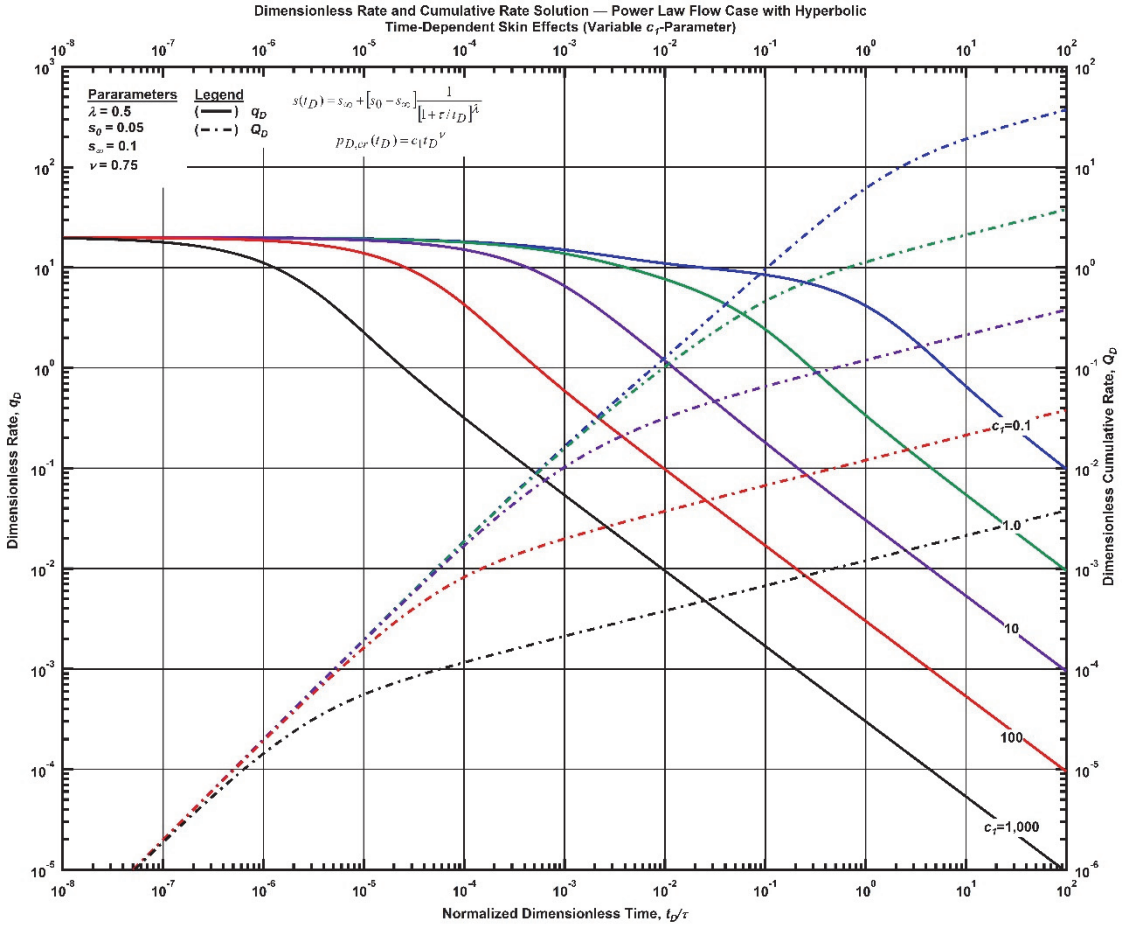

Figure 4.24 — Log-log plot (constant pressure dimensionless cumulative production solution) for the power-law flow model combined with the hyperbolic time-dependent skin factor model for select values of the c_1-parameter ($\tau = 0.01$).

As shown in **Fig. 4.25**, the ν-parameter describes the flow regime of the system. The generalization of the power-law flow relation allows for any observed or theoretical reservoir to be evaluated.

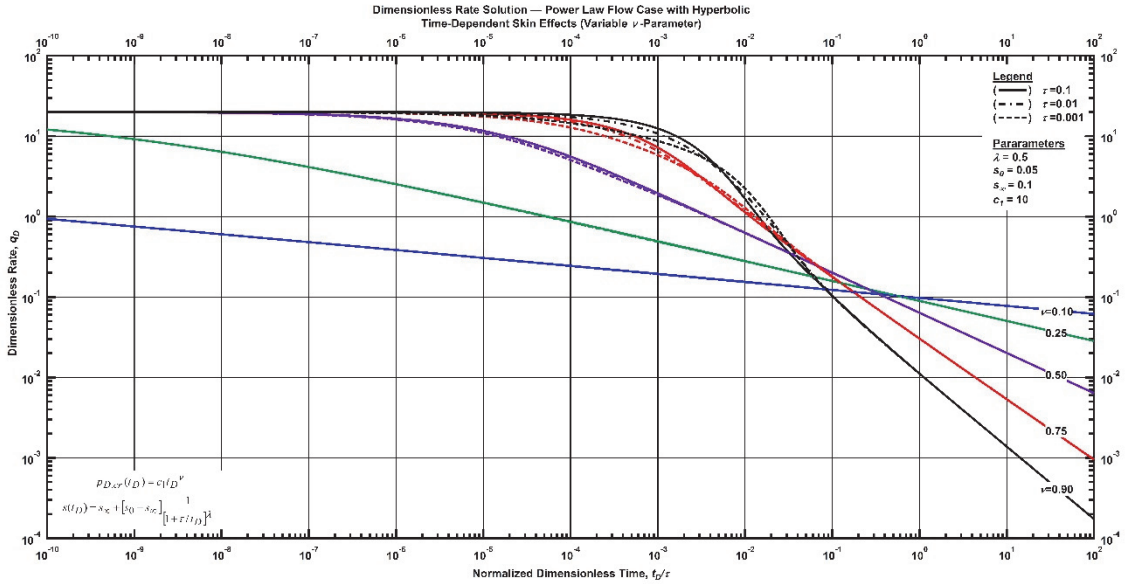

Figure 4.25 — Log-log plot (constant pressure dimensionless rate solution) for the power-law flow model combined with the hyperbolic time-dependent skin factor model for select values of the ν-parameter.

The previous example, evaluating the hyperbolic time-dependent skin effects with the power-law flow model (**Fig. 4.19** — **Fig. 4.25**) represents rate features observed from field data. In a similar fashion as with the cumulative-exponential and exponential time-dependent skin factors, we observe a "hockey-stick" shape, with a rollover (*i.e.,* transition) feature into late-time power-law flow. Unlike the previous two time-dependent skin effect models (cumulative-exponential and exponential) the hyperbolic time-dependent skin factor does not show a rate increase during the transition to late-time flow. Although some of the features may be difficult to resolve in practice, the behavior of the model is noted for possible use to diagnose reservoir behavior.

4.5 Power-Law Flow Relation with Time-Dependent Wellbore Phase Redistribution

Fair (1990) proposed a wellbore phase redistribution pressure based upon empirical data and a single laboratory test to explain anomalous pressure signatures in build-up tests. Incorporation of the phase redistribution pressure profile into the wellbore pressure is fully derived in **Appendix E**. Keeping our diagnostic "procedure" consistent, we examine each parameter within the model and as our method to validate potential application to field data. To assist in diagnostic capabilities, the derivative of the constant pressure solution was also taken and plotted for each parameter. A full evaluation of all plots may be found in **Appendix F**.

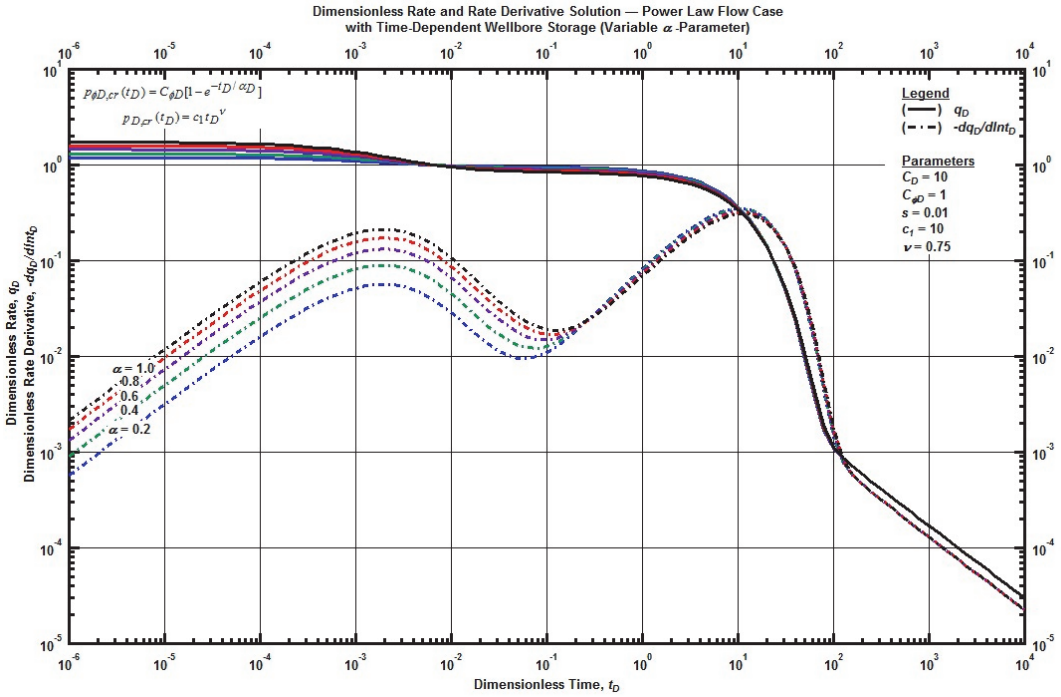

Figure 4.26 — Log-log plot (constant pressure dimensionless rate derivative solution) for the power-law flow model combined with the time-dependent wellbore storage for select values of the α-parameter.

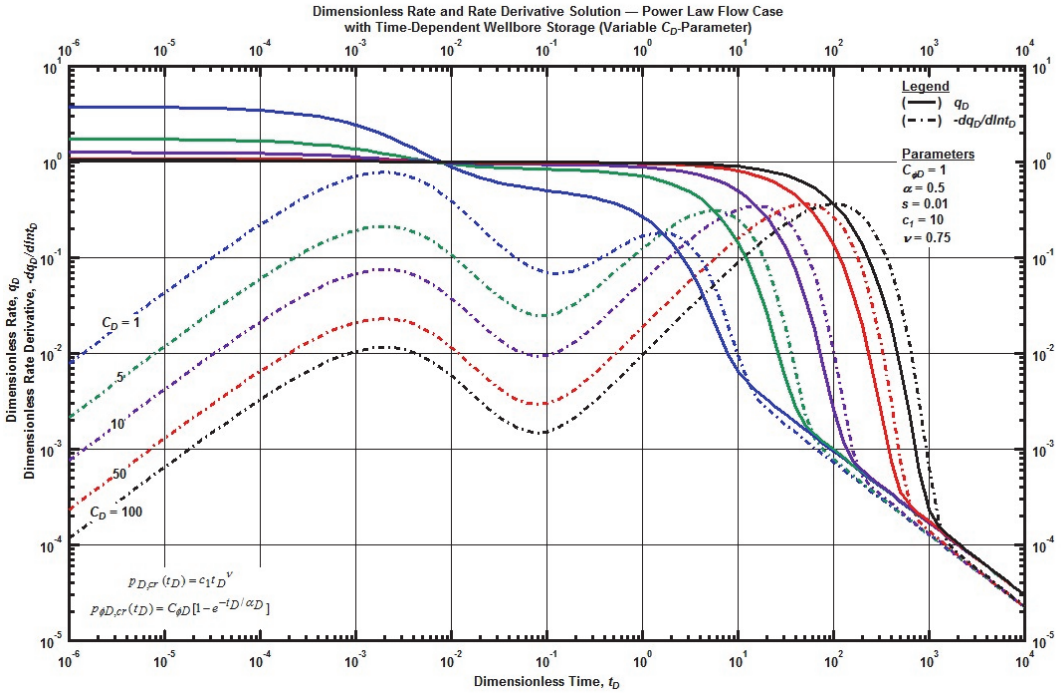

Figure 4.27 — Log-log plot (constant pressure dimensionless rate derivative solution) for the power-law flow model combined with the time-dependent wellbore storage for select values of dimensionless wellbore storage constant.

For the limited range considered, the α-parameter, shown in **Fig. 4.26**, imposes little impact on the constant pressure solution. The derivative has much stronger features than the rate function, and although this function may be difficult to assess in practice, its behavior is noted for possible use as a diagnostic characteristic. The dimensionless wellbore storage constant (C_D), shown in **Fig. 4.27**, provides variations in both early-time behavior and the transition region. As the wellbore storage influence diminishes over time, the rate is governed by the specified power-law flow regime, clearly shown in **Fig. 4.27**.

The dimensionless wellbore phase redistribution constant ($C_{\phi D}$), shown in **Fig. 4.28**, has a similar influence on the solution as the dimensionless wellbore storage constant (C_D), and affects the rate behavior at early-times, merging to yield the power-law flow solution at late-times. The $C_{\phi D}$-parameter yields a consistent shape in the derivative function, displace in time, unlike the C_D-parameter which derivative shape is inconsistent.

The skin factor, as shown in **Fig. 4.29**, imposes little impact on the constant pressure solution. The rate derivative has much stronger features than the rate function as shown by the variation caused by the skin factor. Although the combined effects of skin and wellbore storage may be difficult (or even impossible) to assess in practice, we may be able to develop diagnostic characteristic functions (*i.e.,* derivative ratios, etc.).

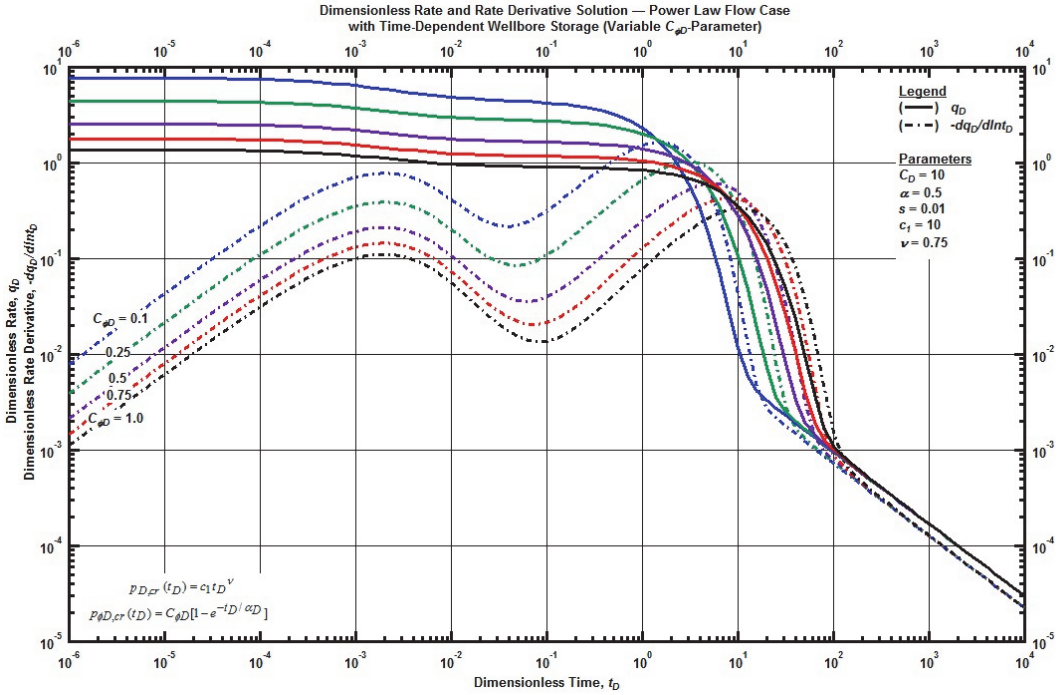

Figure 4.28 — Log-log plot (constant pressure dimensionless rate derivative solution) for the power-law flow model combined with the time-dependent wellbore storage for select values dimensionless phase redistribution constant.

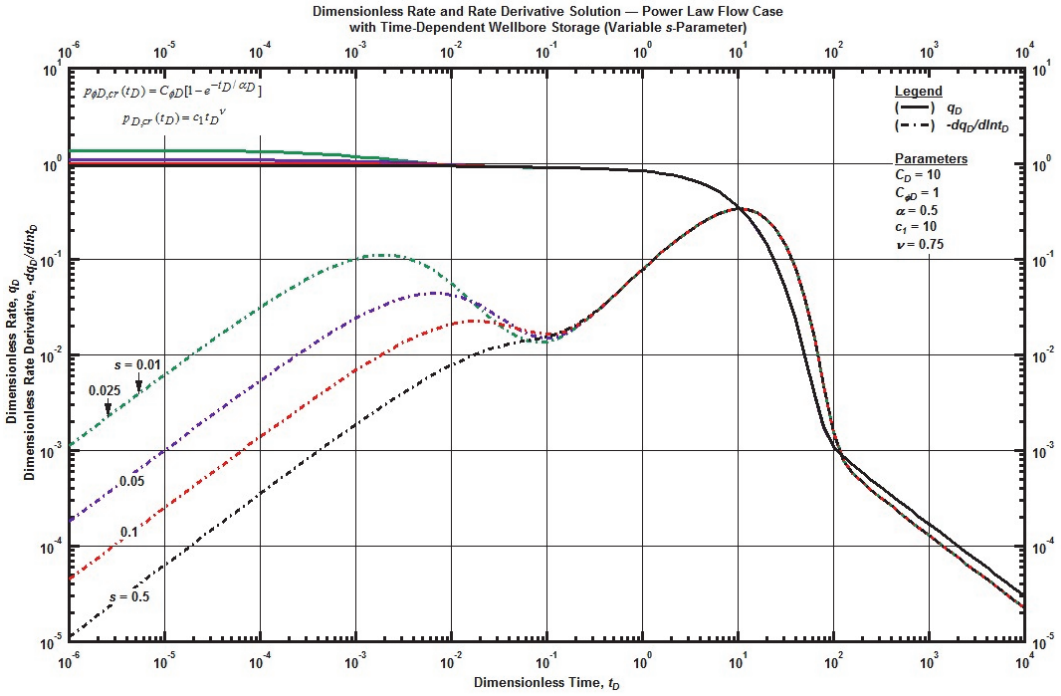

Figure 4.29 — Log-log plot (constant pressure dimensionless rate derivative solution) for the power-law flow model combined with the time-dependent wellbore storage for select values of skin factor.

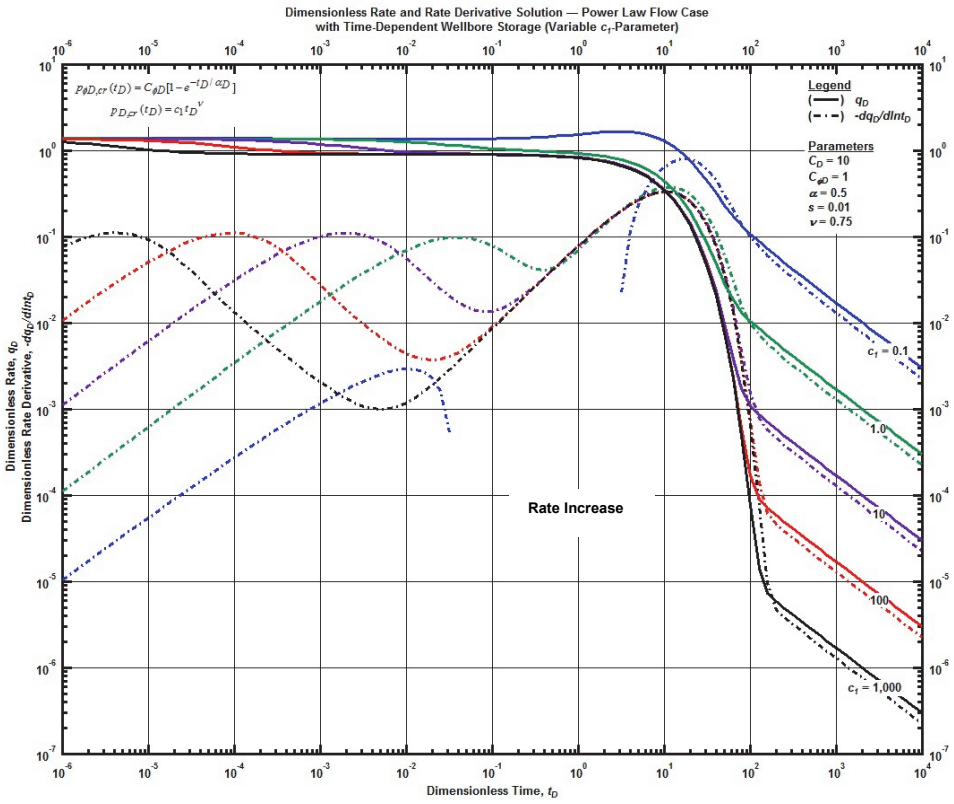

Figure 4.30 — Log-log plot (constant pressure dimensionless rate derivative solution) for the power-law flow model combined with the time-dependent wellbore storage for select values of the c_1-parameter.

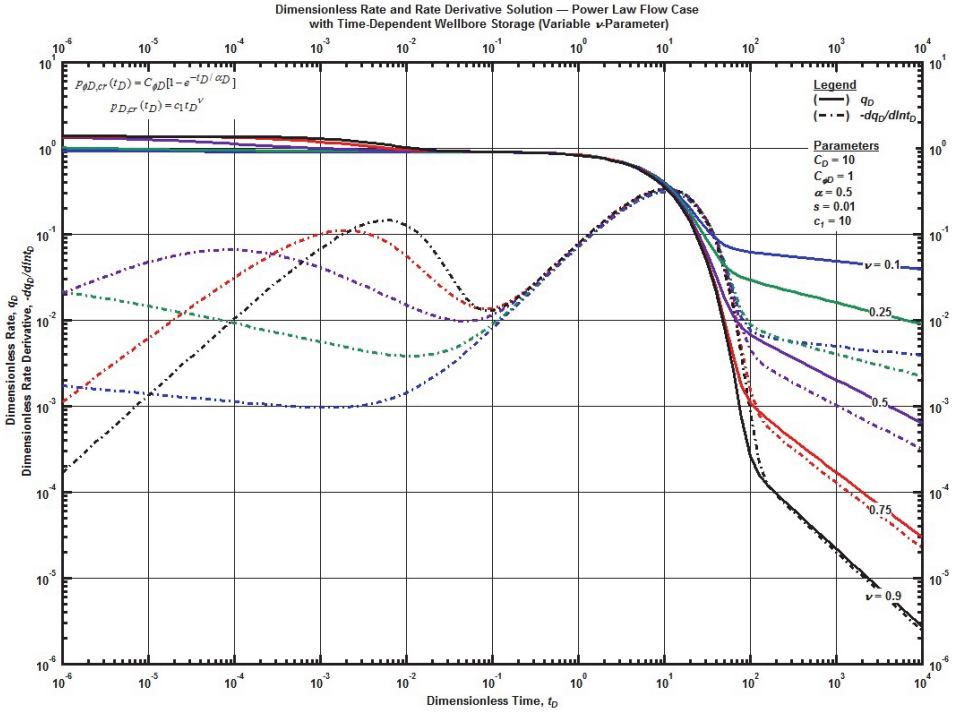

Figure 4.31 — Log-log plot (constant pressure dimensionless rate derivative solution) for the power-law flow model combined with the time-dependent wellbore storage for select values of the ν-parameter.

As shown in **Fig. 4.30**, the c_1-parameter has a significant impact on early-time and late-time flow behavior. At early-time, the c_1-parameter yields a consistent shape offset with time. At late-times, higher values of the c_1-parameter yield a significantly lower dimensionless flowrate.

The ν-parameter significantly affects the rate and rate derivative behavior at both early-times and late-times. As a proxy for the system flow regime (*i.e.,* for linear flow the ν-parameter is ½), late-time behavior is dependent on the exponential ν-parameter, bounded between zero and one for this application.

In summary, the time-dependent wellbore storage model presents a unique diagnostic capability which may be utilized to represent early-time ("flowback") behavior (see **Fig. 4.26** — **Fig. 4.31**). Practically, the use of all diagnostic plots (*i.e.,* dimensionless rate, dimensionless rate derivative, dimensionless cumulative rate, time-normalized dimensionless cumulative rate and dimensionless pressure and dimensionless pressure derivative) provide some mechanism to diagnose time-dependent wellbore storage effects.

4.6 Linear Flow Relation

The linear flow regime, proposed in Chapter III, is based upon the work of Gringarten, Ramey and Raghavan (1974) provides a behavioral model for fluid flow from the matrix to the fracture. Fully derived in **Appendix A**, we apply each of our time-dependent models to the linear flow regime to quantify "early-time" performance of a vertically fractured well. The linear flow relation is displayed below for reference:

$$p_{D,cr}(t_D) = \sqrt{\pi}\sqrt{t_D} \quad \text{.....(4.2)}$$

The following sections examine the time-dependent skin factor and wellbore storage models with the linear flow relation.

4.7 Linear Flow Relation with Cumulative-Exponential Time-Dependent Skin Effects

The cumulative-exponential time-dependent skin factor model is based on empirical observations from ultra-low permeability reservoirs. **Appendix D** provides a derivation of the constant pressure solution in the Laplace domain with cumulative-exponential time-dependent skin effects and the linear flow regime.

As with the power-law flow regime, similar unique trends have been observed within the flowrate data. In this regard, we examine each parameter within the model, along with other relevant diagnostic plots to validate the applicability of our time-dependent relation.

The λ-parameter, shown in **Fig. 4.32** imposes little impact on the dimensionless flowrate except for the potential for cause a slight rate increase during the transition between early-time and late-time linear flow. The rate derivative flow, shown in **Fig. 4.33**, highlights the increase in flowrate causing the derivative term to tend towards a zero value, creating a unique diagnostic feature for potential field application.

The s_0-parameter, shown in **Fig. 4.34**, affects the initial flowrate. As a proxy for the initial skin value, the lower the initial skin, the higher the initial flowrate. A lower boundary for the skin term is developed through the s_∞-parameter (**Fig. 4.35**). Validation of this time-dependent skin factor model is achieved as the s_0- and s_∞-parameters approach zero — *i.e.,* the time-dependent skin effects become negligible yielding the linear flow solution.

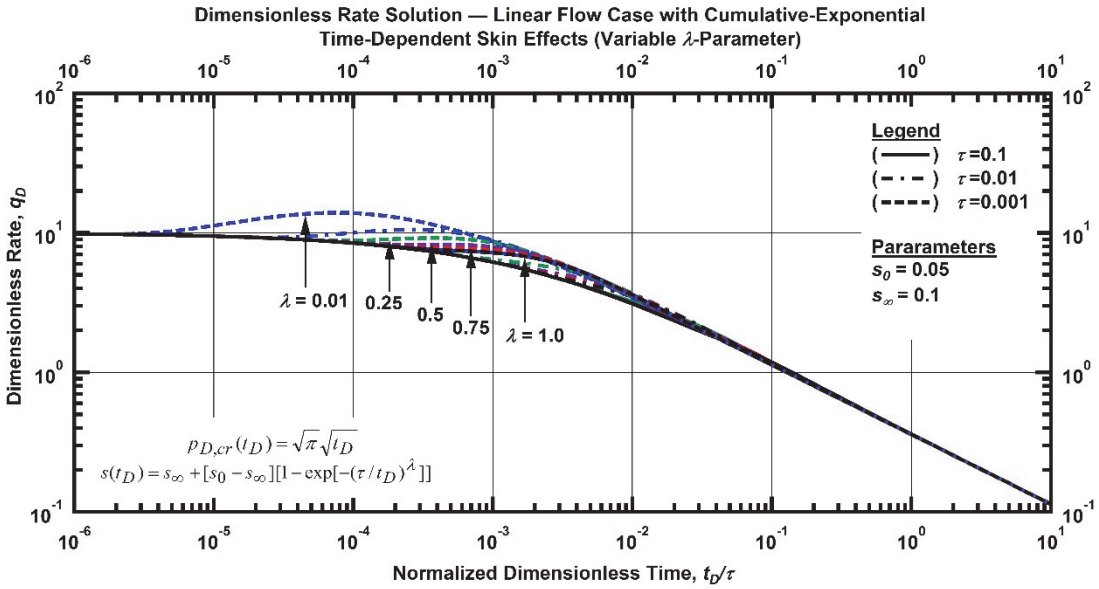

Figure 4.32 — Log-log plot (constant pressure dimensionless rate solution) for the linear flow model combined with the cumulative-exponential time-dependent skin effects for select values of the λ-parameter.

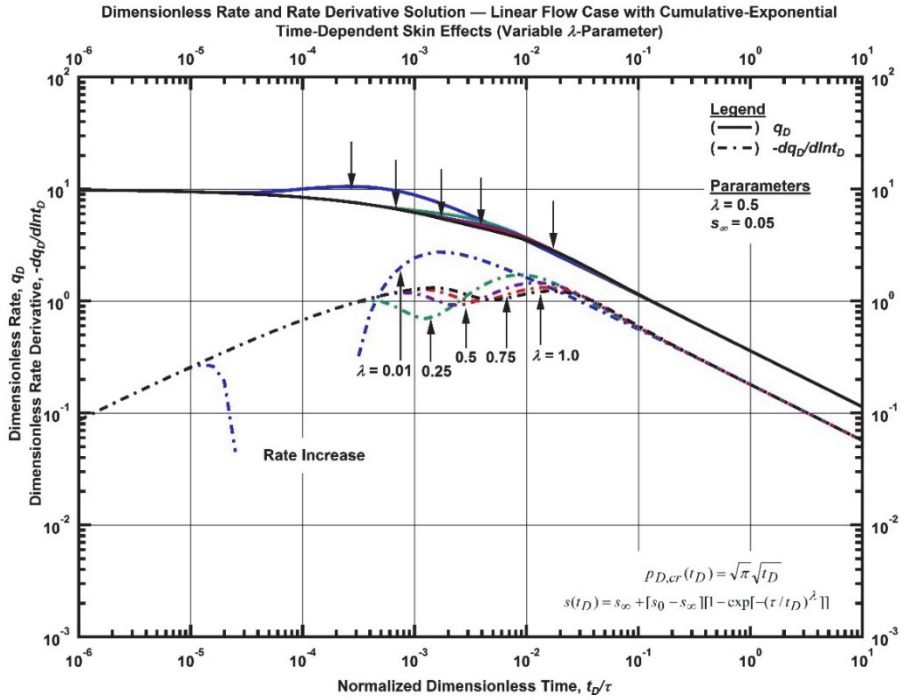

Figure 4.33 — Log-log plot (constant pressure dimensionless rate derivative solution) for the linear flow model combined with the cumulative-exponential time-dependent skin effects for select values of the λ-parameter ($\tau = 0.01$).

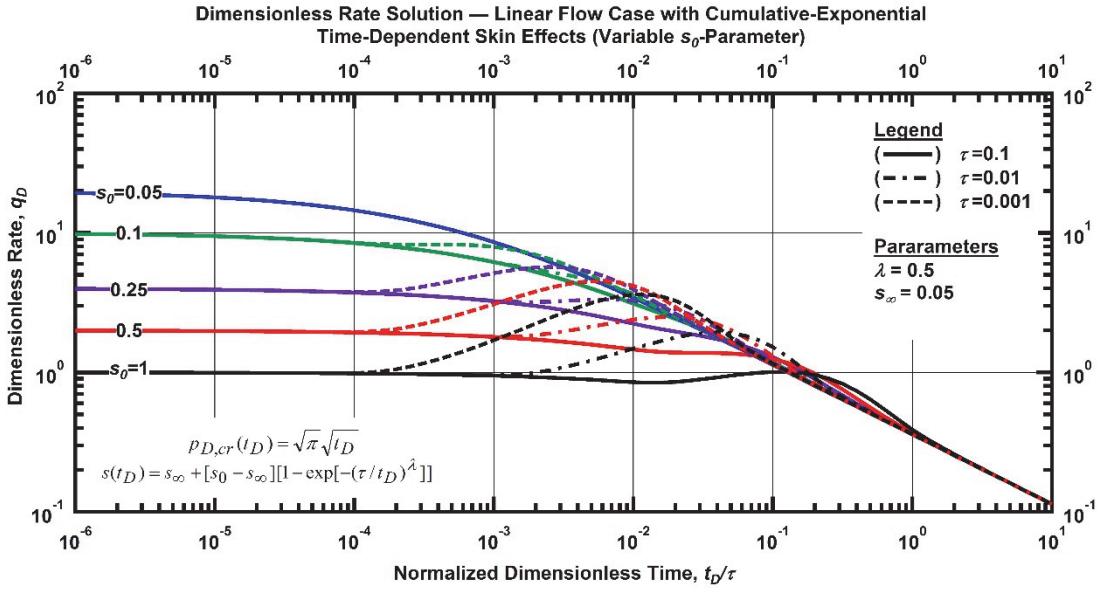

Figure 4.34 — Log-log plot (constant pressure dimensionless rate solution) for the linear flow model combined with the cumulative-exponential time-dependent skin effects for select values of the s_0-parameter.

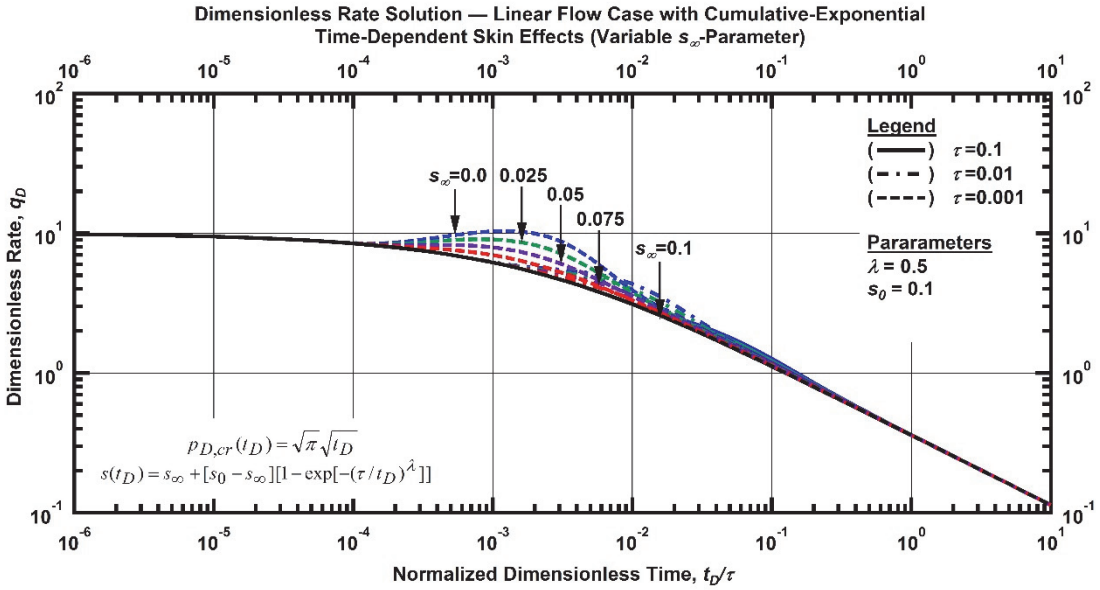

Figure 4.35 — Log-log plot (constant pressure dimensionless rate solution) for the linear flow model combined with the cumulative-exponential time-dependent skin effects for select values of the s_∞-parameter.

As shown in the previous examples (**Fig. 4.32** — **Fig. 4.35**) the cumulative-exponential time-dependent skin factor is used to represent observed rate features — including the desired "hockey-stick" shape, where the flowrate is flat or steadily increasing (derivative is positive) at early-time before reaching a transition feature in which the flowrate demonstrates a "hump" or rate increase, before dissipating to late-time linear flow.

4.8 Linear Flow Relation with Exponential Time-Dependent Skin Effects

The exponential time-dependent skin factor model is based on empirical observations from ultra-low permeability reservoirs. **Appendix D** provides a derivation of the constant pressure solution in the Laplace domain with exponential time-dependent skin effects and the linear flow regime.

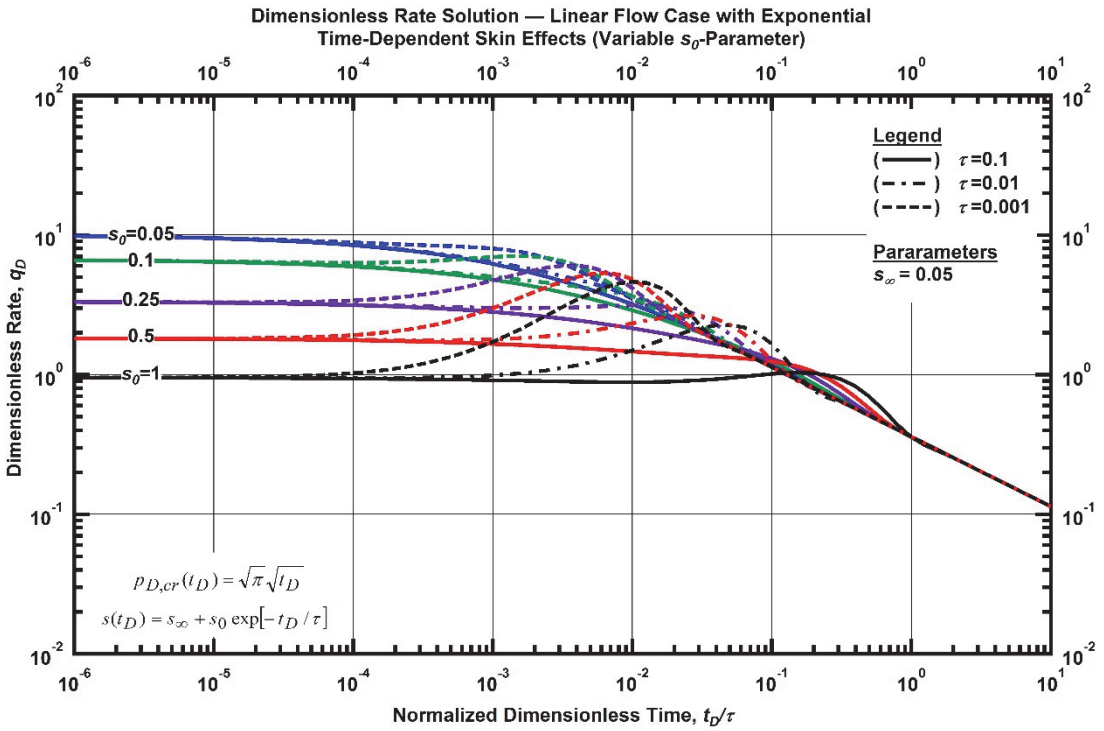

Figure 4.36 — Log-log plot (constant pressure dimensionless rate solution) for the linear flow model combined with the exponential time-dependent skin effects for select values of the s_0-parameter.

The exponential time-dependent skin factor with linear flow relation performs in an almost identical manner as the exponential time-dependent skin factor with power law flow relation. This confirms the additive nature of the time-dependent skin factor to the pressure relation having the same effect on the

dimensionless flowrate regardless the characteristic flow of the reservoir. For thoroughness, we will evaluate each parameter to validate the applicability of our model.

The s_0-parameter affects the initial flowrate, as shown by **Fig. 4.36**, creating a characteristic rate "hump" during the transition to late-time linear flow. The greater difference between the s_∞- and s_0-parameter, the larger the rate increase (*i.e.,* system cleanup) required to dissipate into the reservoir characteristic linear flow regime.

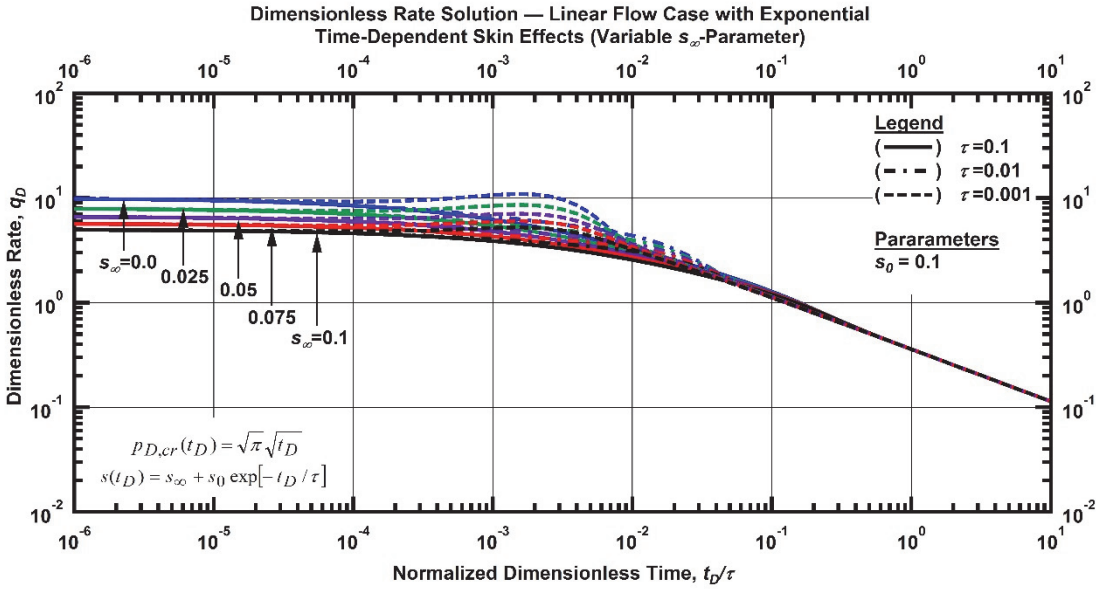

Figure 4.37 — Log-log plot (constant pressure dimensionless rate solution) for the linear flow model combined with the exponential time-dependent skin effects for select values of the s_∞-parameter.

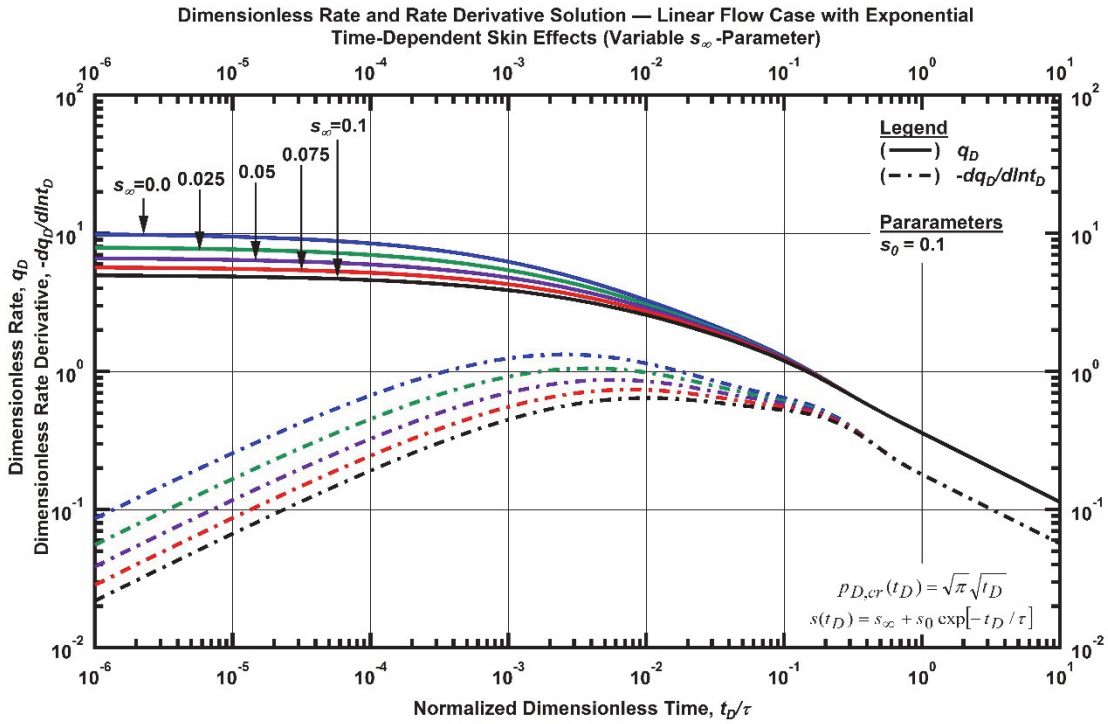

Figure 4.38 — Log-log plot (constant pressure dimensionless rate derivative solution) for the linear flow model combined with the exponential time-dependent skin effects for select values of the s_∞-parameter ($\tau = 0.01$).

The s_∞-parameter, shown in **Fig. 4.37** with the rate derivative shown in **Fig. 4.38**, affects the transition region between early-time and late-time linear flow. The larger the difference between the s_∞- and s_0-parameters, the greater the rate "hump" feature observed.

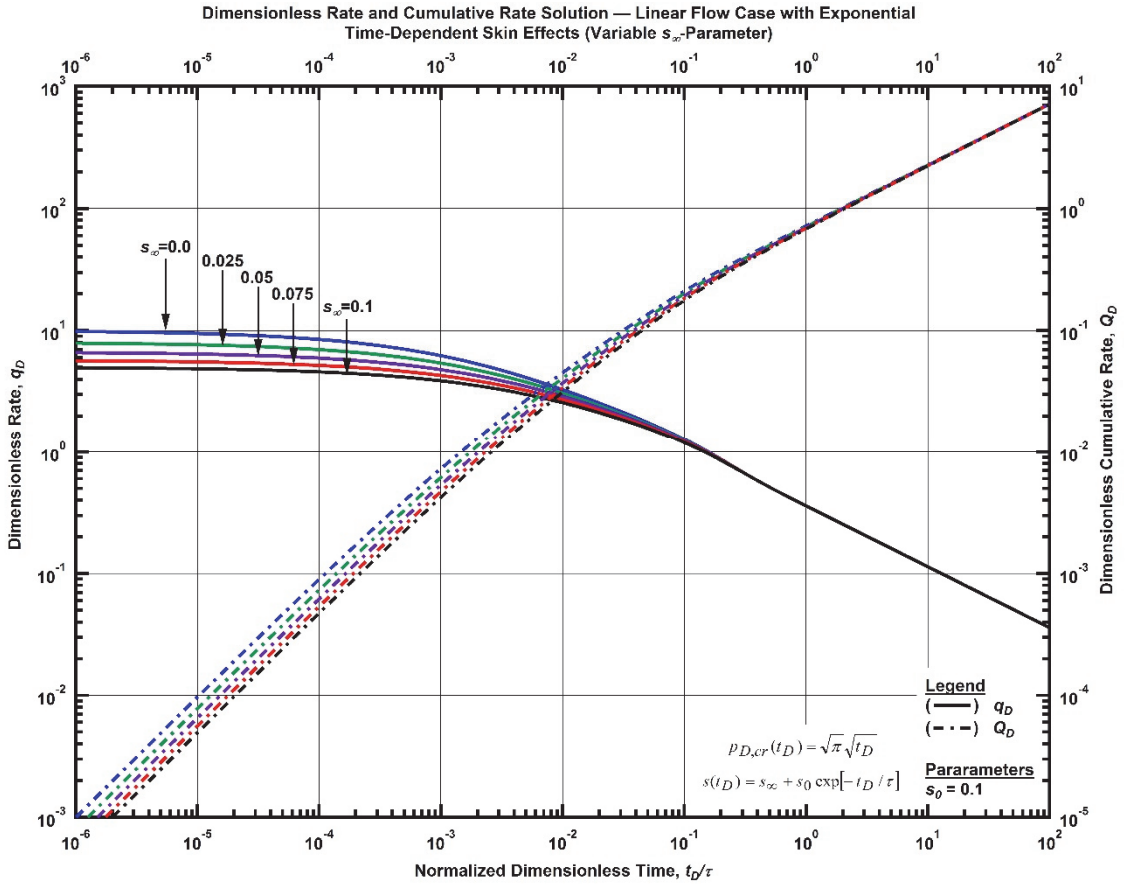

Figure 4.39 — Log-log plot (constant pressure dimensionless cumulative production solution) for the linear flow model combined with the exponential time-dependent skin effects for select values of the s_∞-parameter ($\tau = 0.01$).

The dimensionless cumulative production (**Fig. 4.39**) and the time-normalized dimensionless cumulative rate (**Fig. 4.40**) provide additional diagnostic tools, which may be used to evaluate the reservoir behavioral characteristics.

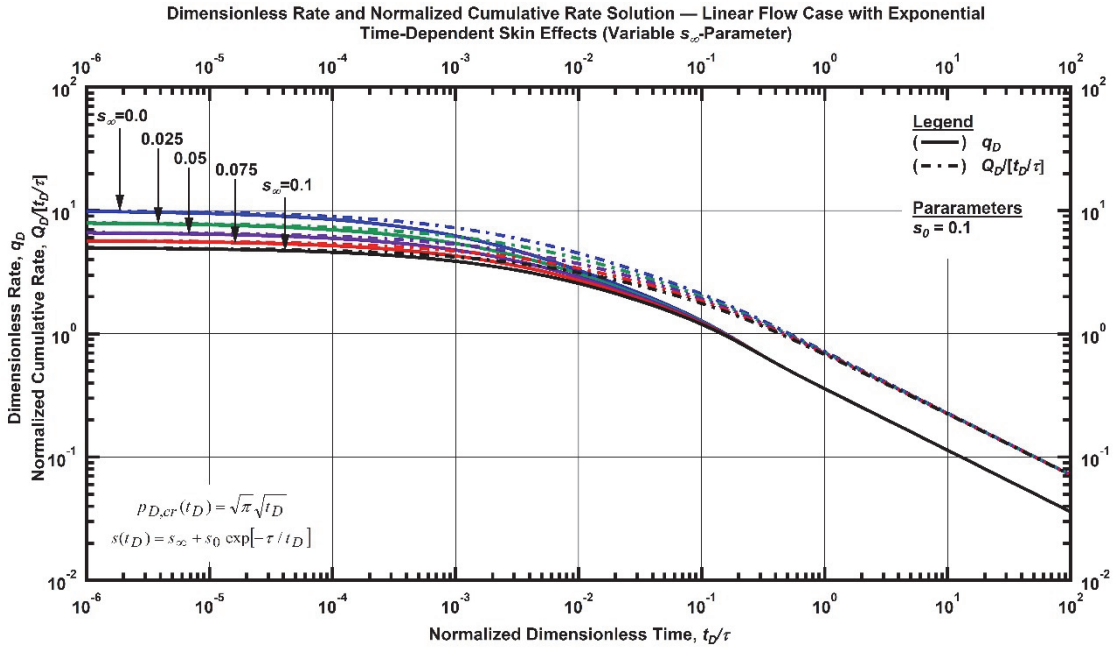

Figure 4.40 — Log-log plot (constant pressure time-normalized dimensionless cumulative rate solution) for the linear flow model combined with the exponential time-dependent skin effects for select values of the s_∞-parameter ($\tau = 0.01$).

The previous examples (**Fig. 4.36** — **Fig. 4.40**) demonstrate that the exponential time-dependent skin factor with linear flow has the same form and function as with the power-law flow relation, with the only difference being the late-time reservoir characteristic flow behavior. Diagnostic features include the desired "hockey-stick" flow profile, with an early-time flat or gently increasing (derivative is positive) flowrate, a rollover (*i.e.,* transition) feature with rate increase potential, dissipating into the late-time linear flow regime, characteristic of the reservoir. These diagnostic features, representing empirical data, potentially provide the ability to quantify early-time or "flow-back" behavior. All diagnostic plots may be found in **Appendix F**.

4.9 Linear Flow Relation with Hyperbolic Time-Dependent Skin Effects

The hyperbolic time-dependent skin factor model is based on empirical observations from ultra-low permeability reservoirs. **Appendix D** provides a derivation of the constant pressure solution in the Laplace domain with hyperbolic time-dependent skin effects and the linear flow regime.

The hyperbolic time-dependent skin model, with linear flow, displays the same characteristics in flowrate behavior as with the hyperbolic time-dependent skin model with power-law flow. The only notable difference is the late-time flowrate characterized by the specific one-half slope of the linear flow regime. For thoroughness, we will evaluate each parameter with supporting diagnostic plots to validate the applicability of the hyperbolic time-dependent skin function for field implementation.

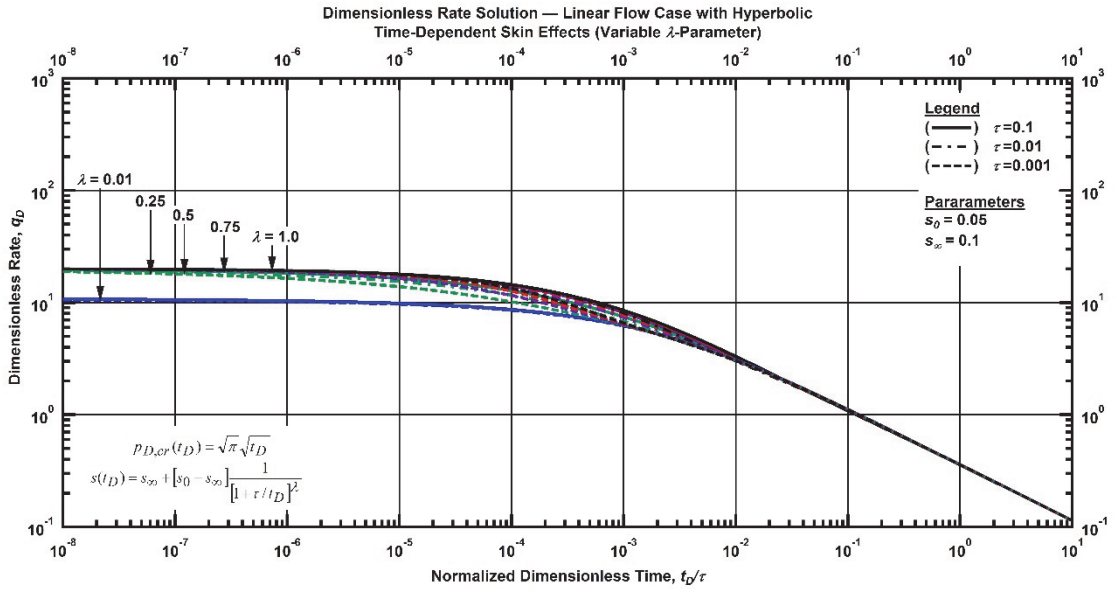

Figure 4.41 — Log-log plot (constant pressure dimensionless rate solution) for the linear flow model combined with the hyperbolic time-dependent skin effects for select values of the λ-parameter.

The λ-parameter imposes little impact on the constant pressure solution, for the limited range considered, as shown in **Fig. 4.41**. Mathematically, the λ-parameter may be any value, however, for this work we chose to bound the value between zero and one in order to maintain consistency with the cumulative-exponential time-dependent skin factor.

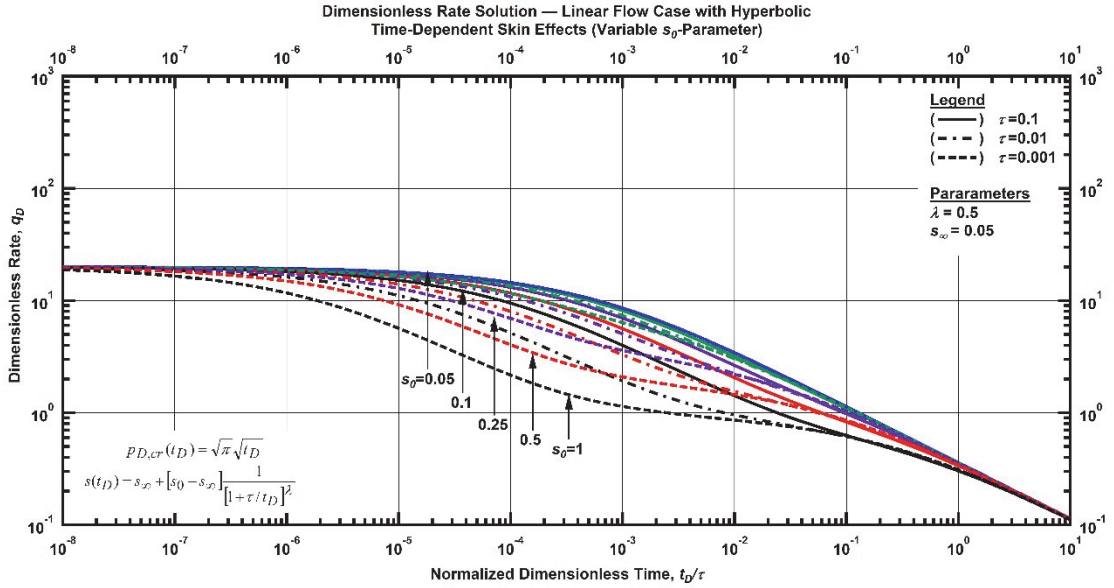

Figure 4.42 — Log-log plot (constant pressure dimensionless rate solution) for the linear flow model combined with the hyperbolic time-dependent skin effects for select values of the s_0-parameter.

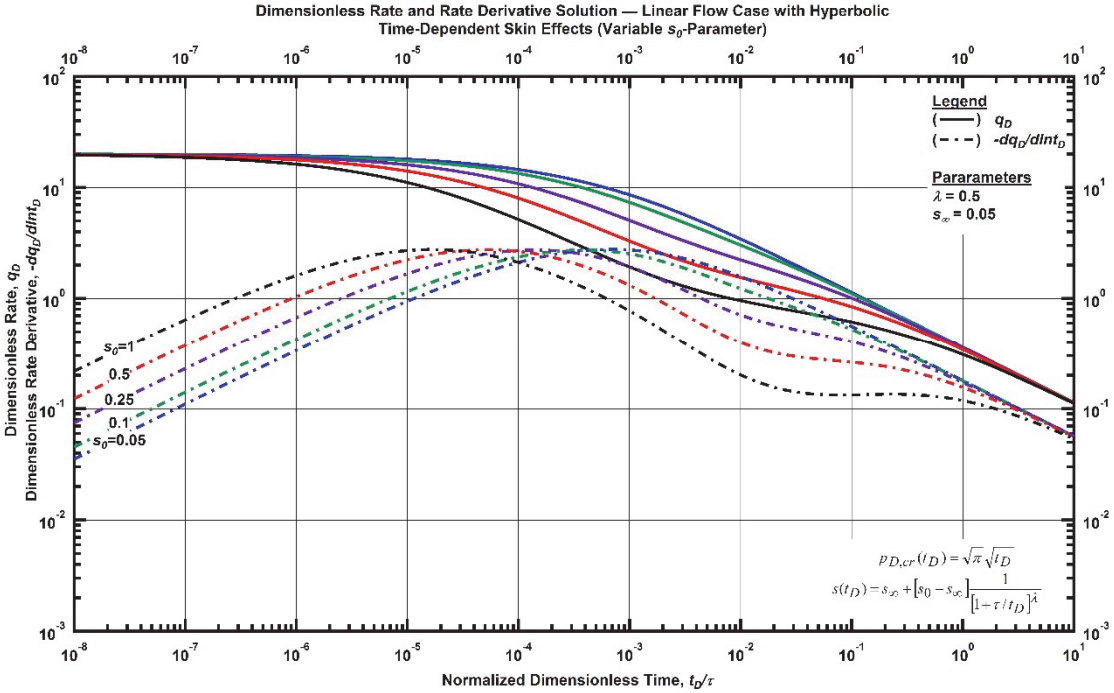

Figure 4.43 — Log-log plot (constant pressure dimensionless rate derivative solution) for the linear flow model combined with the hyperbolic time-dependent skin effects for select values of the s_0-parameter ($\tau = 0.01$).

As shown in **Fig. 4.42**, the s_0-parameter affects the rate at which late-time linear flow is achieved. As a proxy for the systems maximum skin, the higher the s_0-parameter, the more time required to achieve linear flow. The author notes the significant amount of time required, approximately five log-cycles, when the s_0-parameter is very large. The dimensionless rate derivative, shown in **Fig. 4.43**, highlights the features of the dimensionless rate.

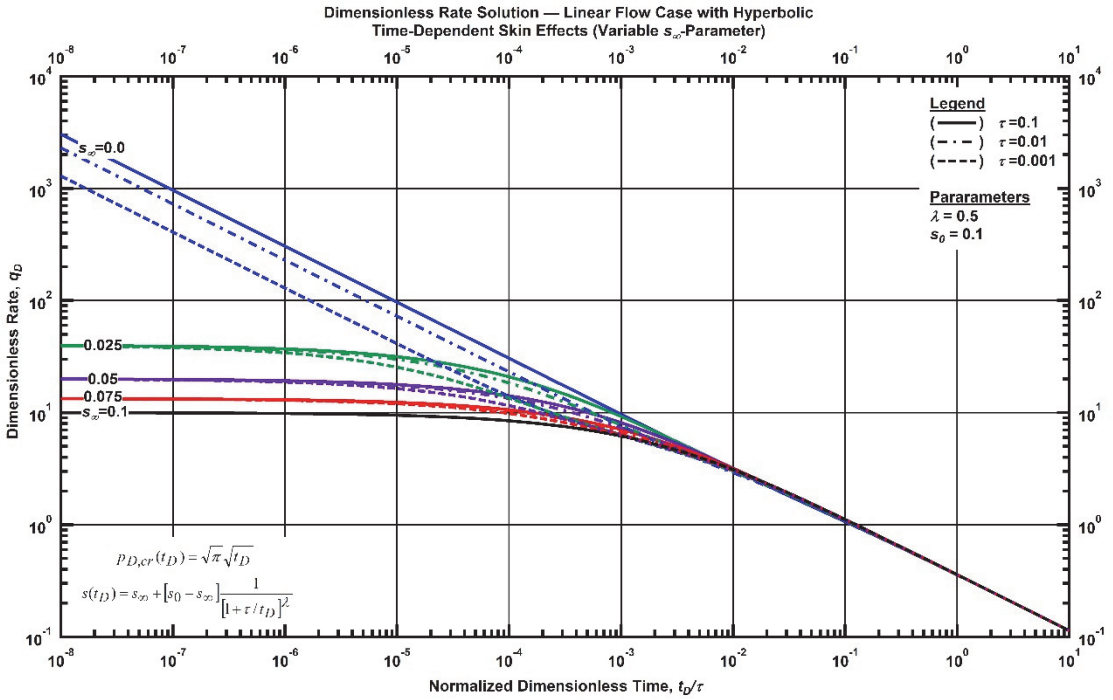

Figure 4.44 — Log-log plot (constant pressure dimensionless rate solution) for the linear flow model combined with the hyperbolic time-dependent skin effects for select values of the s_∞-parameter.

The s_∞-parameter, the lower boundary for skin in this formulation shown in **Fig. 4.44**, affects the initial dimensionless flowrate. The lower the s_∞-parameter, the higher the initial flowrate. The time-normalized dimensionless cumulative rate, shown in **Fig. 4.45**, provides additional diagnostic capabilities when attempting to utilize this methodology to evaluate reservoir behavior. Validation of this model is achieved as the s_∞- and s_0-parameters approach zero — *i.e.,* the time-dependent skin effects become negligible which yield the linear flow regime.

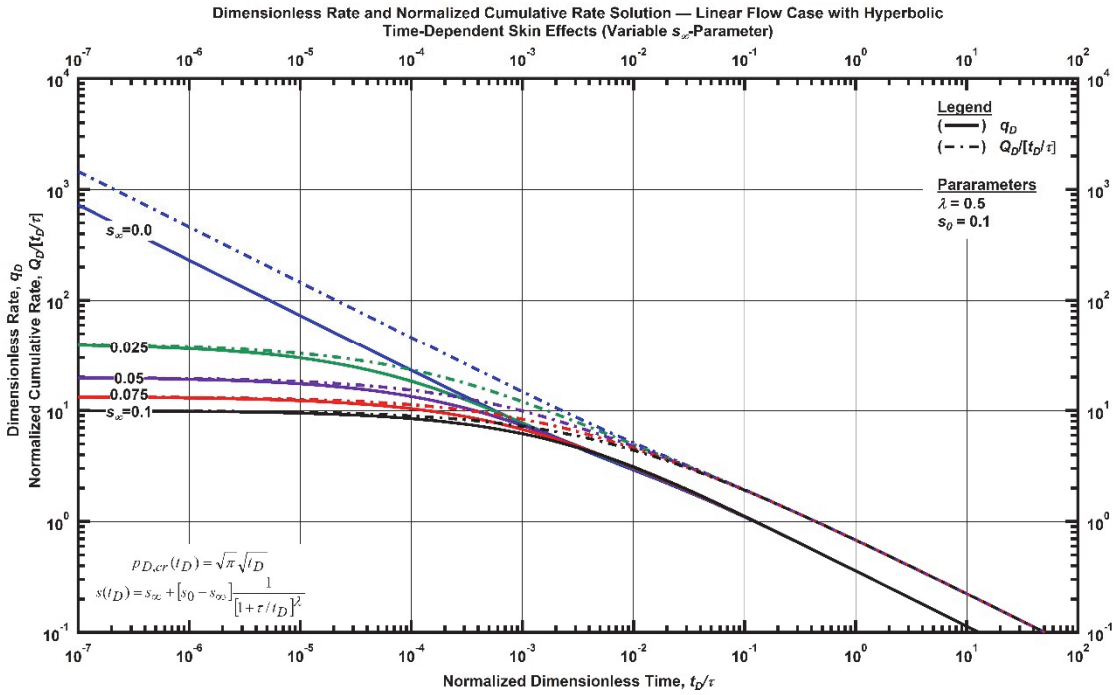

Figure 4.45 — Log-log plot (constant pressure time-normalized dimensionless cumulative rate solution) for the linear flow model combined with the hyperbolic time-dependent skin effects for select values of the s_∞-parameter ($\tau = 0.01$).

From this example, (**Fig. 4.41** — **Fig. 4.45**), we observe that the hyperbolic time-dependent skin effects occur at very small values of dimensionless time, resulting in potentially challenging application to field data where rate measurements are typically taken at a longer time intervals. Although quantitatively this may result in a challenging application, qualitatively, this methodology may serve as a diagnostic tool for reservoir characterization.

4.10 Linear Flow Relation with Time-Dependent Wellbore Phase Redistribution

Fair (1990) proposed a wellbore phase redistribution pressure based upon empirical data and a single laboratory test to explain anomalous pressure signatures in build-up tests. Incorporation of the phase redistribution pressure profile into the wellbore pressure is fully derived in **Appendix E**. To demonstrate the viability of this work, we examine each parameter within the model and the potential application to field data. To assist in diagnostic capabilities, the derivative of the constant pressure solution was also taken and plotted for each parameter. To supplement the dimensionless rate and rate derivative plots, we have further included a variety of other diagnostic plots to further validate the application of this model. A full evaluation of all plots may be found in **Appendix F**.

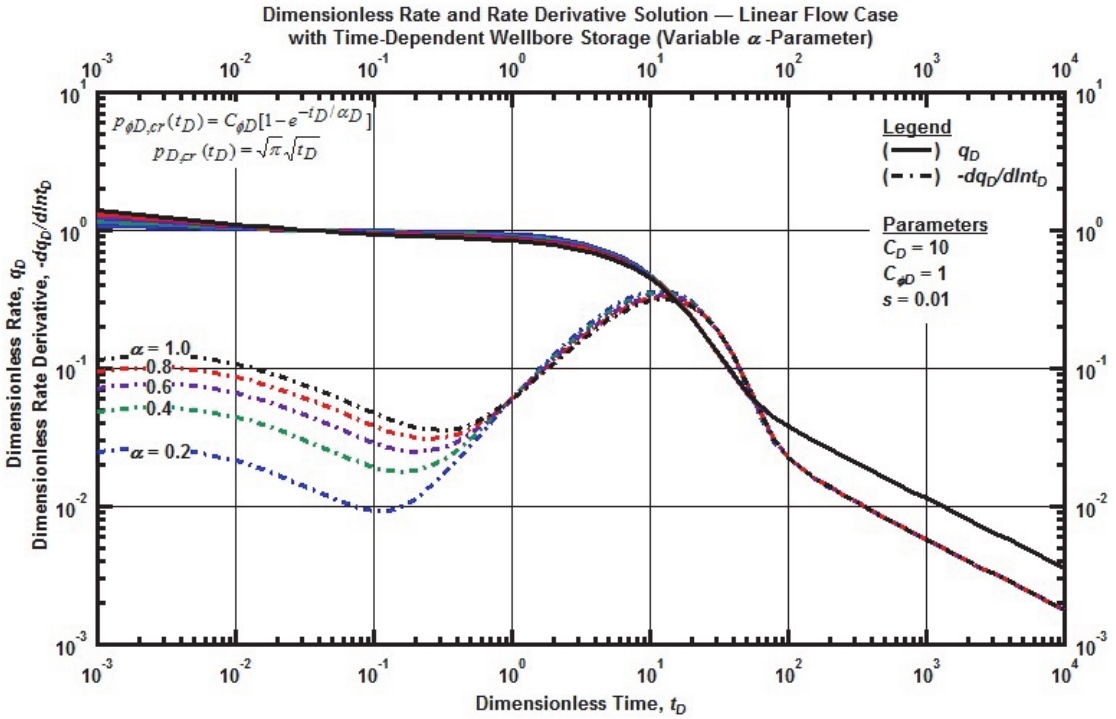

Figure 4.46 — Log-log plot (constant pressure dimensionless rate and rate derivative solution) for the linear flow model combined with the time-dependent wellbore storage for select values of the α-parameter.

For the limited range we considered, the α-parameter, shown in **Fig. 4.46**, imposes little impact on the constant pressure solution. The derivative displays much stronger features than the rate function, and

although this function may be difficult to assess in practice, its behavior is noted for possible use as a diagnostic characteristic.

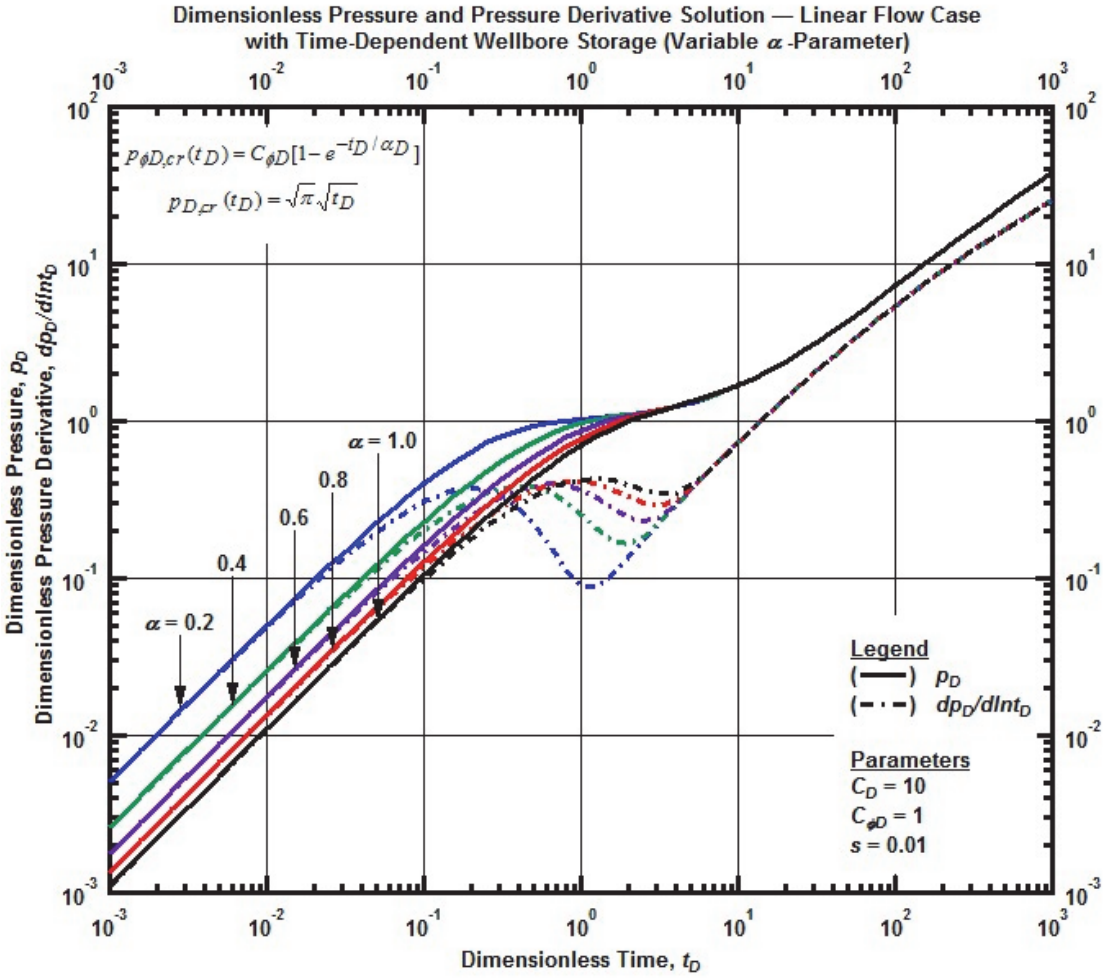

Figure 4.47 — Log-log plot (constant rate dimensionless pressure and pressure derivative solution) for the linear flow model combined with the time-dependent wellbore storage for select values of the α-parameter.

For comparative purposes, the constant rate dimensionless pressure solution was created to demonstrate features characteristic to wellbore storage. Shown in **Fig. 4.47**, we observe the unit slope wellbore storage line with a wellbore storage "bubble" during the transition into late-time linear flow.

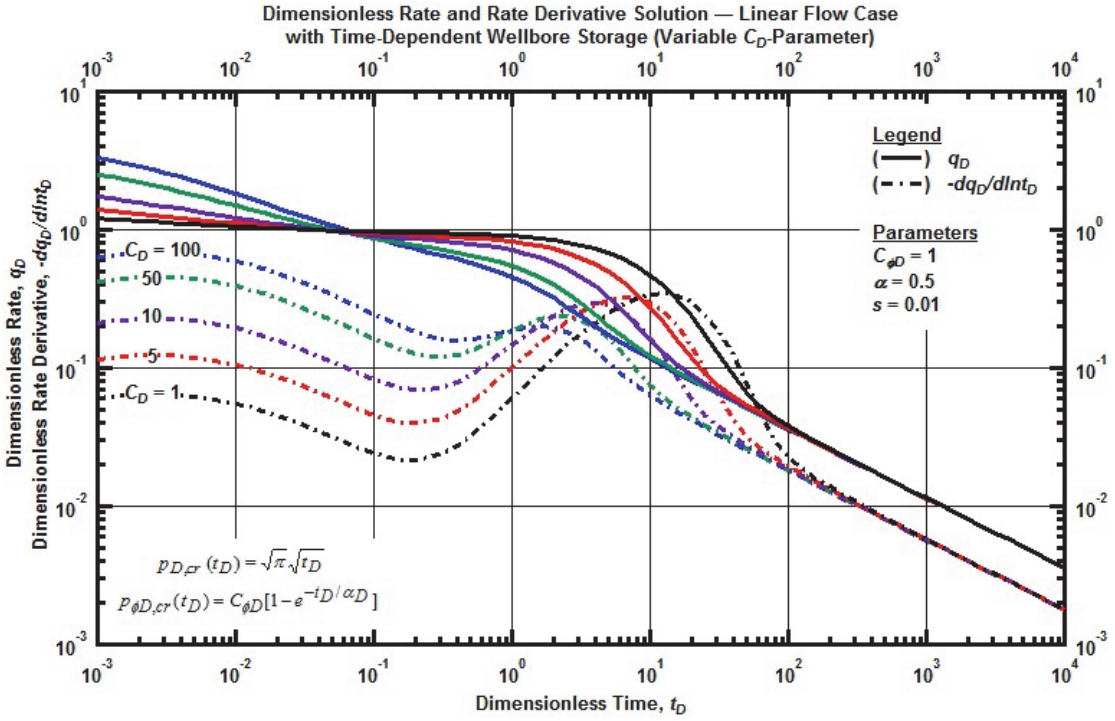

Figure 4.48 — Log-log plot (constant pressure dimensionless rate and rate derivative solution) for the linear flow model combined with the time-dependent wellbore storage for select values of dimensionless wellbore storage constant

The dimensionless wellbore storage constant (C_D) shown in **Fig. 4.48**, provides variations in both early-time behavior and the transition region. As the wellbore storage influence diminishes over time, the rate is governed by the specified linear flow solution. Additional diagnostic features may be explored, through the evaluation of the dimensionless cumulative flowrate (**Fig. 4.49**) and time-normalized dimensionless cumulative flowrate (**Fig. 4.50**) highlighting the transition region between early-time and late-time linear flow.

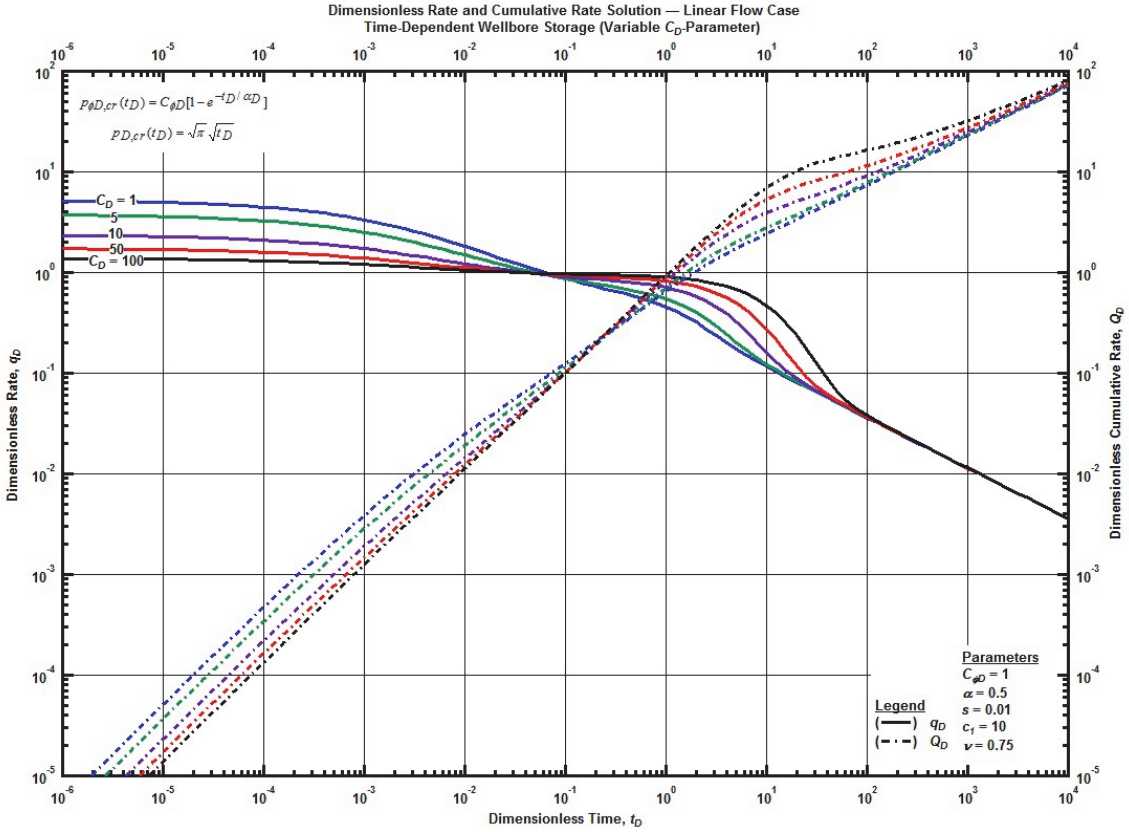

Figure 4.49 — Log-log plot (constant pressure dimensionless cumulative production solution) for the linear flow model combined with the time-dependent wellbore storage for select values of dimensionless wellbore storage constant.

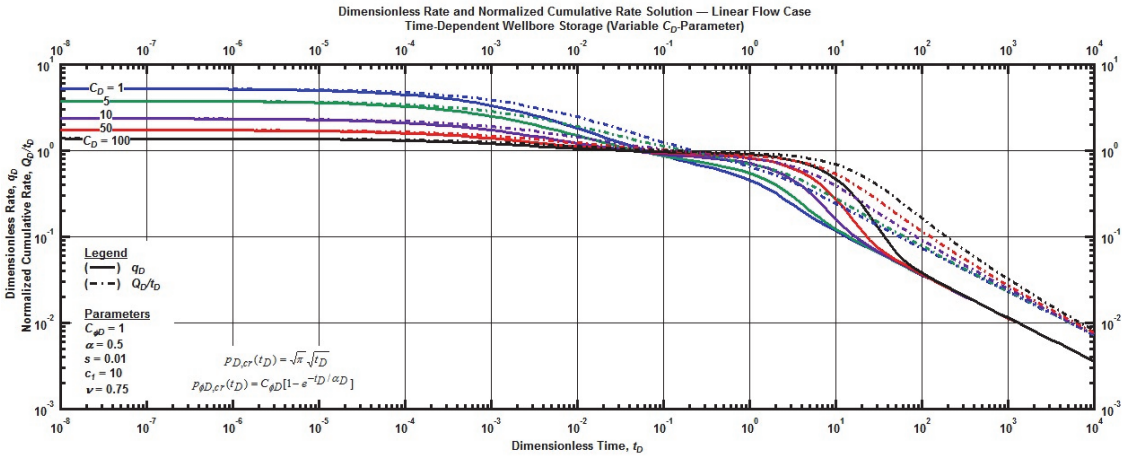

Figure 4.50 — Log-log plot (constant pressure time-normalized dimensionless cumulative rate solution) for the linear flow model combined with the time-dependent wellbore storage for select values of dimensionless wellbore storage constant.

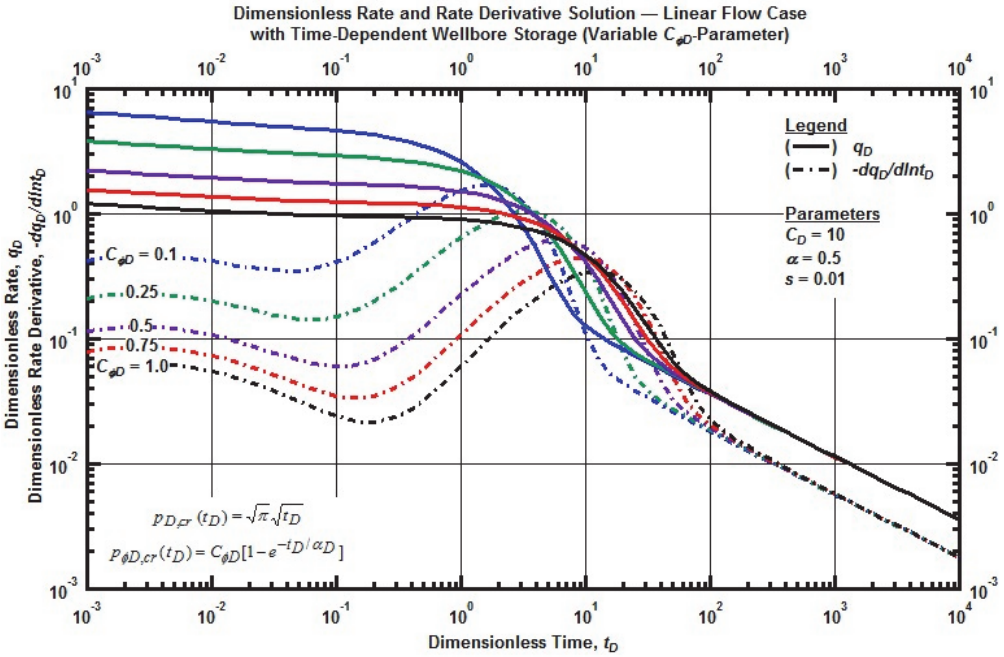

Figure 4.51 — Log-log plot (constant pressure dimensionless rate and rate derivative solution) for the linear flow model combined with the time-dependent wellbore storage for select values of dimensionless wellbore phase redistribution constant.

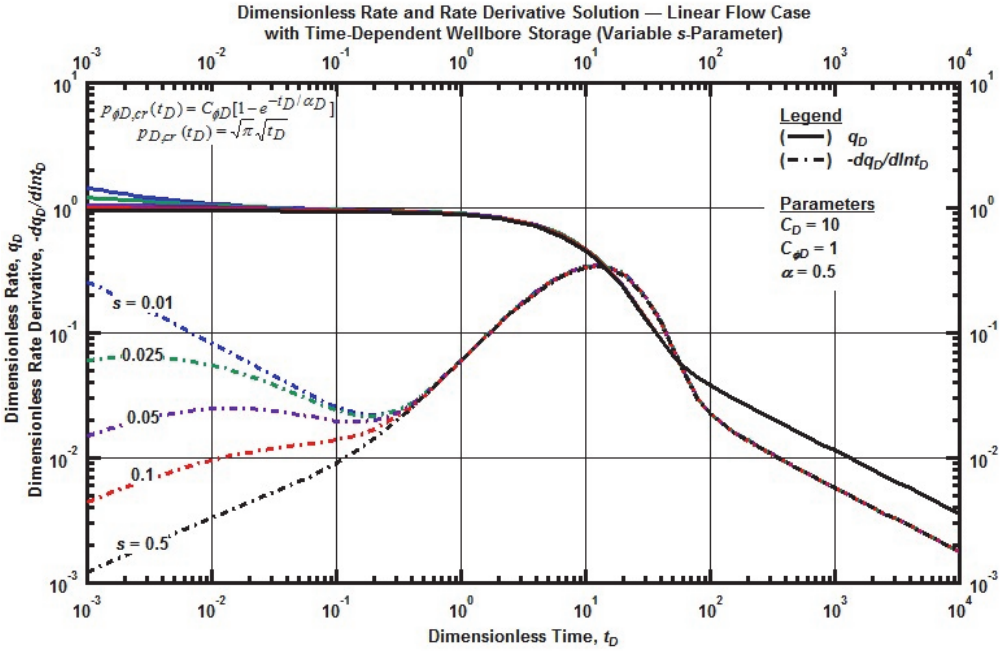

Figure 4.52 — Log-log plot (constant pressure dimensionless rate and rate derivative solution) for the linear flow model combined with the time-dependent wellbore storage for select values of constant skin factor.

The dimensionless wellbore phase redistribution constant ($C_{\phi D}$), shown in **Fig. 4.51**, displays similar features as the dimensionless wellbore storage constant (C_D), affecting the rate at early-times and dissipating to yield the linear flow solution at late-times. The $C_{\phi D}$-parameter rate derivative profile yields a consistent shape displaced in time, unlike the C_D-parameter which does not influence the shape in a constant manner.

The skin factor imposes little impact on the constant pressure solution shown in **Fig. 4.52**. The rate derivative has much stronger features than the rate function as shown by the early-time variations in the skin factor rate derivative. Although the combined effects of skin and wellbore storage may be difficult (or even impossible) to assess in practice, we may be able to develop diagnostic characteristic functions (*e.g.,* derivative ratios etc.)

As shown in the previous example (**Fig. 4.46 — Fig. 4.52**) a time-dependent wellbore storage model (with constant skin factor) is used to represent rate features observed from field data. Features include flat or gently decreasing rates at early-times and a convergence to the reservoir signature (*e.g.,* linear flow) at late-times via a rollover (*i.e.,* transition) attribute. The dimensionless rate derivative function highlights the transition feature where, for time-dependent wellbore storage, all cases exhibit a "hump" indicative of a wellbore storage "bubble" (which is commonly seen in the constant rate dimensionless pressure function.

4.11 Bilinear Flow Relation

The bilinear flow regime, developed in Chapter III, based upon the work of Cinco and Samaniego (1981a) provides a behavioral model for fluid flow from the matrix through the fracture to the wellbore. Fully derived in **Appendix A**, we apply each of our time-dependent models to the bilinear flow regime to quantify "early-time" performance of a vertically fractured well. The linear flow relation is displayed below for reference:

$$p_{D,cr}(t_D) = \frac{\pi}{\Gamma(5/4)\sqrt{2(k_f w_f)_D}} \sqrt[4]{t_D} \quad \text{.....(4.3)}$$

The following sections examine the time-dependent skin factor and wellbore storage models with the linear flow relation.

4.12 Bilinear Flow Relation with Cumulative-Exponential Time-Dependent Skin Effects

The cumulative-exponential time-dependent skin factor model is based on empirical observations from ultra-low permeability reservoirs. **Appendix D** provides a derivation of the constant pressure solution in the Laplace domain with cumulative-exponential time-dependent skin effects and the bilinear flow regime.

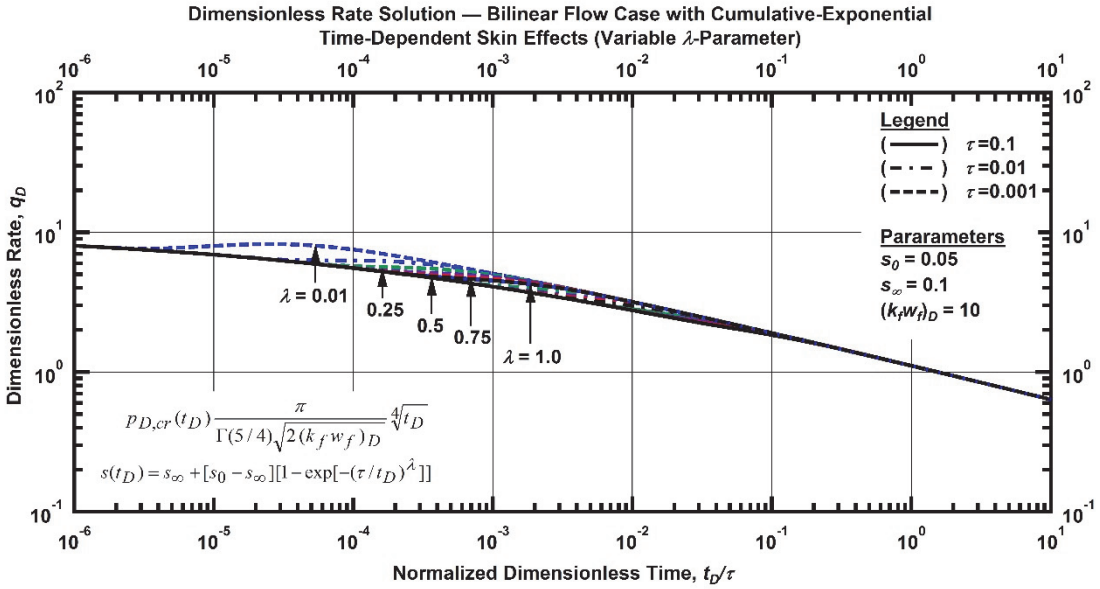

Figure 4.53 — Log-log plot (constant pressure dimensionless rate solution) for the bilinear flow model combined with the cumulative-exponential time-dependent skin effects for select values of λ-parameter.

The λ-parameter, shown in **Fig. 4.53**, imposes little impact on the constant pressure solution, as was evident with both the linear and power-law flow regimes, except for the slight increase in rate during the transition from early-time flow to late-time bilinear flow. In this application, the λ-parameter must be bounded between zero and one.

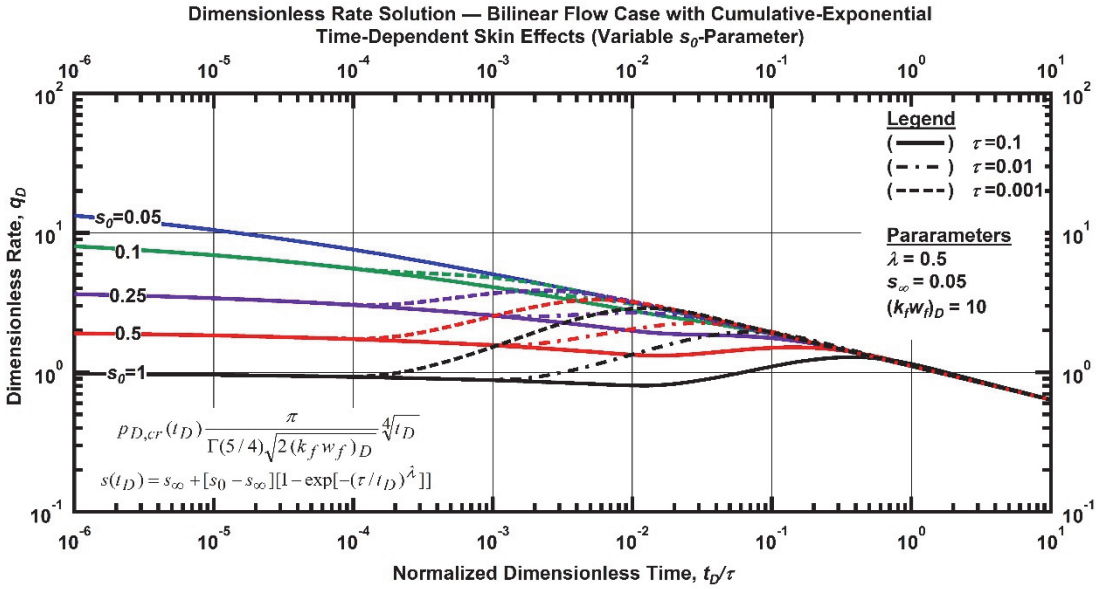

Figure 4.54 — Log-log plot (constant pressure dimensionless rate solution) for the bilinear flow model combined with the cumulative-exponential time-dependent skin effects for select values of s_0-parameter.

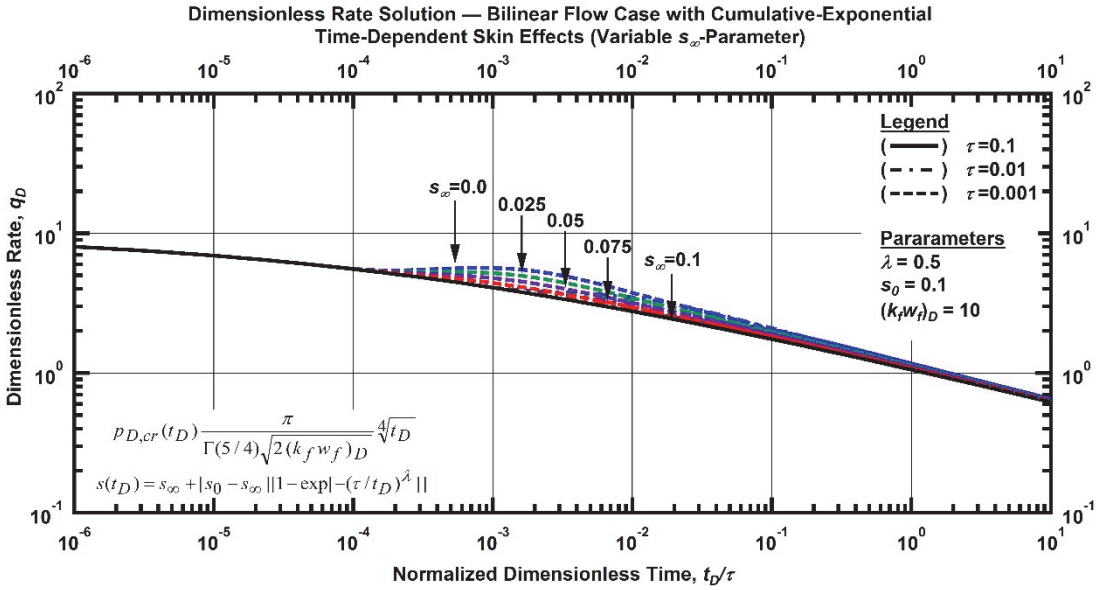

Figure 4.55 — Log-log plot (constant pressure dimensionless rate solution) for the bilinear flow model combined with the cumulative-exponential time-dependent skin effects for select values of s_∞-parameter.

As shown in **Fig. 4.54**, the s_0-parameter affects the initial flowrate. The higher the value of the s_0-parameter, a proxy for the maximum skin available to the system, the lower the initial flowrate. Shown in

Fig. 4.55, the s_∞-parameter, a proxy for the minimum skin boundary, affects the transition region potentially increasing the dimensionless flowrate, between early-time and late-time-bilinear flow. Validation of this model is achieved as the s_0- and s_∞-parameters approach zero, the time dependent skin effects become negligible yielding the late-time bilinear flow regime.

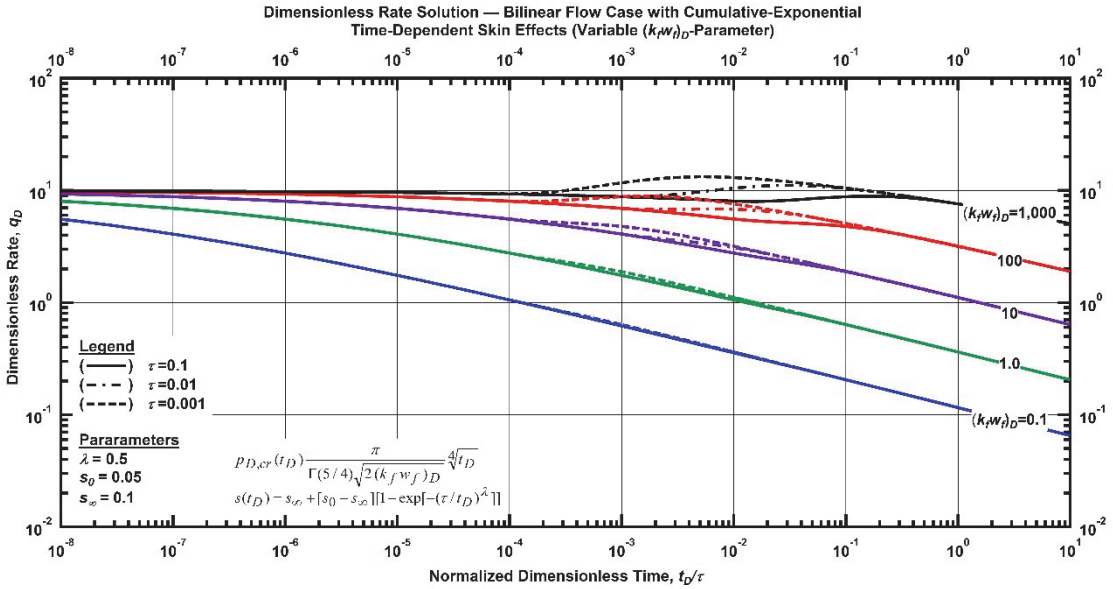

Figure 4.56 — Log-log plot (constant pressure dimensionless rate solution) for the bilinear flow model combined with the cumulative-exponential time-dependent skin effects for select values of dimensionless fracture conductivity.

The effect of the cumulative-exponential time-dependent skin effects remains consistent regardless of the flow regime to which it is associated. The example posed above (shown in **Fig. 4.53** — **Fig. 4.56**), the cumulative-exponential time-dependent skin model with bilinear flow regime, differs from the linear and power law model only in regards to the late-time reservoir signature — *i.e.,* early-time and transitional behavior are consistent are regardless of the flow regime experienced by the reservoir.

4.13 Bilinear Flow Relation with Exponential Time-Dependent Skin Effects

The exponential time-dependent skin factor model is based on empirical observations from ultra-low permeability reservoirs. **Appendix D** provides a derivation of the constant pressure solution in the Laplace domain with exponential time-dependent skin effects and the bilinear flow regime.

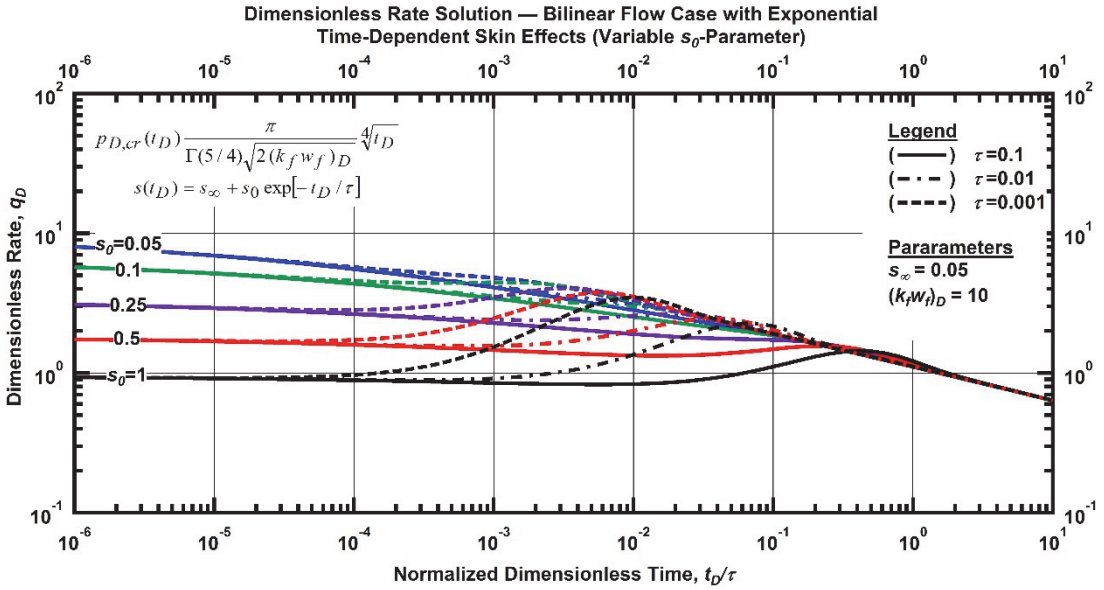

Figure 4.57 — Log-log plot (constant pressure dimensionless rate solution) for the bilinear flow model combined with the exponential time-dependent skin effects for select values of s_0-parameter.

The s_0-parameter affects initial dimensionless flowrate and therefore, the size of the rate "hump" required to return to the late-time quarter slope (*i.e.,* bilinear flow) on a log-log scale. The higher the s_0-parameter, the lower the initial flowrate and larger of a transition feature before dissipating into late-time bilinear flow, as demonstrated in **Fig. 4.57**. The derivative of the dimensionless rate solution, evaluating the s_0-parameter, clearly shows this rate increase, shown in **Fig. 4.58**.

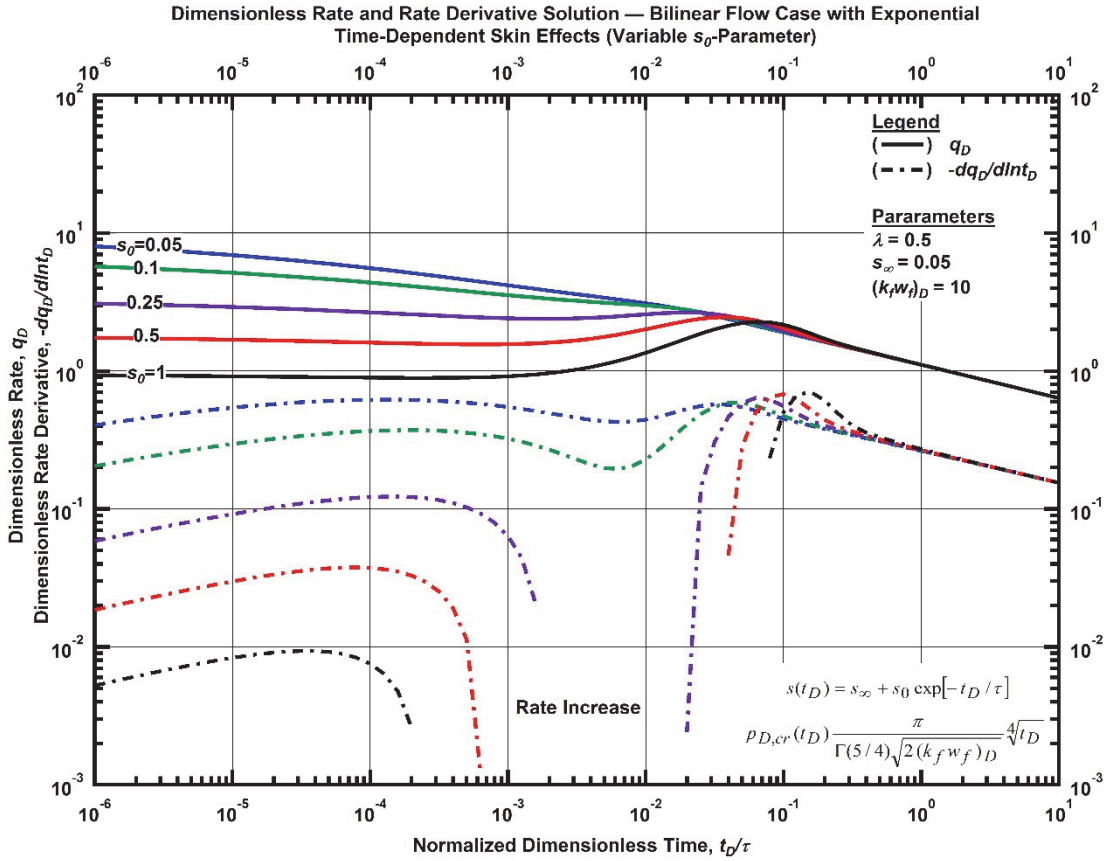

Figure 4.58 — Log-log plot (constant pressure dimensionless rate derivative solution) for the bilinear flow model combined with the exponential time-dependent skin effects for select values of s_0-parameter ($\tau = 0.01$).

The s_∞-parameter has less effect than the s_0-parameter, however, still exhibits the same early-time influence and transitional features, as illustrated by **Fig. 4.59**. The difference between the two parameters (s_∞-and s_0-parameter) proxies for the upper and lower limits of skin observed by the system, defines the magnitude of influence the exponential time-dependent skin factor has on the reservoir characteristic flow regime (*i.e.,* bilinear flow relation). The larger the difference, the more prominent the features.

The dimensionless fracture conductivity plays a significant role on when the system reaches the reservoirs late-time characteristic flow regime (*i.e.,* bilinear flow) as shown by **Fig. 4.60**. Clearly, for a low conductive fracture, the effects of a time-dependent skin factor are negligible. For an infinite conductivity fracture, the choked fracture skin effects are the only impediment to fluid flow within the fracture, therefore, play a significant impact on the transition to late-time reservoir characteristic flow behavior.

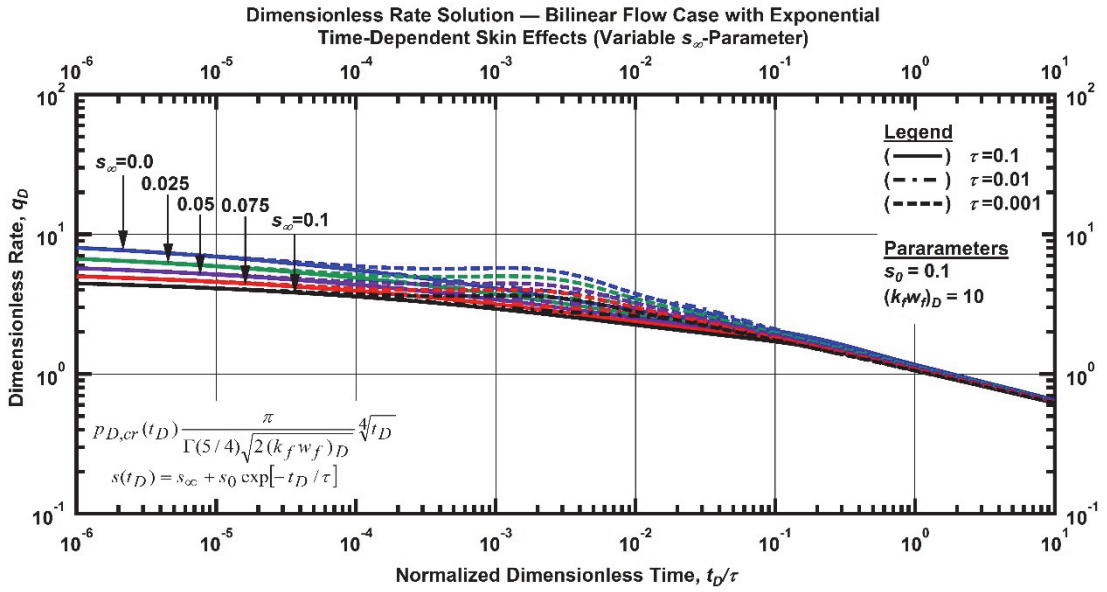

Figure 4.59 — Log-log plot (constant pressure dimensionless rate solution) for the bilinear flow model combined with the exponential time-dependent skin effects for select values of s_∞-parameter.

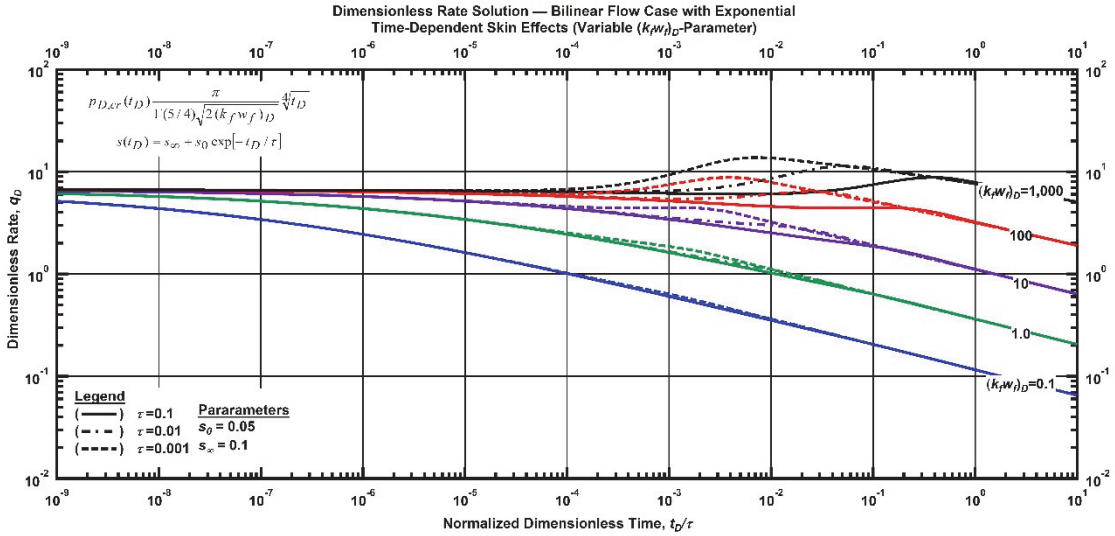

Figure 4.60 — Log-log plot (constant pressure dimensionless rate solution) for the bilinear flow model combined with the exponential time-dependent skin effects for select values of dimensionless fracture conductivity.

We observe, in **Fig. 4.61**, the significance of dimensionless fracture conductivity on the dimensionless cumulative production of the system. As observed, an infinite conductivity fracture will produce more hydrocarbon than a finite conductivity fracture.

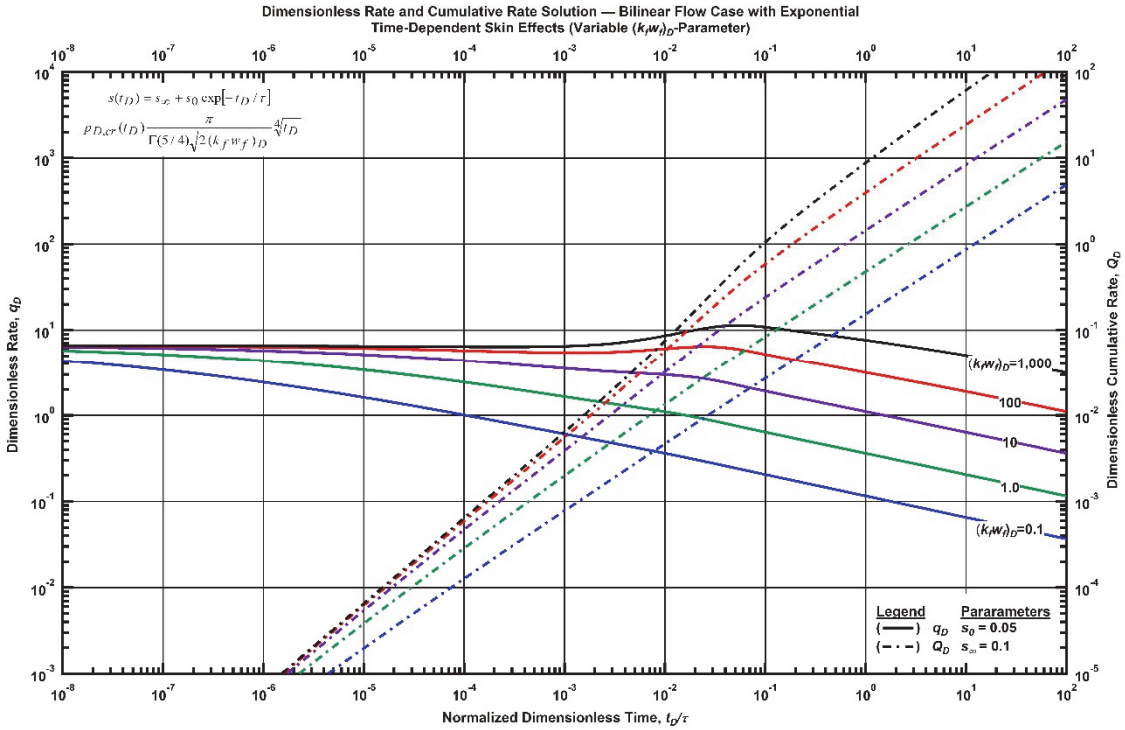

Figure 4.61 — Log-log plot (constant pressure dimensionless cumulative production solution) for the bilinear flow model combined with the exponential time-dependent skin effects for select values of dimensionless fracture conductivity ($\tau = 0.01$).

The previous example (**Fig. 4.57** — **Fig. 4.61**) demonstrates that the exponential time-dependent skin factor with bilinear flow has the same form as the same time-dependent function with the power-law and linear flow relations, the only difference being the late-time reservoir flow behavior. Diagnostic features include the desired "hockey-stick" flow profile, with an early-time flat or gently increasing (derivative is positive) flowrate, a rollover (*i.e.,* transition) feature with rate increase potential, dissipating into the late-time linear flow regime, characteristic of the reservoir. Dimensionless fracture conductivity imposes significant influence on the rate behavior, with higher conductivity fractures being influenced by time-dependent skin effects more than low conductivity fractures. These diagnostic features, representing empirical data, potentially provide the ability to quantify early-time or "flow-back" behavior. All diagnostic plots may be found in **Appendix F**.

4.14 Bilinear Flow Relation with Hyperbolic Time-Dependent Skin Effects

The hyperbolic time-dependent skin factor model is based on empirical observations from ultra-low permeability reservoirs. **Appendix D** provides a derivation of the constant pressure solution in the Laplace domain with exponential time-dependent skin effects and the bilinear flow regime.

As with previous flow regimes, following we examine the effect of each parameter, from the hyperbolic-time dependent skin factor, on the constant pressure solution to evaluate the potential application to field data.

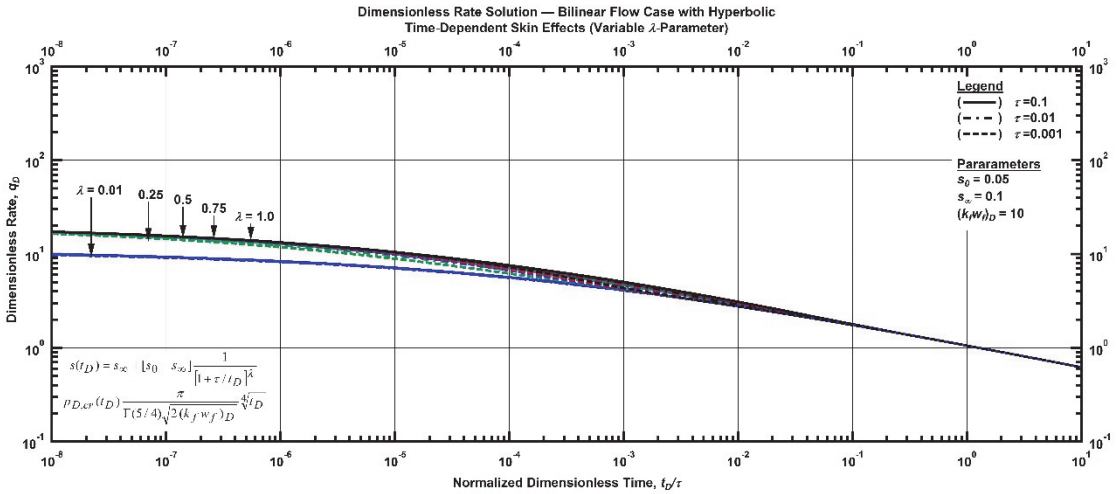

Figure 4.62 — Log-log plot (constant pressure dimensionless rate solution) for the bilinear flow model combined with the hyperbolic time-dependent skin effects for select values of λ-parameter.

Bounding the λ-parameter between zero and one for this work, in order to maintain consistency with the cumulative-exponential time-dependent skin factor, we notice little impact on the constant pressure solution, as shown by **Fig. 4.62**. The dimensionless rate derivative solution, shown in **Fig. 4.63**, has stronger features than the dimensionless rate solution providing behavioral characteristics for diagnosis, despite the potential difficulty in assessing this function in practice.

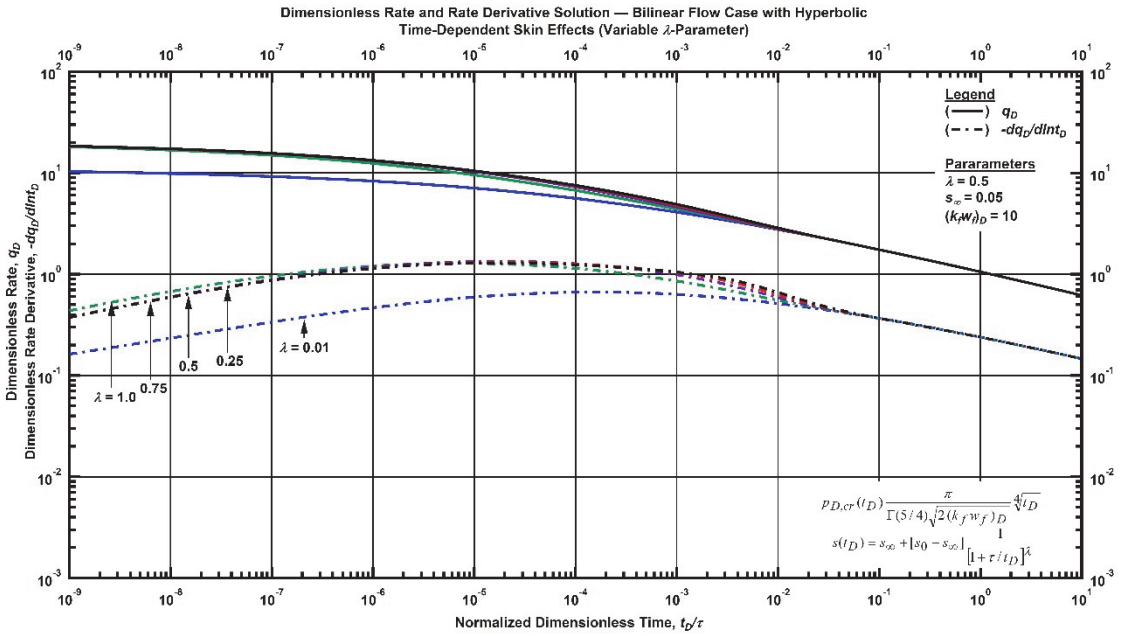

Figure 4.63 — Log-log plot (constant pressure dimensionless rate derivative solution) for the bilinear flow model combined with the hyperbolic time-dependent skin effects for select values of λ-parameter ($\tau = 0.01$).

A proxy for the systems maximum skin, the s_0-parameter affects the rate at which the system reaches the reservoir characteristic flow (*i.e.,* bilinear flow) as shown in **Fig. 4.64**. The s_∞-parameter affects the initial dimensionless flowrate as shown in **Fig. 4.65**, where the higher the s_∞-parameter, the lower the initial dimensionless flowrate. Validation of this model is achieved as the s_∞- and s_∞-parameters approach zero — *i.e.,* the time-dependent skin effects become negligible yielding only the bilinear flow regime.

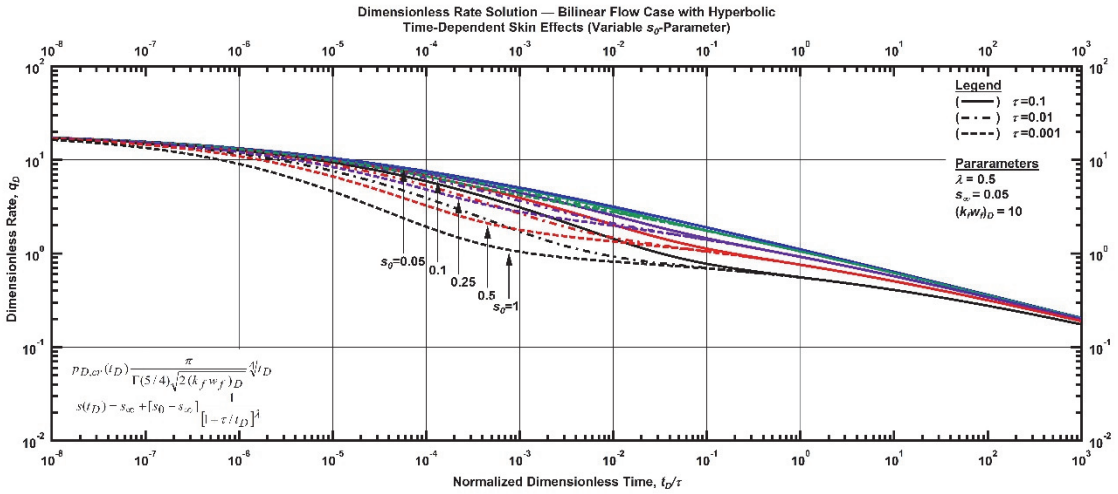

Figure 4.64 — Log-log plot (constant pressure dimensionless rate solution) for the bilinear flow model combined with the hyperbolic time-dependent skin effects for select values of s_0-parameter.

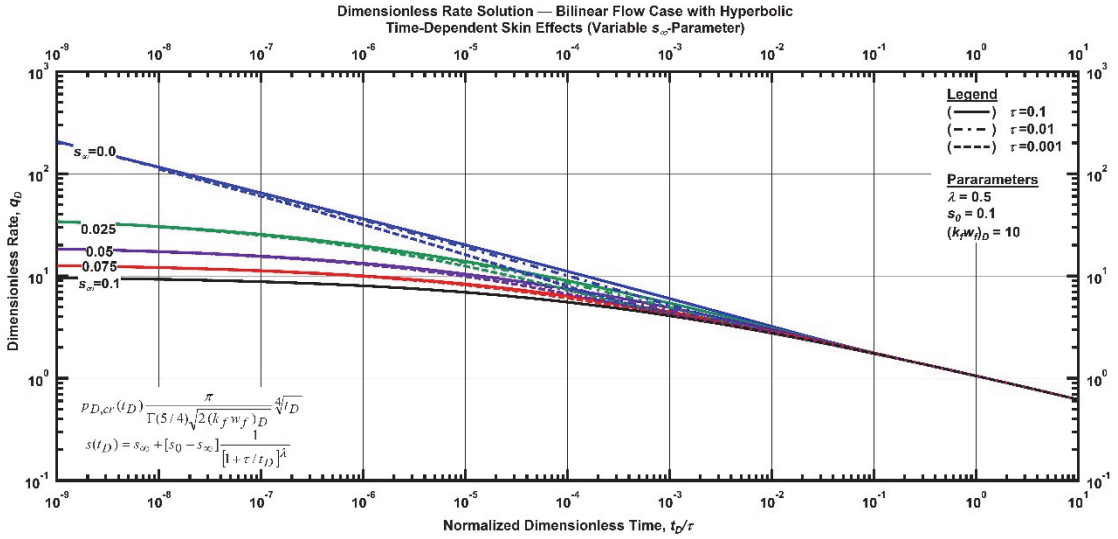

Figure 4.65 — Log-log plot (constant pressure dimensionless rate solution) for the bilinear flow model combined with the hyperbolic time-dependent skin effects for select values of s_∞-parameter.

The dimensionless fracture conductivity, shown in **Fig. 4.66**, imposes a significant impact on the final system flowrate. As observed with the power-law flow regime, the higher the fracture conductivity, the faster the system reaches reservoir characteristic flow (*i.e.,* bilinear flow). The dimensionless derivative rate solution yields more distinct features than the dimensionless rate solution, as shown in **Fig. 4.67**, providing further potential to diagnose reservoir behavioral characteristics.

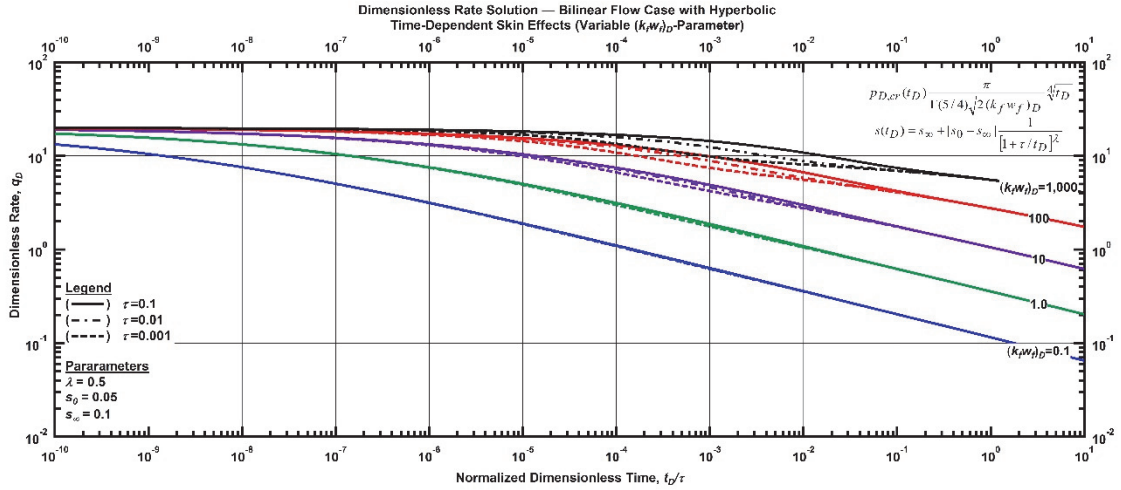

Figure 4.66 — Log-log plot (constant pressure dimensionless rate solution) for the bilinear flow model combined with the hyperbolic time-dependent skin effects for select values of the dimensionless fracture conductivity.

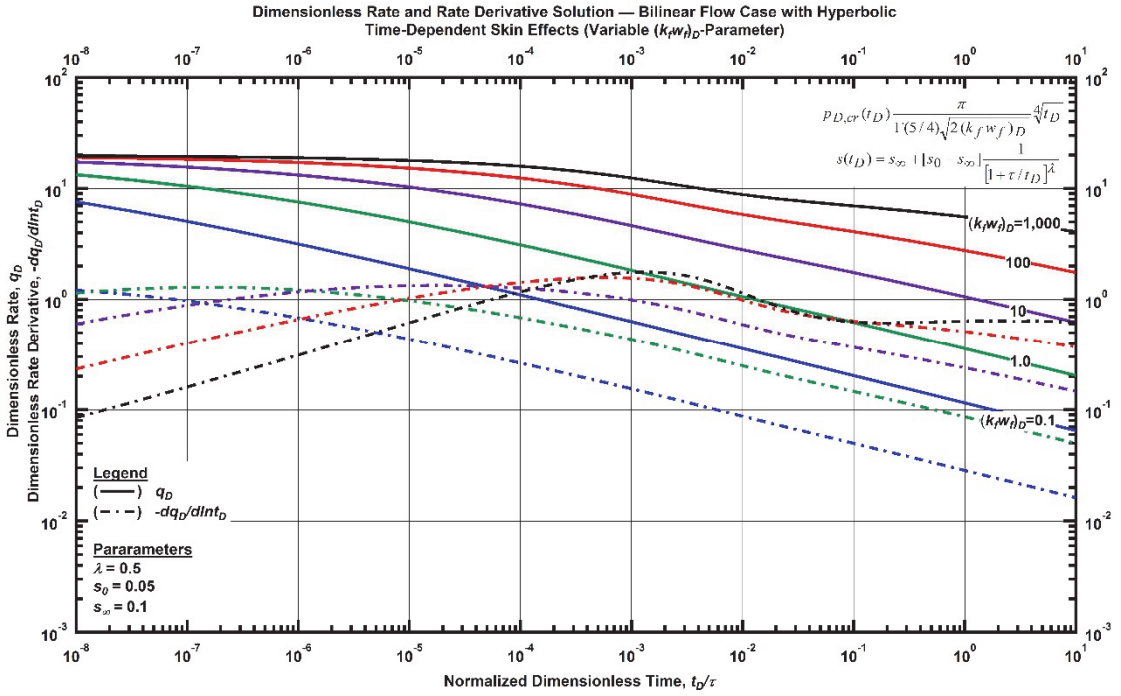

Figure 4.67 — Log-log plot (constant pressure dimensionless rate derivative solution) for the bilinear flow model combined with the hyperbolic time-dependent skin effects for select values of the dimensionless fracture conductivity (τ = 0.01).

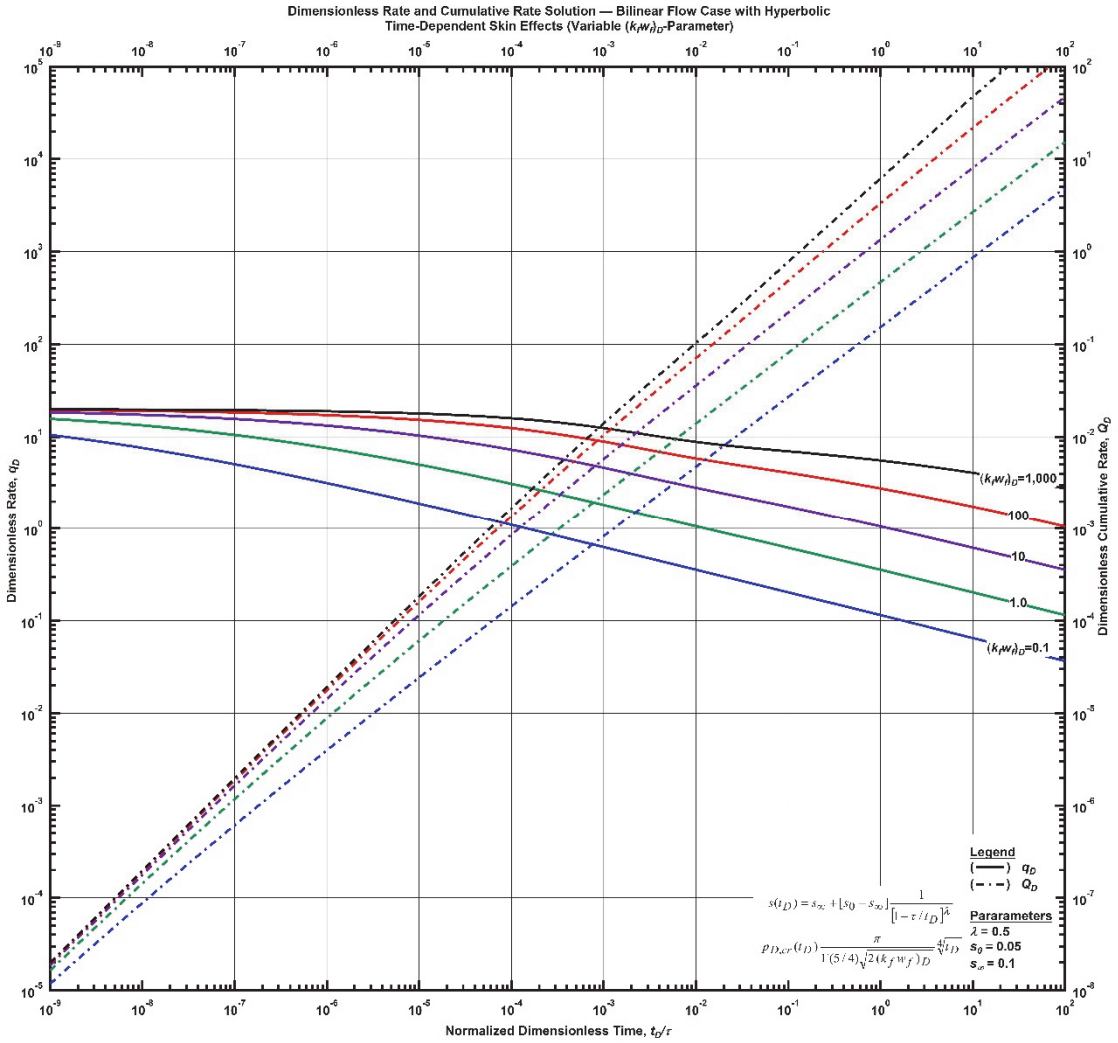

Figure 4.68 — Log-log plot (constant pressure dimensionless cumulative production solution) for the bilinear flow model combined with the hyperbolic time-dependent skin effects for select values of the dimensionless fracture conductivity ($\tau = 0.01$).

The dimensionless cumulative production solution, shown in **Fig. 4.68**, demonstrates the impact that a higher fracture conductivity has on the total production of a system. A highly conductive fracture (the author notes this evaluation was performed over 5 orders of magnitude for comparative purposes) will yield orders of magnitude more total production than a low-conductivity fracture.

Although the features observed in the time-normalized dimensionless cumulative rate solution, shown in **Fig. 4.69** are not unique in and of themselves, in conjunction with the dimensionless rate solution and other diagnostic plots demonstrated above, may provide additional diagnostic tool in order to characterize reservoir behavior

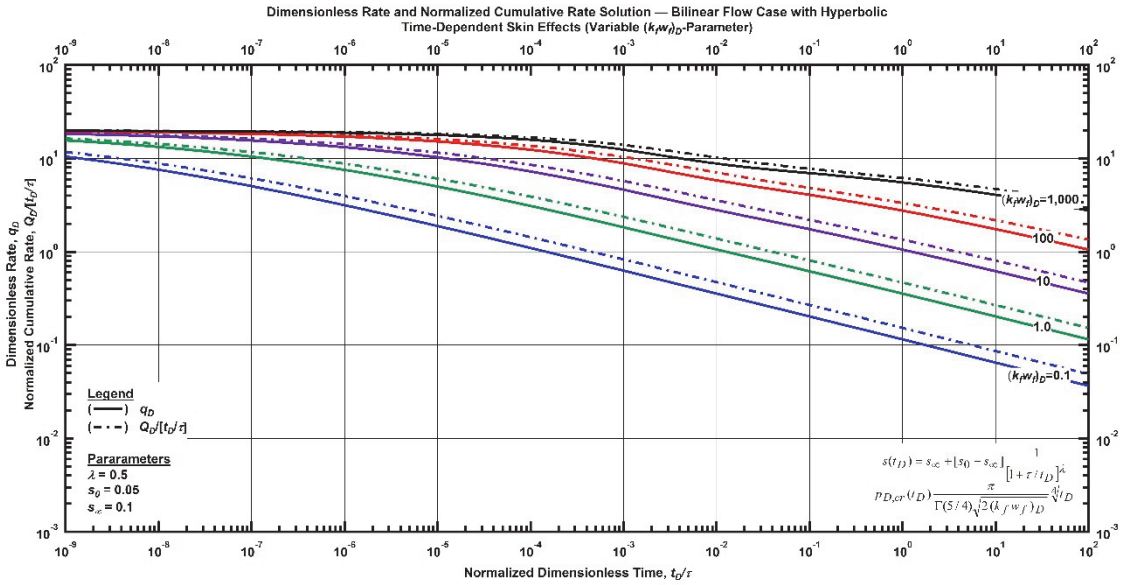

Figure 4.69 — Log-log plot (constant pressure time-normalized dimensionless cumulative rate solution) for the bilinear flow model combined with the hyperbolic time-dependent skin effects for select values of the dimensionless fracture conductivity ($\tau = 0.01$).

The hyperbolic time-dependent skin factor models are consistent regardless of the flow regime to which it is applied, as is demonstrated through the examples in **Sections 4.4** and **4.8**. The hyperbolic time-dependent skin effects only differ from example to example only based on the late-time reservoir signature — *i.e.,* early-time and transitional behavior are consistent are regardless of the reservoir characteristic flow regime.

4.15 Bilinear Flow Relation with Time-Dependent Wellbore Storage

As with previous examples, we apply the concept of Fair (1990) proposed wellbore phase redistribution pressure on the bilinear flow regime to compare performance against the other two flow relations examined. Fully derived in **Appendix E**, we demonstrate the viability of this work by evaluating the effect of each parameter within the model plotting the constant pressure dimensionless rate solution against dimensionless time. Further diagnostic plots are generated including the dimensionless rate derivative solution, the dimensionless cumulative production solution and the time-normalized dimensionless cumulative rate solution to further evaluate the validity of this model. This section contains a summary of diagnostic plots for this model, while a comprehensive examination may be found in **Appendix F**.

Over the limited range considered, the α-parameter, shown in **Fig. 4.70**, imposes little impact on the constant pressure solution. The dimensionless derivative rate solution has much stronger features than the dimensionless rate solution, and although this may be difficult to assess in practice, we note this behavior for the potential diagnostic capabilities.

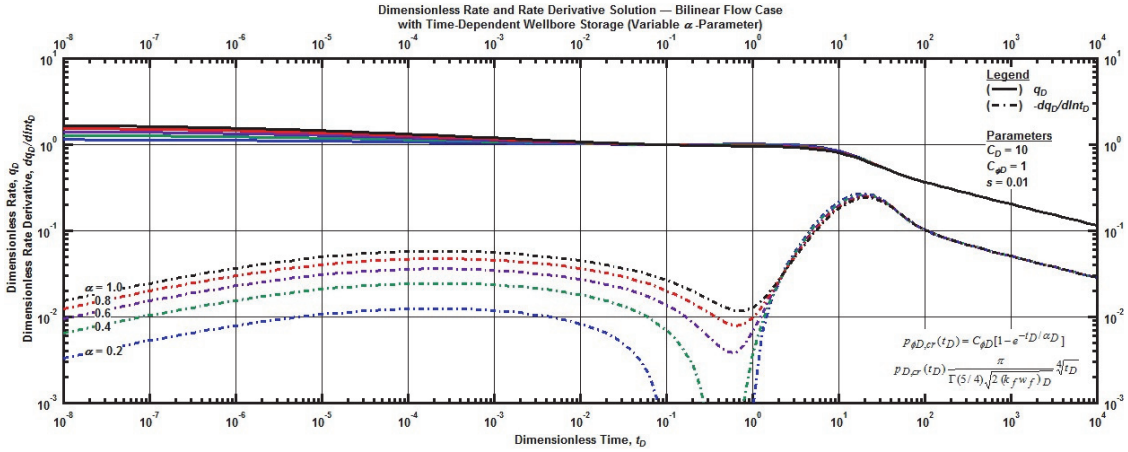

Figure 4.70 — Log-log plot (constant pressure dimensionless rate and rate derivative solution) for the bilinear flow model combined with the time-dependent wellbore storage for select values of the α-parameter.

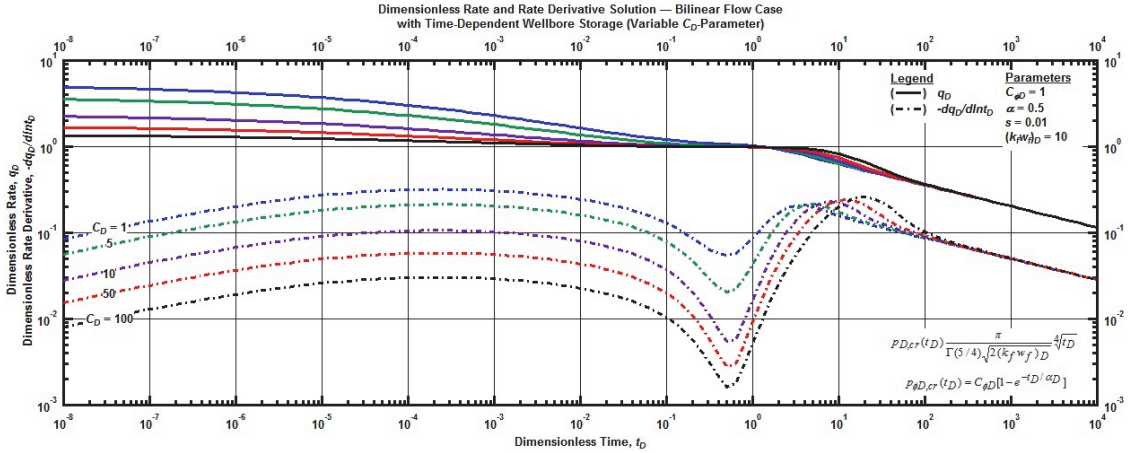

Figure 4.71 — Log-log plot (constant pressure dimensionless rate and rate derivative solution) for the bilinear flow model combined with the time-dependent wellbore storage for select values of dimensionless wellbore storage constant.

As shown in **Fig. 4.71**, the dimensionless wellbore storage constant (C_D) provides variations in both early-time behavior and during the rollover (*i.e.,* transition) region before dissipating into late-time bilinear flow. This behavior is nearly identical to that found with the power-law and linear flow regimes, save for the late-time reservoir flow characteristics are altered. As the wellbore storage influence diminishes with time, the rate is governed by bilinear flow regime.

The dimensionless wellbore phase redistribution constant ($C_{\phi D}$), shown in **Fig. 4.72**, has a similar influence as the dimensionless wellbore storage constant (C_D), affecting both early-time and the transition region.

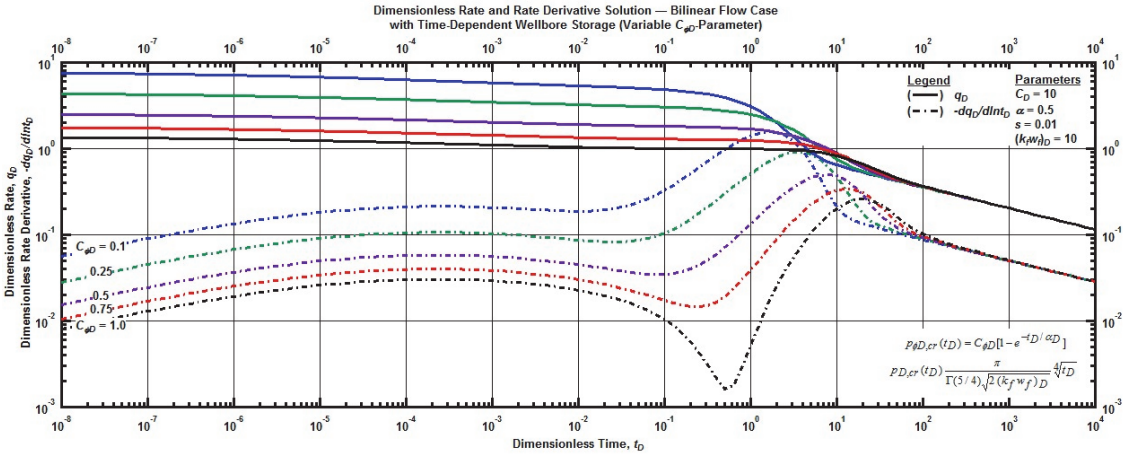

Figure 4.72 — Log-log plot (constant pressure dimensionless rate and rate derivative solution) for the bilinear flow model combined with the time-dependent wellbore storage for select values of dimensionless wellbore phase redistribution constant.

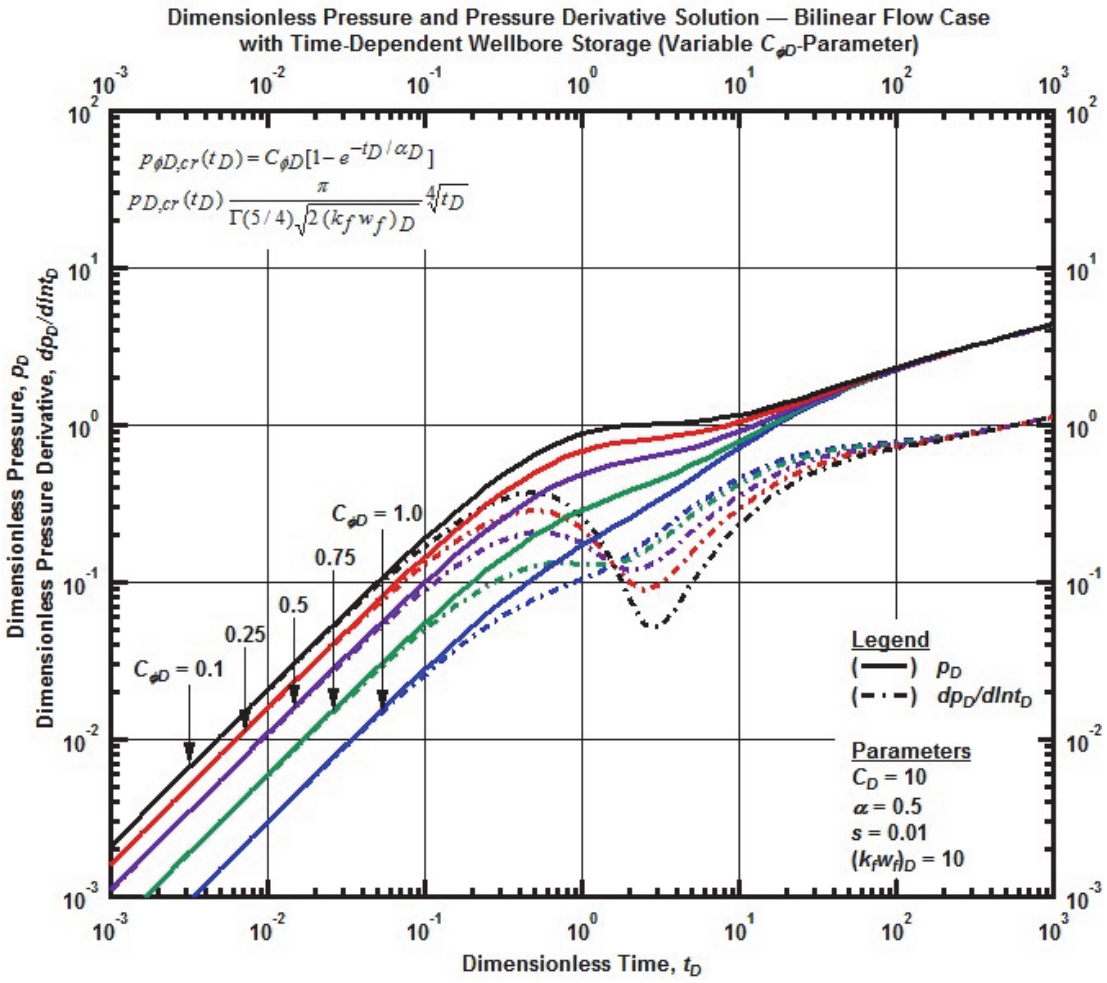

Figure 4.73 — Log-log plot (constant rate dimensionless pressure and pressure derivative solution) for the bilinear flow model combined with the time-dependent wellbore storage for select values of dimensionless wellbore phase redistribution constant.

The constant-rate dimensionless pressure derivative "bubble" feature is demonstrated through evaluation of the dimensionless wellbore phase redistribution constant ($C_{\phi D}$), shown in **Fig. 4.72**. This "anomalous" pressure build-up is the basis of Fair's (1981) work, which we have captured in our constant pressure solution.

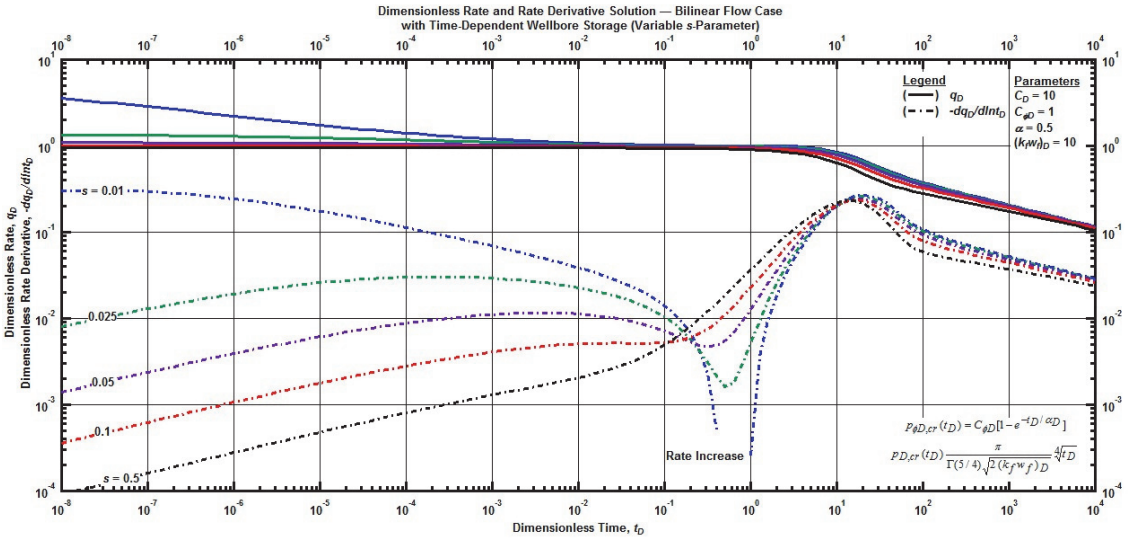

Figure 4.74 — Log-log plot (constant pressure dimensionless rate and rate derivative solution) for the bilinear flow model combined with the time-dependent wellbore storage for select values of constant skin factor.

The skin factor, held constant for the time-dependent wellbore storage case, imposes little impact on the constant pressure solution (over the range considered). The rate derivative has much stronger features than the rate function as shown in the early-time variations demonstrated in **Fig. 4.74**. At small values of skin, a rate increase is observed highlighted by the derivative trending towards zero. As with the other flow regimes, the combined effect of skin and time-dependent wellbore storage may be difficult (if impossible) to assess in practice, however, diagnostic features may be developed in order to characterize reservoir behavior.

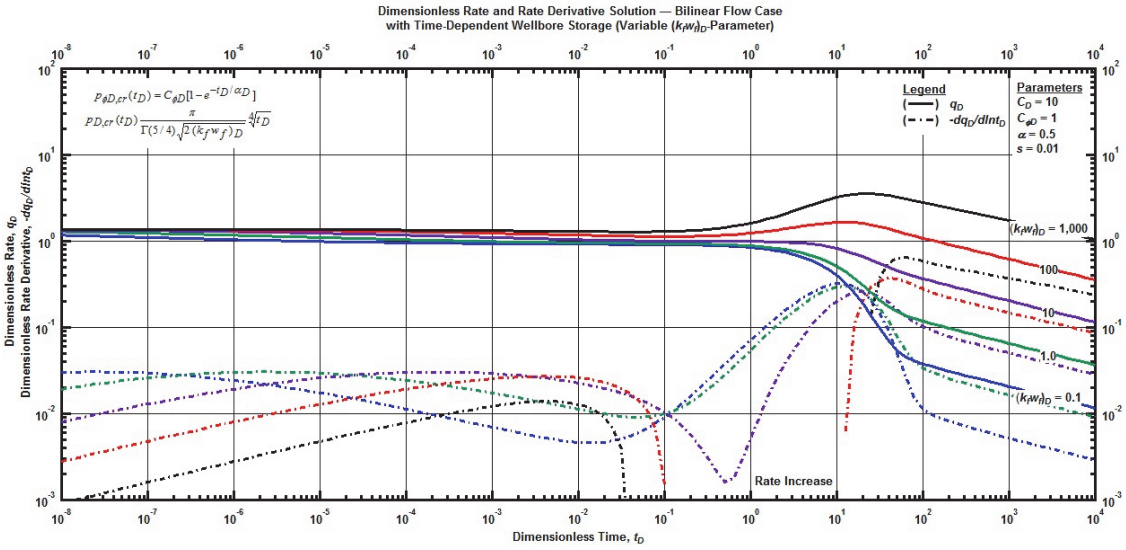

Figure 4.75 — Log-log plot (constant pressure dimensionless rate and rate derivative solution) for the bilinear flow model combined with the time-dependent wellbore storage for select values of dimensionless fracture conductivity.

The dimensionless fracture conductivity, shown in **Fig. 4.75**, imposes a significant impact on the constant pressure solution. A large fracture conductivity may cause the dimensionless rate to increase during the transition region before dissipating into the reservoir characteristic flow (*i.e.,* bilinear flow).

As shown in the previous example (**Fig. 4.70** — **Fig. 4.75**) a time-dependent wellbore storage model (inclusive of a constant skin factor) may be used to represent observed features from field data. These features include flat to gently increasing (derivative is positive) at early-time rate transitioning into a late-time bilinear flow. The dimensionless flowrate during the transition region may rollover directly, or increase slightly before the late-time reservoir flow signature is reached. In all cases, the dimensionless rate derivative exhibit a "hump" feature indicative of a commonly observed wellbore storage "bubble" (which is seen in the constant-rate dimensionless pressure function, **Fig. 4.73** for reference).

4.16 Time-Dependent Wellbore Storage and Skin Effects

Recognizing that time-dependent wellbore storage and time-dependent skin effects will, individually, be very challenging to distinguish within field data, we never-the-less continue our work along it logical progression and examine the combined effects of both time-dependent models. Evaluating the cumulative-exponential time-dependent skin effects with time-dependent wellbore storage, yields the following diagnostic plots.

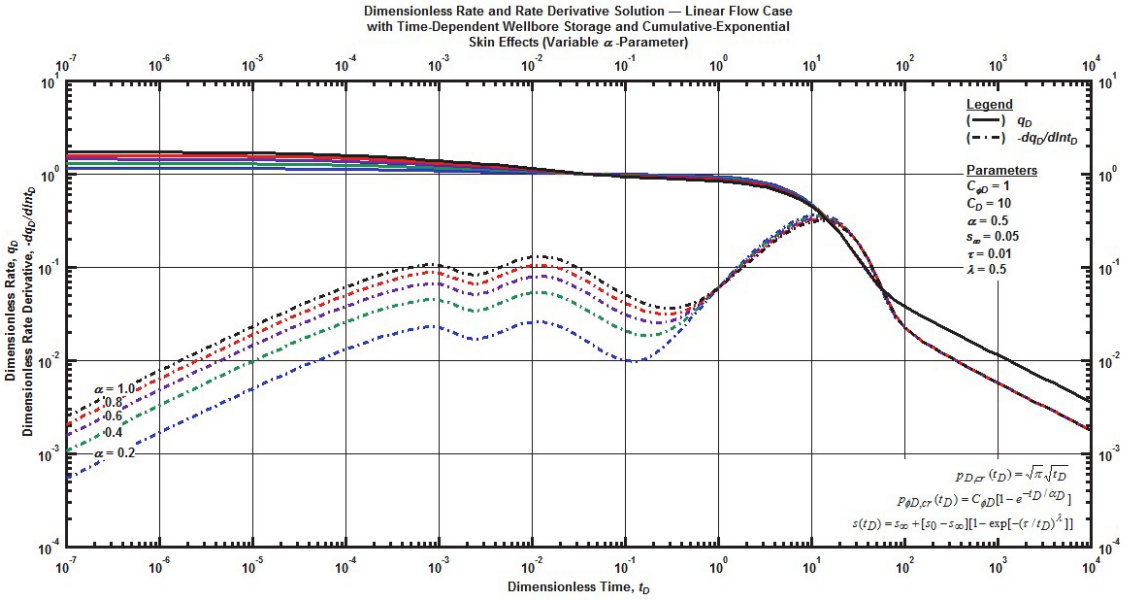

Figure 4.76 — Log-log plot (constant pressure dimensionless rate and rate derivative solution) for the linear flow model combined with the time-dependent wellbore storage and cumulative-exponential skin effects for select values of the α-parameter.

For the limited range we considered, the α-parameter, shown in **Fig. 4.76**, imposes little impact on the constant pressure solution. The derivative displays much stronger features than the rate function. The author acknowledges the difficulty in assessing this function in practice — however, the "double-hump" in the constant pressure derivative is a notable feature, which may be possible for use as a diagnostic characteristic.

The dimensionless wellbore storage constant (C_D) shown in **Fig. 4.77**, provides variations in both early-time behavior and the transition region. As the wellbore storage influence diminishes over time, the rate is governed by the specified linear flow solution. The dimensionless wellbore phase redistribution constant ($C_{\phi D}$), shown in **Fig. 4.78**, displays similar features as the dimensionless wellbore storage constant (C_D),

affecting the rate at early-times and dissipating to yield the linear flow solution at late-times. Both parameters rate derivative plot display the characteristic "double-hump" as shown in the rate derivative of the α-parameter.

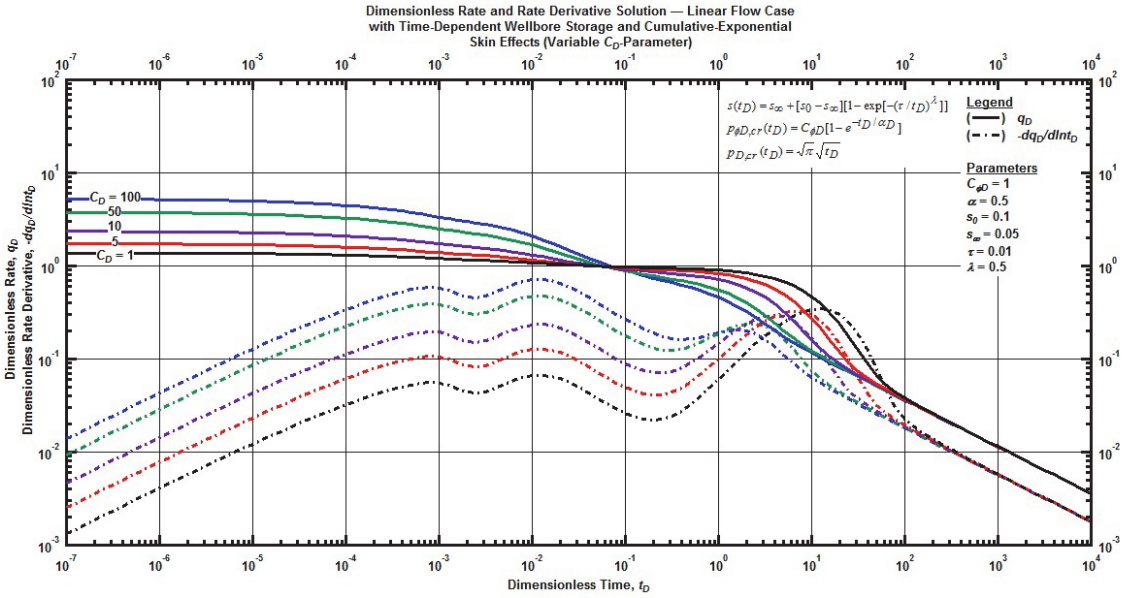

Figure 4.77 — Log-log plot (constant pressure dimensionless rate and rate derivative solution) for the linear flow model combined with the time-dependent wellbore storage and cumulative-exponential skin effects for select values of dimensionless wellbore storage constant.

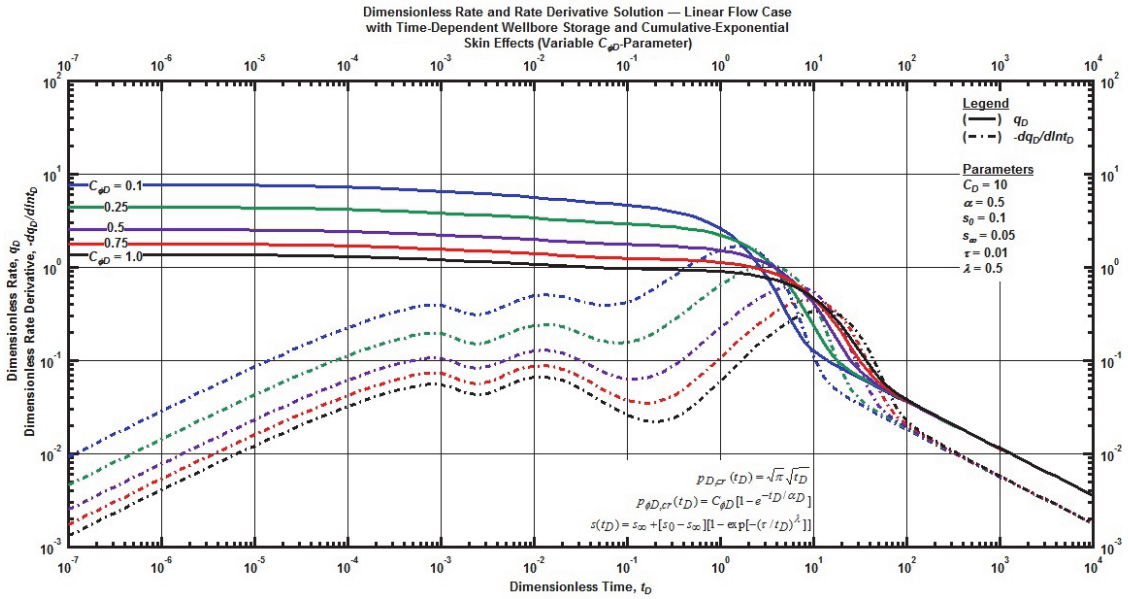

Figure 4.78 — Log-log plot (constant pressure dimensionless rate and rate derivative solution) for the linear flow model combined with the time-dependent wellbore storage and cumulative-exponential skin effects for select values of dimensionless phase redistribution constant.

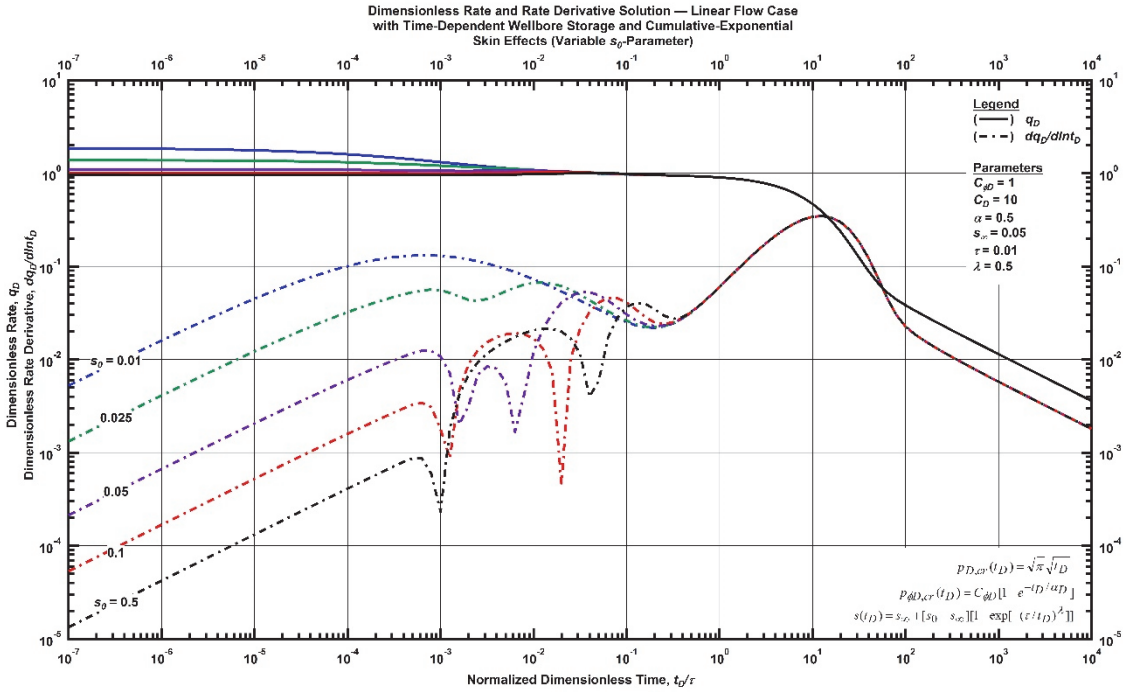

Figure 4.79 — Log-log plot (constant pressure dimensionless rate and rate derivative solution) for the linear flow model combined with the time-dependent wellbore storage and cumulative-exponential skin effects for select values of the s_0-parameter.

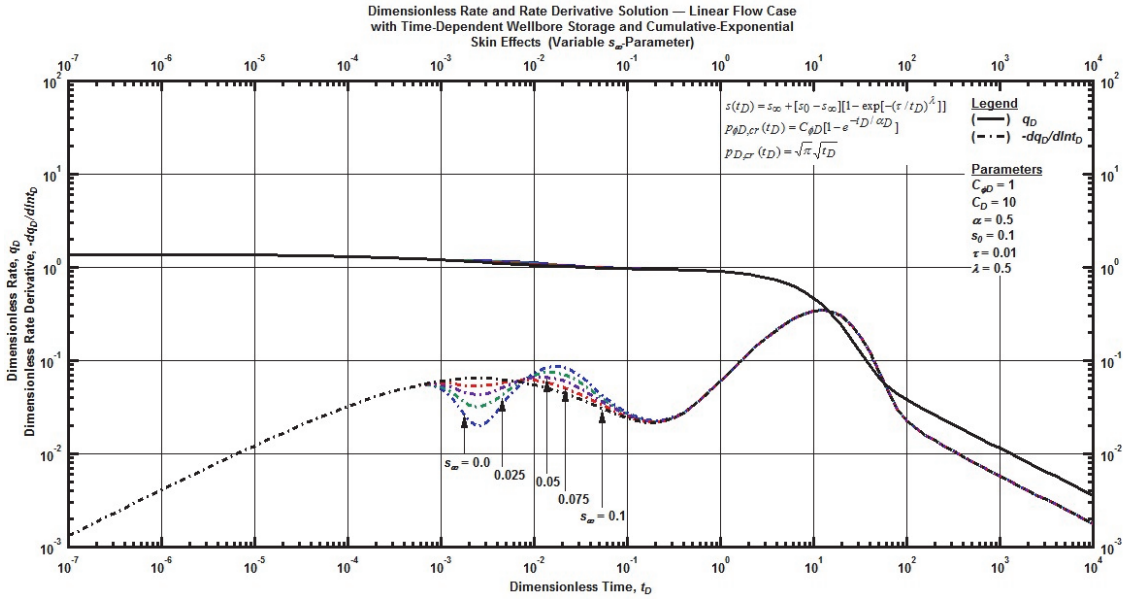

Figure. 4.80 — Log-log plot (constant pressure dimensionless rate and rate derivative solution) for the linear flow model combined with the time-dependent wellbore storage and cumulative-exponential skin effects for select values of the s_∞-parameter.

The s_0-parameter and s_∞-parameter affect the flow rate before the transition "rollover" feature to late time linear flow. The s_0-parameter, shown in **Fig. 4.79**, causes the rate to increase slightly. The rate derivative then illustrates the double change in slope by twice tending towards a zero value. The time-dependent skin effect is clearly illustrated in **Fig. 4.80** examining the rate derivative. In all previous examples, the skin factor has had a negligible effect on the time-dependent wellbore storage, which is clearly not the case in this example.

From the previous example, (**Fig. 4.76** — **Fig. 4.80**), we observe a unique behavior that, theoretically, has the potential to provide diagnostic characteristics for a vertically fractured well. However, in practice, we acknowledge the difficult, if impossible, task of evaluate the combined effects of time-dependent wellbore storage and skin factor from field data.

CHAPTER V

SUMMARY, CONCLUSIONS, AND RECOMMENDATIONS FOR FUTURE WORK

5.1 Summary

In an effort to quantify "early-time" or "flowback" performance of a hydraulically fractured vertical well, we have postulated a series of time-dependent wellbore storage and skin factor models which appear to describe observed features from field data. Using, as a foundation, Larsen and Kviljo's (1990) hyperbolic variable skin model, developed to describe the lowering skin factor during wellbore cleanup, our time-dependent skin factor models are given as:

$$s(t_D) = s_\infty + [s_0 - s_\infty][1 - \exp[-(\tau / t_D)^\lambda]] \quad \text{(cumulative-exponential, } s(t)\text{)} \quad (5.1)$$

$$s(t_D) = s_\infty + s_0 \exp[-(t_D / \tau)] \quad \text{(exponential, } s(t)\text{)} \quad (5.2)$$

$$s(t_D) = s_\infty + [s_0 - s_\infty]\frac{1}{[1 + \tau / t_D]^\lambda} \quad \text{(hyperbolic, } s(t)\text{)} \quad (5.3)$$

Fair (1981) proposed a wellbore phase redistribution pressure to account for the anomalous pressure "humps" sometimes observed during pressure build-up tests conducted in two-phase flow systems. Fair's (1981) exponential wellbore phase redistribution pressure is given as:

$$p_{\phi D}(t_D) = C_{\phi D}(1 - e^{-t_D / \alpha_D}) \quad \text{(wellbore phase redistribution)} \quad (5.4)$$

In this work, we wanted to keep our concepts simple so we assumed that reservoir flow is dominated by linear or bilinear flow regimes with "base" approximations for formation flow regimes given as:

$$p_{D,cr}(t_D) = c_1 t_D^{\,v} \quad \text{(general power-law flow)} \quad (5.5)$$

$$p_{D,cr}(t_D) = \sqrt{\pi}\sqrt{t_D} \quad \text{(formation linear flow)} \quad (5.6)$$

$$p_{D,cr}(t_D) = \frac{\pi}{\Gamma(5/4)\sqrt{2(k_f w_f)_D}}\sqrt[4]{t_D} \quad \text{(bilinear flow)} \quad (5.7)$$

Through the use of the convolution integral, with most of our algebraic manipulations performed in the Laplace domain, we examine the performance of the constant pressure rate solutions, numerically inverting the Laplace domain formulations using the Stehfest algorithm. Unfortunately, analytical solutions of the proposed formulations are essentially impossible to generate due to the complexity of the algebraic forms of these formulations in the Laplace domain.

We examine the performance of each time-dependent wellbore storage and skin model with each reservoir flow regime, evaluating the effects of each model parameter on the computed rate performance. Our results indicate that the proposed time-dependent models demonstrate characteristics similar to those

observed in field data (*i.e.,* rate "humps" and nearly constant rate performance at early times). In theory, this would could provide diagnostic capabilities for early-time well performance behavior during "clean-up" after well stimulation. We acknowledge that our proposed models have yet to be directly verified against field cases.

A major accomplishment of this work is the development of a general procedure for modeling early-time well clean-up behavior. We believe that this theory may be applicable to other fields of research — including multi-fracture horizontal wells.

5.2 Conclusions

- The time-dependent skin factor models yield features observed in field data. Subtle differences between models will likely yield an optimal model for practical application.
  - All time-dependent skin factor models exhibit certain features including the "hockey-stick" shape, with dimensionless flowrate gently increasing at early times, followed by a "rollover" (*i.e.,* transition) feature, with all flowrates converging to the characteristic reservoir (*i.e.,* power-law, linear or bilinear) flow regime (which is the reservoir model for the constant pressure case).
  - The cumulative-exponential time dependent skin factor demonstrates a rate increase during the "rollover" feature, and has a strong "transition" regime as the performance tends to be dominated by the reservoir flow behavior. This makes it likely to be the most applicable in practice.
  - The exponential time dependent skin factor demonstrates a rate increase during the "rollover" feature, but has a fixed duration of the time-dependent skin effect.
  - The hyperbolic time-dependent skin factor does not demonstrate a rate increase during the "rollover" feature — however, this model can be tuned to have a very long transition period.
- For the time-dependent wellbore storage case, we observe a monotonically decreasing dimensionless rate profile that is roughly "s-shaped," where all cases converge to the characteristic reservoir flow regime (*i.e.,* power-law, linear or bilinear) at late times.
- We believe that the derivative of the constant pressure dimensionless rate function has the potential to provide diagnostic capabilities. We would also comment that the cumulative production, and normalized cumulative production functions also have good character, but less sharpness in features compared to the derivative of the constant pressure dimensionless rate function.

5.3 Recommendations for Future Work

- Perform field tests to verify the applicability of each time-dependent functional form.
- Perform analytical inversion of the models from the Laplace domain (currently not possible).
- This workflow should be exhaustively applied to field cases for vertically fractured wells.
- This workflow should be extended to field cases for multi-fractured horizontal wells.

REFERENCES

Abramowitz, M. & Stegun, I. A. 1972. *Handbook of Mathematical Functions with Formulas, Graphs and Mathematical Tables*, New York City, Dover Publishing Inc.

Agarwal, R. G., Al-Hussainy, R., & Ramey, H. J., 1970. An Investigation of Wellbore Storage and Skin Effect in Unsteady Liquid Flow: I. Analytical Treatment. SPE-2455, http://dx.doi.org/10.2118/2466-PA

Blasingame, T.A. 1994. Development and Application of Concepts in Wellbore Storage Distortion, *Class Notes PETE 620*, College Station, TX, Texas A&M University. http://www.pe.tamu.edu/blasingame/data/z_zCourse_Archive/P620_15C/P620_15C_Lectures_(base)/P620_Lec_27_Mod4_ResFlw_08_WellboreStrg.pdf

Bourgeois, M. J. & Horne, R. H., 1993. Well-Test-Model Recognition with Laplace Space. SPE-22682. http://dx.doi.org/10.2118/22682-PA

Cheng, A. H-D., Sidauruk, P., & Abousleiman, Y., 1994. Approximate Inversion of the Laplace Transform. The Mathematica Journal. 4 (2): 76-82

Cinco-Ley, H. & Samaniego, V. F. 1977. Effect of Wellbore Storage and Damage on the Transient Pressure Behavior of Vertically Fractured Wells. Presented at the 52nd Annual Fall Technical Conference and Exhibition. SPE-6752. http://dx.doi.org/10.2118/6752-MS

Cinco-Ley, H., Samaniego, V. F. & Dominguez, A. N., 1978. Transient Pressure Behavior for a Well with a Finite-Conductivity Vertical Fracture. Presented at the 51st Annual Fall Technical Conference and Exhibition. SPE-6014. http://dx.doi.org/10.2118/6014-MS

Cinco-Ley, H. & Samaniego V. F., 1981a. Transient Pressure Analysis for Fractured Wells. SPE-7490. http://dx.doi.org/10.2118/7490-PA

Cinco-Ley, H. & Samaniego V. F., 1981b. Transient Pressure Analysis: Finite Conductivity Fracture Case Versus Damaged Fracture Case. Presented at 56th Annual Fall Technical Conference and Exhibition. SPE-10179. http://dx.doi.org/10.2118/10179-PA

Cinco-Ley, H. & Samaniego V. F., 1982. Pressure Transient Analysis for Naturally Fractured Reservoirs. Presented at 57th Annual Fall Technical Conference and Exhibition. SPE-11026. http://dx.doi.org/10.2118/11026-MS

Cinco-Ley, H. 1982. Evaluation of Hydraulic Fracturing by Transient Pressure Analysis Methods. Presented at the International Petroleum Exhibition and Technical Symposium. SPE-10043. http://dx.doi.org/10.2118/10043-MS

Cohen, A. M., 2007. Quadrature Methods. In *Numerical Methods for Laplace Transform Inversion,* Vol. 5 Springer Publishing, Chap. 4.4, 87. New York, USA

Davis, B. & Martin, B., 1979. Numerical Inversion of the Laplace Tansform: A Survey and Comparison of Methods. *Journal of Computational Physics*. Vol. 33. No. 1. 0021-9991/79/100001

Earlougher, R. C., 1977. *Advances in Well Test Analysis*. Monograph Vol. 5. Chap. 2, 2-20. Richardson, TX, SPE.

Economides, M. J., Hill, A. D., Ehlig-Economides, C., Zhu., D., 2013. *Petroleum Production Systems.* 2nd Edition. Chapter 1, pp. 1-18. Upper Saddle River, New Jersey, USA. Pearson Education, Inc.

Ehlig-Economides, C. A., 1979. *Well Test Analysis for Wells Produced at a Constant Pressure*. PhD Dissertation, Stanford University, Stanford, California (June 1979)

Fair, W. B. Jr., 1981. Pressure Buildup Analysis with Wellbore Phase Redistribution. SPE-8206. http://dx.doi.org/10.2118/8206-PA

Gringarten, A.C., Ramey, H. J., & Raghavan, R., 1974. Unsteady-State Pressure Distributions Created by a Well with a Single Infinite-Conductivity Vertical Fracture. SPE 4051. http://dx.doi.org/10.2118/4050-PA

Gringarten, A.C., Ramey, H. J., & Raghavan, R., 1974. Applied Pressure Analysis for Fractured Wells. SPE 5496. http://dx.doi.org/10.2118/5496-PA

Larson, L. & Kviljo, K., 1990. Variable-Skin and Cleanup Effects in Well-Test Data. SPE-15581. http://dx.doi.org/10.2118/15581-PA

Lee, J. Rollins, J.B., & Spivey, J.P., 2003. *Pressure Transient Testing*, Richardson, TX: Society of Petroleum Engineers.

Ramey, H. J., 1970. Short-Time Well Test Data Interpretation in the Presence of Skin Effect and Wellbore Storage. *Journal of Petroleum Technology*. **January** (1970): 97-104. SPE-2336

Roberts, G.E., & Kaufman, H., 1966. *Table of Laplace Transforms*. Philadelphia, PA: W. B. Saunders Company.

Spiegel, M. R., 1971. *Schaum's Outline of Advanced Mathematics for Engineers and Scientists.* USA. The McGraw-Hill Companies, Inc.

Stegemeier, G. L., & Matthews, C. S., 1958. A Study of Anomalous Pressure Build-Up Behavior. *Petroleum Transactions, AIME*. **213**: 44-50. SPE-927G. http://dx.doi.org/10.2118/SPE-927-G.

Valdes-Perez, A. R., Pulido, H., Cinco-Ley, H., & Galicia-Munoz, G., 2011. A New Bilinear Flow Model for Naturally Fractured Reservoirs with Transient Interporosity Transfer. Presented at the 36th Workshop on Geothermal Reservoir Engineering, Stanford University, Stanford, California, January 31 – February 2, 2011. SGP-TR-191

Valkó, P.P and Abate, K., 2004. Comparison of Sequence Accelerators for the Gaver Method of Numerical Laplace Transform Inversion, *Computers and Mathematics with Application*, **48** (Iss. 3-40) pp 629-636.

Van Everdingen, A. F., 1953. The Skin Effect and Its Influence on the Productive Capacity of a Well. *Petroleum Transactions,* AIME. **198**: 171-176. SPE-203. http://dx.doi.org/10.2118/203-G

Van Everdingen, A. F., & Hurst, W., 1949. The Application of the Laplace Transformation to Flow Problems in Reservoirs. *Petroleum Transactions,* AIME. **December**: 305-324B. SPE-2732. http://dx.doi.org/10.2118/2732

Wolfram Mathematica 10, 2007. https://www.wolfram.com/mathematica/

NOMENCLATURE

Field Variables

B = Formation volume factor, [bbl/STB] or [Rm^3/Sm^3]
c_t = Total compressibility, $(M/Lt^2)^{-1}$ [Pa^{-1}] or [psi^{-1}]
C_s = Wellbore storage constant, $L^2/(M/Lt^2)$ [bbl/psi] or [m^3/Pa]
C_Φ = Wellbore phase redistribution constant, $L^2/(M/Lt^2)$ [bbl/psi] or [m^3/Pa]
h = Net pay thickness, L [m] or [ft]
k = Permeability, L^2 [mD] or [m^2]
k_f = Fracture permeability, L^2 [mD] or [m^2]
k_s = Damaged reservoir permeability, L^2 [mD] or [m^2]
k_{fs} = Damaged fracture permeability, L^2 [mD] or [m^2]
$k_f w_f$ = Fracture conductivity, L^3 [mD-ft] or [m^3]
p = Pressure, M/Lt^2 [Pa] or [psi]
p_i = Initial reservoir pressure, M/Lt^2 [Pa] or [psi]
p_f = Fracture pressure, M/Lt^2 [Pa] or [psi]
p_s = Wellbore flowing pressure inclusive wellbore skin, M/Lt^2 [Pa] or [psi]
p_{wf} = Wellbore flowing pressure, M/Lt^2 [Pa] or [psi]
p_Φ = Wellbore phase redistribution pressure, M/Lt^2 [Pa] or [psi]
p_t = Tubing flowing pressure at surface, M/Lt^2 [Pa] or [psi]
r = Radial distance, L [m] or [ft]
r_s = Damaged skin zone radial distance, L [m] or [ft]
r_w = Wellbore radius, L [m] or [ft]
r_D = Dimensionless radius, dimensionless
s = Skin factor, dimensionless
s_f = Fracture face skin factor, dimensionless
$s_{f,ch}$ = Choked fracture skin factor, dimensionless
s_o = Maximum skin factor, dimensionless
s_∞ = Minimum skin factor, dimensionless
q = Flowrate, L^3/t [m^3/sec] or [ft^3/s]
q_D = Dimensionless flowrate, dimensionless
$q_{sf\alpha}$ = Sandface flowrate, L^3/t [m^3/sec] or [ft^3/s]
t = Time, t [sec]
t_D = Dimensionless time, dimensionless
u = Laplace transform variable
V_i = Stehfest extrapolation coefficient, dimensionless
V_{wb} = Wellbore volume, L^3 [m^3] or [ft^3]
w_f = Fracture width, L [m] or [ft]
w_s = Damaged zone width, L [m] or [ft]
x_f = Fracture half length, L [m] or [ft]
x_w = Wellbore length in x-direction, L [m] or [ft]
y_w = Wellbore length in y-direction, L [m] or [ft]

Dimensionless Field Variables

C_D = Dimensionless wellbore storage constant
$C_{\Phi D}$ = Dimensionless wellbore phase redistribution constant
k_{fD} = Dimensionless damaged fracture permeability
$(k_f w_f)_D$ = Dimensionless fracture conductivity
p_D = Dimensionless wellbore flowing pressure
p_{wD} = Dimensionless wellbore flowing pressure inclusive wellbore storage and skin
p_{sD} = Dimensionless wellbore flowing pressure inclusive skin
p_{tD} = Dimensionless tubing flowing pressure at surface
$p_{\Phi D}$ = Dimensionless Wellbore phase redistribution pressure
w_{fD} = Dimensionless fracture width
x_D = Dimensionless fracture length
x_{wD} = Dimensionless wellbore length in *x*-direction
y_{wD} = Dimensionless wellbore length in *y*-direction

Greek Variables

α = Wellbore phase redistribution time constant, *t* [sec]
α_D = Dimensionless wellbore phase redistribution time constant, dimensionless
λ = Time-dependent skin effect exponential parameter ($0 \le \lambda \le 1$)
μ = Newtonian Viscosity, M/Lt [cp] or [lb_m/ft•s]
ν = Power-law flow regime exponential parameter ($0 \le \nu \le 1$)
η = Hydraulic diffusivity, L/t^2 [md/cp•Pa^{-1}] or [m^2/(lb_m/ft•s) •psi^{-1}]
η_D = Dimensionless hydraulic diffusivity, dimensionless
ρ = Density, M/L^3 [kg/m^3] or [lb_m/ft^3]
σ = Variable for substitution
ϕ = Porosity, fraction
τ = Convolution variable

Subscripts

cls = Continuous line source
cp = Constant pressure production
cr = Constant rate production
frac = Fracture
WBS = Wellbore Storage

Mathematical Functions

E_i = Exponential integral
erf = Error function
Γ = Gamma function
K_0 = Modified Bessel Functions of the first kind, zero order
K_1 = Modified Bessel Functions of the first kind, first order

APPENDIX A
FORMATION LINEAR FLOW REGIME PRESSURE RELATION DERIVATION

This Appendix presents the derivation of the transient pressure behavior of an infinite-conductivity vertical fracture, derived from the line source solution, as proposed by Gringarten, Ramey and Raghavan (1974) in the formulation of formation linear flow from the matrix to the fracture. Assumptions used for the formulation of this derivation are:

- A vertical well penetrates the entire thickness of the reservoir.
- The reservoir thickness is uniform (constant).
- The reservoir is initially at pressure p_i.
- The reservoir is infinite in size.
- The well produces from a constant flowrate
- The rock properties are constant.
- The fracture has infinite conductivity.
- The fracture is infinite in length.
- Flow to the wellbore occurs only through the vertical fracture.
- The system contains a "slightly-compressible" fluid.
- The effects of gravity are negligible.
- The fracture has a uniform pressure distribution.

The continuous line source solution, as presented by Carslaw and Jaeger (1946) presents the foundation of this work. Although Gringarten, Ramey and Raghavan (1974) presented their solution using Greens Functions, we propose an alternative derivation in this Appendix resulting in the same final solution. The continuous line source solution is presented as Eq. A.1 below.

$$\Delta p_{cls}(x,y,t) = \frac{1}{4\pi\eta_f}\int_0^t q_{cls}(\tau)\exp\left[-\frac{(x-x_w)^2+(y-y_w)^2}{4\eta_f(t-\tau)}\right]\frac{d\tau}{t-\tau} \quad \text{.....(A.1)}$$

Where

$$q_{cls}(\tau) = \frac{q(t)B_o}{\phi h c_t} \quad \text{.....(A.2)}$$

$$\eta_f = \frac{k}{\phi\mu c_t} \quad \text{.....(A.3)}$$

Assuming a constant flowrate, then Eq. A.1 may be reduced to:

$$\Delta p_{cls}(x,y,t) = \frac{q_{cls}}{4\pi\eta_f}\int_0^t \exp\left[-\frac{(x-x_w)^2+(y-y_w)^2}{4\eta_f\tau}\right]\frac{d\tau}{\tau} \quad \text{.....(A.4)}$$

In order to solve this integral, we first define a variable for substitution:

$$\sigma = \frac{(x-x_w)^2+(y-y_w)^2}{4\eta_f\tau} \quad \text{.....(A.5)}$$

Taking the derivative of Eq. A.5 with respect to the τ-parameter yields:

$$\frac{d\sigma}{d\tau} = -\frac{1}{\tau}\frac{(x-x_w)^2+(y-y_w)^2}{4\eta_f\tau} \quad \text{.....(A.6)}$$

Substituting Eq. A.5 into A.6 yields:

$$\frac{d\sigma}{d\tau} = -\frac{\sigma}{\tau} \quad \text{.....(A.7)}$$

Rearranging Eq. A.7 yields a form to substitute back into Eq. A.4:

$$\frac{\tau}{d\tau} = -\frac{\sigma}{d\sigma} \quad \text{.....(A.8)}$$

Where the limits of integration are:

$$\tau = 0\,,\ \sigma = \infty \quad \text{.....(A.9)}$$

$$\tau = t\,,\ \sigma = \frac{(x-x_w)^2+(y-y_w)^2}{4\eta_f\tau} \quad \text{.....(A.10)}$$

Substituting Eq.A.5 and Eq. A.7 through A.10 into Eq. A.4 yields:

$$\Delta p_{cls}(x,y,t) = \frac{q_{cls}}{4\pi\eta_f}\int_0^{\frac{(x-x_w)^2+(y-y_w)^2}{4\eta_f(t-\tau)}} \frac{\exp[-\sigma]}{\sigma}d\sigma \quad \text{.....(A.11)}$$

Reversing the limits of integration yields:

$$\Delta p_{cls}(x,y,t) = \frac{q_{cls}}{4\pi\eta_f} \int_{\frac{(x-x_w)^2+(y-y_w)^2}{4\eta_f(t-\tau)}}^{\infty} \frac{\exp[-\sigma]}{\sigma} d\sigma \quad \text{.....(A.12)}$$

Recalling the definition of the exponential integral from Schaum's (1971):

$$E_i(x) = \int_x^{\infty} \frac{\exp[-u]}{u} du \quad \text{.....(A.13)}$$

We can substitute the definition of the exponential integral into Eq. A.12 resulting in:

$$\Delta p_{cls}(x,y,t) = \frac{q_{cls}}{4\pi\eta_f} Ei\left[\frac{(x-x_w)^2+(y-y_w)^2}{4\eta_f\tau}\right] \quad \text{.....(A.14)}$$

Where the function evaluated at infinity is zero. Eq. A.14 is the continuous line source solution for radial flow. For a fractured well, we create a plane along the x-axis and integrate. Rearranging Eq. A.14 for a continuous fracture, assuming the wellbore is in the center of the fracture, yields:

$$\Delta p_{cls}(x,y,t) = \frac{q_{cls}}{4\pi\eta_f} \int_{x_w'-x_f}^{x_w'+x_f} Ei\left[\frac{(x-x_w)^2+(y-y_w)^2}{4\eta_f\tau}\right] dx_w \quad \text{.....(A.15)}$$

Eq. A.15 assumes the fracture half-length is notated by x_f while the wellbore length is x_w. The constant flowrate into the fracture is denoted by:

$$q_{frac} = \frac{qB_o}{2\phi c_t h x_f} \quad \text{.....(A.16)}$$

Non-dimensionalizing Eq. A.15 requires the following equations:

$$\eta_f = \frac{k}{\phi\mu c_t} \quad \text{.....(A.17)}$$

$$x_D = \frac{x}{x_f} \quad \text{.....(A.18)}$$

$$y_D = \frac{y}{x_f} \quad \text{.....(A.19)}$$

$$p_D = 2\pi \frac{kh}{qB\mu}[p_i - p(x,y,z)] \quad \text{.....(A.20)}$$

$$t_D = \frac{k}{\phi\mu c_t {x_f}^2} \quad \text{.....(A.21)}$$

Substituting Eq. A.16 through A.21 into Eq. A.15 yields:

$$\Delta p_{cls}(x,y,t) = \left[\frac{qB_o}{2\phi c_t h x_f}\right]\left[\frac{\phi\mu c_t}{4\pi k}\right]\int_{x_w'-x_f}^{x_w'+x_f} Ei\left[\frac{(x-x_w)^2+(y-y_w)^2}{4kt/\phi\mu c_t}\right]dx_w \quad \text{.....(A.22)}$$

Multiplying the exponential integral function by $[1/{x_f}^2]/[1/{x_f}^2]$ and simplifying terms yields:

$$\Delta p_{cls}(x,y,t) = \frac{1}{4}\left[\frac{qB_o\mu}{2\pi h}\right]\left[\frac{\phi\mu c_t}{4\pi k}\right]\int_{x_w'-x_f}^{x_w'+x_f} Ei\left[\frac{(x/x_f - x_w/x_f)^2+(y/x_f - y_w/x_f)^2}{4kt/\phi\mu c_t}\right]\frac{dx_w}{x_f} \quad \text{.....(A.23)}$$

Defining further a dimensionless variable for substitution:

$$x_{wD} = \frac{x_w}{x_f} \quad \text{.....(A.24)}$$

Differentiating Eq. A.24 yields:

$$dx_{wD} = \frac{1}{x_f}dx_w \quad \text{.....(A.25)}$$

where the limits of integration are:

$$x_w = x_w' + x_f, \quad x_{wD} = \frac{x_w'}{x_f} + \frac{x_f}{x_f} \quad \text{.....(A.26)}$$

$$x_w = x_w' - x_f, \quad x_{wD} = \frac{x_w'}{x_f} - \frac{x_f}{x_f} \quad \text{.....(A.27)}$$

Eq. A.26 and A.27 may be rewritten as:

$$x_w = x_w' + x_f, \quad x_{wD} = x_{wD}' + 1 \quad \text{.....(A.28)}$$

$$x_w = x_w' - x_f, \quad x_{wD} = x_{wD}' - 1 \quad \text{.....(A.29)}$$

Substitution of Eq. A.28 and A.29 into Eq. A.23, and multiplication by $\frac{2\pi hk}{qB_o\mu}$ yields:

$$\frac{2\pi hk}{qB\mu}\Delta p_{cfrac}(x,y,t)=\frac{1}{4}\int_{x_{wD}'-1}^{x_{wD}'+1}E_i\left[\frac{(x_D-x_{wD})^2+(y_D-y_{wD})^2}{4t_D}\right]dx_{wD} \quad \text{.....(A.30)}$$

Recalling Eq. A.20, we define the dimensionless fracture pressure as:

$$\Delta p_{D,cfrac}(x_D,y_D,t_D)=\frac{1}{4}\int_{x_{wD}'-1}^{x_{wD}'+1}E_i\left[\frac{(x_D-x_{wD})^2+(y_D-y_{wD})^2}{4t_D}\right]dx_{wD} \quad \text{.....(A.31)}$$

Assuming that the well is at the center of the fracture (*i.e.,* $x_{wD}'=0$) with negligible length compared to the fracture half-length, and that the fracture has no thickness (*i.e.,* $y_D=y_{wD}=0$), we can rewrite Equation A.31 as:

$$\Delta p_{D,cfrac}(x_D,t_D)=\frac{1}{4}\int_{-1}^{+1}E_i\left[\frac{(x_D-x_{wD})^2}{4t_D}\right]dx_{wD} \quad \text{.....(A.32)}$$

To solve this integral, we begin by creating a variable for substitution as:

$$z^2=\frac{(x_D-x_{wD})^2}{4t_D} \quad \text{.....(A.33)}$$

Taking the square root of all terms in Eq. A.33 yields:

$$z=\frac{x_D-x_{wD}}{2\sqrt{t_D}} \quad \text{.....(A.34)}$$

Taking the derivative of Eq. A.34 with respect to x_{wD}:

$$\frac{dz}{dx_{wD}}=\frac{-1}{2\sqrt{t_D}} \quad \text{.....(A.35)}$$

Rewriting Eq. A.35 yields:

$$dx_{wD}=-2\sqrt{t_D}\,dz \quad \text{.....(A.36)}$$

Evaluating the limits of integration:

$$x_{wD} = 1, \quad z = \frac{x_D - 1}{2\sqrt{t_D}} \quad \text{.....(A.38)}$$

$$x_{wD} = -1, \quad z = \frac{x_D + 1}{2\sqrt{t_D}} \quad \text{.....(A.39)}$$

Returning these results to Eq. A.33, we rewrite the dimensionless fracture pressure difference as:

$$\Delta p_{D,cfrac}(x_D, t_D) = \frac{-\sqrt{t_D}}{2} \int_{\frac{x_D+1}{2\sqrt{t_D}}}^{\frac{x_D-1}{2\sqrt{t_D}}} E_i[z^2]dz \quad \text{.....(A.40)}$$

Performing a second variable substitution, we introduce:

$$m = z^2 \quad \text{.....(A.41)}$$

Taking the derivative of Eq. A.41 yields:

$$dm = 2z\,dz \quad \text{.....(A.42)}$$

Substituting Eq. A.42 into Eq. A.40:

$$\Delta p_{D,cfrac}(x_D, t_D) = \frac{-\sqrt{t_D}}{2} \int_{\frac{x_D+1}{2\sqrt{t_D}}}^{\frac{x_D-1}{2\sqrt{t_D}}} E_i[m]\frac{dm}{2z} \quad \text{.....(A.43)}$$

We cannot take this integral; therefore, we rewrite Eq. A.41 as:

$$z = \sqrt{m} \quad \text{.....(A.44)}$$

Returning Eq. A.44 to A.43:

$$\Delta p_{D,cfrac}(x_D, t_D) = \frac{-\sqrt{t_D}}{2} \int_{\frac{x_D+1}{2\sqrt{t_D}}}^{\frac{x_D-1}{2\sqrt{t_D}}} E_i[m]\frac{dm}{2\sqrt{m}} \quad \text{.....(A.45)}$$

Naming variables to use in integration by parts let:

$$u = E_i[m] \quad \text{.....(A.46)}$$

$$v' = 2\sqrt{m} \quad \text{.....(A.47)}$$

Therefore:

$$u' = \frac{e^{-m}}{m} \quad \text{.....(A.48)}$$

$$v = -\sqrt{m} \quad \text{.....(A.49)}$$

Applying integration by parts to solve Eq. A.45 yields:

$$p_{D,cfrac}(x_D, t_D) = \frac{-\sqrt{t_D}}{2}\left[-\sqrt{m}E_i[m]\Big|_{\frac{x_D+1}{2\sqrt{t_D}}}^{\frac{x_D-1}{2\sqrt{t_D}}} + \int_{\frac{x_D+1}{2\sqrt{t_D}}}^{\frac{x_D-1}{2\sqrt{t_D}}} \frac{e^{-m}}{m}\sqrt{m}\,dm \right] \quad \text{.....(A.50)}$$

Performing a second substitution in order to solve the integral remaining in Eq. A.50, we define:

$$u = \sqrt{m} \quad \text{.....(A.51)}$$

Taking the derivative of Eq. A.51 yields:

$$du = \frac{dm}{2\sqrt{m}} \quad \text{.....(A.52)}$$

Substituting Eq. A.51 and A.52 into A.50 yields:

$$p_{D,cfrac}(x_D, t_D) = \frac{-\sqrt{t_D}}{2}\left[-\sqrt{m}E_i[m]\Big|_{\frac{x_D+1}{2\sqrt{t_D}}}^{\frac{x_D-1}{2\sqrt{t_D}}} + 2\int_{\frac{x_D+1}{2\sqrt{t_D}}}^{\frac{x_D-1}{2\sqrt{t_D}}} e^{-u^2}\,du \right] \quad \text{.....(A.53)}$$

We rewrite the integral of Eq. A.53 as a sum of integrals across the limits of integration as shown:

$$2\int_{\frac{x_D+1}{2\sqrt{t_D}}}^{\frac{x_D-1}{2\sqrt{t_D}}} e^{-u^2}\,du = 2\int_{\frac{x_D+1}{2\sqrt{t_D}}}^{0} e^{-u^2}\,du + 2\int_{0}^{\frac{x_D-1}{2\sqrt{t_D}}} e^{-u^2}\,du \quad \text{.....(A.54)}$$

Recalling the error function from Schaum's (1974):

$$erf(x) = \frac{2}{\sqrt{\pi}} \int_0^x e^{-u^2}\, du \quad \text{.....(A.55)}$$

Rewriting Eq. A.54,

$$2 \int_{\frac{x_D+1}{2\sqrt{t_D}}}^{\frac{x_D-1}{2\sqrt{t_D}}} e^{-u^2}\, du = -2 \int_0^{\frac{x_D+1}{2\sqrt{t_D}}} e^{-u^2}\, du + 2 \int_0^{\frac{x_D-1}{2\sqrt{t_D}}} e^{-u^2}\, du \quad \text{.....(A.56)}$$

Substituting the definition of the error function into Eq. A.56 yields:

$$2 \int_{\frac{x_D+1}{2\sqrt{t_D}}}^{\frac{x_D-1}{2\sqrt{t_D}}} e^{-u^2}\, du = -\sqrt{\pi} erf\left[\frac{x_D+1}{2\sqrt{t_D}}\right] + \sqrt{\pi} erf\left[\frac{x_D-1}{2\sqrt{t_D}}\right] \quad \text{.....(A.57)}$$

Returning this result to Eq. A.53 yields:

$$p_{D,cfrac}(x_D, t_D) = \frac{-\sqrt{t_D}}{2}\left[-\sqrt{m} E_i[m] \Big|_{\frac{x_D+1}{2\sqrt{t_D}}}^{\frac{x_D-1}{2\sqrt{t_D}}} + -\sqrt{\pi} erf\left[\frac{x_D+1}{2\sqrt{t_D}}\right] + \sqrt{\pi} erf\left[\frac{x_D-1}{2\sqrt{t_D}}\right] \right] \quad \text{.....(A.58)}$$

Substituting Eq. Eq. A.44 into Eq. A.58 yields:

$$p_{D,cfrac}(x_D, t_D) = \frac{-\sqrt{t_D}}{2}\left[-zE_i[z^2] \Big|_{\frac{x_D+1}{2\sqrt{t_D}}}^{\frac{x_D-1}{2\sqrt{t_D}}} + -\sqrt{\pi} erf\left[\frac{x_D+1}{2\sqrt{t_D}}\right] + \sqrt{\pi} erf\left[\frac{x_D-1}{2\sqrt{t_D}}\right] \right] \quad \text{.....(A.59)}$$

Applying the limits to the exponential integral and substituting Eq. A.34, results in:

$$p_{D,cfrac}(x_D,t_D)=\frac{-\sqrt{t_D}}{2}\left[\left[\frac{x_D-1}{2\sqrt{t_D}}\right]E_i\left[\frac{(x_D-1)^2}{4t_D}\right]-\left[\frac{x_D+1}{2\sqrt{t_D}}\right]E_i\left[\frac{(x_D+1)^2}{4t_D}\right]\right.$$
$$\left.-\sqrt{\pi}erf\left[\frac{x_D+1}{2\sqrt{t_D}}\right]+\sqrt{\pi}erf\left[\frac{x_D-1}{2\sqrt{t_D}}\right]\right]$$

.....(A.60)

Multiplying through by $-\sqrt{t_D}/2$ results in:

$$p_{D,cfrac}(x_D,t_D)=-\left[\frac{x_D-1}{4}\right]E_i\left[\frac{(x_D-1)^2}{4t_D}\right]+\left[\frac{x_D+1}{4}\right]E_i\left[\frac{(x_D+1)^2}{4t_D}\right]$$
$$+\frac{\sqrt{\pi t_D}}{2}erf\left[\frac{x_D+1}{2\sqrt{t_D}}\right]-\frac{\sqrt{\pi t_D}}{2}erf\left[\frac{x_D-1}{2\sqrt{t_D}}\right]\Bigg]$$

.....(A.61)

Combining like terms within Eq. A.60 yields:

$$p_{D,cfrac}(x_D,t_D)=\frac{\sqrt{\pi t_D}}{2}\left[erf\left[\frac{x_D+1}{2\sqrt{t_D}}\right]-erf\left[\frac{x_D-1}{2\sqrt{t_D}}\right]\right]$$
$$-\left[\frac{x_D-1}{4}\right]E_i\left[\frac{(x_D-1)^2}{4t_D}\right]+\left[\frac{x_D+1}{4}\right]E_i\left[\frac{(x_D+1)^2}{4t_D}\right]$$

.....(A.62)

Applying the negative sign in the error and exponential integral terms, we can rearrange to the form produced by Gringarten, Ramey and Raghavahn (1974).

$$p_{D,cfrac}(x_D,t_D)=\frac{\sqrt{\pi t_D}}{2}\left[erf\left[\frac{1+x_D}{2\sqrt{t_D}}\right]+erf\left[\frac{1-x_D}{2\sqrt{t_D}}\right]\right]$$
$$+\left[\frac{1-x_D}{4}\right]E_i\left[\frac{(1-x_D)^2}{4t_D}\right]+\left[\frac{1+x_D}{4}\right]E_i\left[\frac{(1+x_D)^2}{4t_D}\right]$$

.....(A.63)

The short term solution for Eq. A.63, as described by the authors, describes the formation linear flow regime utilized within this thesis. Evaluating the error function, as dimensionless time approaches zero leads towards a solution of one, while the exponential integral approaches negative infinity. Applying this to Eq. A.63 yields:

$$p_{D,frac}(x_D = 0, t_D) = \frac{\sqrt{\pi}\sqrt{t_D}}{2}[1+1] \quad \text{.....(A.64)}$$

Simplification of Eq. A.64 results in:

$$p_{D,frac}(x_D = 0, t_D) = \sqrt{\pi}\sqrt{t_D} \quad \text{.....(A.65)}$$

Which is the short term approximation for the dimensionless pressure relation of an infinite conductivity vertical fracture displaying formation linear flow regimes between the reservoir matrix and the fracture.

APPENDIX B
BILINEAR FLOW REGIME PRESSURE RELATION DERIVATION

This Appendix presents the derivation of the transient pressure behavior of a finite-conductivity vertical fracture as proposed by Cinco and Samaniego (1981). Assumptions used for the formulation of this derivation are:

- A vertical well penetrates the entire thickness of the reservoir.
- The reservoir thickness is uniform (constant).
- The reservoir is initially at pressure, p_i.
- The reservoir is infinite in size.
- The well produces from a constant flowrate
- The rock properties are constant.
- The fracture has finite conductivity.
- The fracture is infinite in length.
- Flow to the wellbore occurs only through the vertical fracture.
- The system contains a "slightly-compressible" fluid.
- The effects of gravity are negligible.
- The pressure gradients are small.
- The system obeys Darcy's law.

Assuming linear flow within the fracture, and that fracture tip effects are not felt at early-times, we recall the full pressure behavior of the system as described (Eq. B.1) by Cinco and Samaniego's (1981a) in Eq. B.1. Derivation of the full pressure behavior is based on mass balance and continuity principles, however, is not of direct relevance to this paper and not produced in this work.

$$\frac{\partial^2 p_{fD,cr}}{\partial {x_D}^2} + \frac{2}{(k_f w_f)_D} \frac{\partial p_D}{dy_D}\bigg|_{y_D=0} = \frac{1}{\eta_{fD}} \frac{\partial p_{fD}}{dt_D} \quad (0 < x_D < \infty) \quad \text{.....(B.1)}$$

The initial condition for Eq. B.1 is:

$$p_{fD,cr}(x_D, t_D = 0) = 0 \quad \text{..... (B.2)}$$

The boundary conditions for Eq. B.1 are:

$$\frac{\partial p_{fD,cr}}{\partial x_D}\bigg|_{x_D=0} = \frac{-\pi}{(k_f w_f)_D} \qquad \text{(inner boundary condition)..... (B.3)}$$

$$\lim_{x_D \to \infty} p_{fD,cr}(x_D, t_D) = 0 \qquad \text{(outer boundary condition)} \quad \text{(B.4)}$$

The transient flow behavior from the formation can be described with the following partial differential equation.

$$\frac{\partial^2 p_D}{\partial {y_D}^2} = \frac{\partial p_D}{\partial t_D} \quad (0 < y_D < \infty,\ t_D > 0) \quad \text{(B.5)}$$

The initial condition for Eq. B.5 is:

$$p_D(y_D, t_D = 0) = 0 \quad \text{(B.6)}$$

The boundary conditions for Eq. B.5 are:

$$p_D(y_D = 0, t_D) = p_{fD,cr}(x_D, t_D) \qquad \text{(inner boundary condition)} \quad \text{(B.7)}$$

$$\lim_{y_D \to \infty} P_D(y_D \to \infty, t_D) = 0 \qquad \text{(outer boundary condition)} \quad \text{(B.8)}$$

Method of Solution

Taking the differential equation for fracture flow into the Laplace domain yields the following relation:

$$\frac{\partial^2 \bar{p}_{fD,cr}}{\partial {x_D}^2} + \frac{2}{(k_f w_f)_D} \left. \frac{\partial p_D}{dy_D} \right|_{y_D = 0} = \frac{u}{\eta_{fD}} \bar{p}_{fD,cr} \quad (0 < x_D < \infty) \quad \text{(B.9)}$$

The initial condition for Eq. B.9 is:

$$\bar{p}_{fD,cr}(x_D, u) = 0 \quad \text{(B.10)}$$

The boundary conditions, in the Laplace domain, for Eq. B.9 are:

$$\left. \frac{\partial \bar{p}_{fD,cr}}{\partial x_D} \right|_{x_D = 0} = \frac{\frac{-\pi}{(k_f w_f)_D}}{u} \qquad \text{(inner boundary condition)} \quad \text{(B.11)}$$

$$\lim_{x_D \to \infty} \bar{p}_{cr,fD}(x_D, u) = 0 \qquad \text{(outer boundary condition)} \quad \text{(B.12)}$$

Taking the differential equation for reservoir flow into the Laplace domain yields the following relation:

$$\frac{\partial^2 \overline{p}_D}{\partial {y_D}^2} = u\overline{p}_D \ \ (0 < y_D < \infty) \quad \text{(B.13)}$$

The initial condition for Eq. B.13 is:

$$\overline{p}_D(y_D, u) = 0 \quad \text{(B.14)}$$

The boundary conditions for Eq. B.13 are:

$$\overline{p}_D(y_D = 0, u) = 0 = \overline{p}_{fD,cr}(x_D, u) \quad \text{(B.15)}$$

$$\lim_{y_D \to \infty} \overline{p}_D(y_D, u) \quad \text{(B.16)}$$

The solution for Eq. B.13 results in a second order linear differential equation with a general solution of the form:

$$y(t) = K_1 e^{\sqrt{B}x} + K_2 e^{-\sqrt{B}x} \quad \text{(B.17)}$$

Applying Equation B.13 into the known form of the differential equation,

$$\overline{p}_D(u) = K_1 e^{\sqrt{u}y_D} + K_2 e^{-\sqrt{u}y_D} \quad \text{(B.18)}$$

Applying the outer boundary condition Eq. B.16 to B.15 yields:

$$0 = K_1 e^{\sqrt{u}(\infty)} + K_2 e^{-\sqrt{u}(\infty)} \quad \text{(B.19)}$$

Evaluating, the second term on the right hand side will tend towards zero.

$$0 = K_1 e^{\sqrt{u}(\infty)} \quad \text{(B.20)}$$

leading to K_1=0. Returning to Eq. B.18, substituting our first constant yielding:

$$\overline{p}_D(u) = K_2 e^{-\sqrt{u}y_D} \quad \text{(B.21)}$$

Applying the second boundary condition Eq. B.15 to our incomplete solution Eq. B.21,

$$\overline{p}_{fD,cr}(u) = K_2 e^{-\sqrt{u}(0)} \quad \text{(B.22)}$$

Leading to $K_2 = \overline{p}_{fD}$. Returning the solution to the constant to Eq. B.21, yields:

$$\bar{p}_D(u) = \bar{p}_{fD,cr}(u)e^{-\sqrt{u}y_D} \quad \text{.....(B.23)}$$

Taking the derivative of the pressure response with respect to distance from the fracture y_D, yields: yields:

$$\frac{\partial \bar{p}_D(u)}{\partial y_D} = -\sqrt{u}\,\bar{p}_{fD,cr}(u)e^{-\sqrt{u}y_D} \quad \text{.....(B.24)}$$

Solving at the fracture interface,

$$\left.\frac{\partial \bar{p}_D(u)}{\partial y_D}\right|_{y_D=0} = -\sqrt{u}\,\bar{p}_{fD,cr}(u)\,e^{-\sqrt{u}(0)} \quad \text{.....(B.25)}$$

Yielding

$$\left.\frac{\partial \bar{p}_D(u)}{\partial y_D}\right|_{y_D=0} = -\sqrt{u}\,\bar{p}_{fD,cr}(u) \quad \text{.....(B.26)}$$

Which provides an expression for transient reservoir inflow source term which may be substituted into the fracture flow pressure expression Eq. B.9 yielding:

$$\frac{\partial^2 \bar{p}_{fD,cr}}{\partial {x_D}^2} - \frac{2\sqrt{u}}{(k_f w_f)_D}\bar{p}_{fD,cr} = \frac{u}{\eta_{fD}}\bar{p}_{fD,cr}\,, \quad \text{.....(B.27)}$$

Or:

$$\frac{\partial^2 \bar{p}_{fD,cr}}{\partial {x_D}^2} = \left[\frac{u}{\eta_{fD}} + \frac{2\sqrt{u}}{(k_f w_f)_D}\right]\bar{p}_{fD,cr}\,, \quad \text{.....(B.28)}$$

The solution to Eq. B.28 will take the form:

$$y(t) = K_1 e^{\sqrt{B}x} + K_2 e^{-\sqrt{B}x}\,, \quad \text{.....(B.29)}$$

Where substituting Eq. B.28 into the known form of the differential equation, we arrive at:

$$\bar{p}_{fD,cr}(u) = K_1 e^{\sqrt{\frac{u}{\eta_{fD}}+\frac{2\sqrt{u}}{(k_f w_f)_D}}x_D} + K_2 e^{-\sqrt{\frac{u}{\eta_{fD}}+\frac{2\sqrt{u}}{(k_f w_f)_D}}x_D}\,, \quad \text{.....(B.30)}$$

Utilizing boundary conditions to solve for the constants K_1 and K_2, we first apply the outer boundary condition Eq. B.12:

$$0 = K_1 e^{\sqrt{\frac{u}{\eta_{fD}} + \frac{2\sqrt{u}}{(k_f w_f)_D}}(\infty)} + K_2 e^{-\sqrt{\frac{u}{\eta_{fD}} + \frac{2\sqrt{u}}{(k_f w_f)_D}}(\infty)} \quad \text{.....(B.31)}$$

Evaluating, the second term on the RHS will tend towards zero.

$$0 = K_1 e^{\sqrt{\frac{u}{\eta_{fD}} + \frac{2\sqrt{u}}{(k_f w_f)_D}}\infty} \text{,.....(B.32)}$$

Leading to K_1=0. Therefore, we return to Eq. B.31, substituting our first constant yielding:

$$\bar{p}_{fD,cr}(u) = K_2 e^{-\sqrt{\frac{u}{\eta_{fD}} + \frac{2\sqrt{u}}{(k_f w_f)_D}} x_D} \text{,.....(B.33)}$$

Taking the derivative of Eq. B.33, and applying the inner boundary condition, Eq. B.11, yields:

$$\frac{\partial \bar{p}_{fD,cr}}{\partial x_D} = -\frac{\frac{\pi}{(k_f w_f)_D}}{u} = -\sqrt{\frac{u}{\eta_{fD}} + \frac{2\sqrt{u}}{(k_f w_f)_D}} K_2 e^{-\sqrt{\frac{u}{\eta_{fD}} + \frac{2\sqrt{u}}{(k_f w_f)_D}}(0)} \text{, ...(B.34)}$$

Simplifying, we solve for the second constant:

$$K_2 = \frac{\frac{\pi}{(k_f w_f)_D}}{u\sqrt{\frac{u}{\eta_{fD}} + \frac{2\sqrt{u}}{(k_f w_f)_D}}} \text{,.....(B.35)}$$

Returning the second constant to Eq. B.33, we arrive at the expression for pressure behavior along the fracture:

$$\bar{p}_{fD,cr}(u) = \frac{\pi \exp\left(- x_D \left[\frac{u}{\eta_{fD}} + \frac{2\sqrt{u}}{(k_f w_f)_D} \right]^{1/2} \right)}{(k_f w_f)_D u \left[\frac{u}{\eta_{fD}} + \frac{2\sqrt{u}}{(k_f w_f)_D} \right]^{1/2}} \text{, ...(B.36)}$$

Examining the pressure performance at the wellbore $x_D = 0$, we arrive at the final non-dimensional pressure response for the fracture in Laplace space:

$$\bar{p}_{D,cr}(u) = \frac{\pi}{(k_f w_f)_D} \frac{1}{u\left[\frac{u}{\eta_{fD}} + \frac{2\sqrt{u}}{(k_f w_f)_D}\right]^{1/2}} \quad \text{(B.37)}$$

Inversion of Equation B.37 is too complex for practical application; therefore, we will produce short and long time approximations. Beginning with short time behavior, we return to Eq. B.37. Knowing that as the limit of time in the real domain tends towards zero, the Laplace variable u tends towards infinity, yields:

$$\bar{p}_{D,cr}(u) = \frac{\pi}{(k_f w_f)_D} \frac{1}{u\left[\frac{u}{\eta_{fD}}\right]^{1/2}}, \quad \text{(B.38)}$$

Arraying and simplifying, we arrive at,

$$\bar{p}_{D,cr}(u) = \frac{\pi\sqrt{\eta_{fD}}}{(k_f w_f)_D} \frac{1}{u^{3/2}}, \quad \text{(B.39)}$$

The short term pressure behavior of a well in Laplace space. Utilizing the work of Roberts and Kaufman (1966) we apply the following two identities

Table 1 —Laplace Inversion Lookup Table for Short Time Pressure Solution

$g(u)$	$f(t)$	Location
$\frac{1}{u^{3/2}}$	$2\left[\frac{t}{\pi}\right]^{1/2}$	Pg. 206, Eq. 2
$ag(u)$	$af(t)$	Pg. 169, Eq. 1

Utilizing **Table 1,** we assume the general shape of Eq. B.39 is of the form $ag(u)$. Taking the Laplace inversion of $g(u)$ results in:

$$p_{D,cr}(t_D) = \frac{\pi\sqrt{\eta_{fD}}}{(k_f w_f)_D} 2\left[\frac{t}{\pi}\right]^{1/2}, \quad \text{(B.40)}$$

Rearranging,

$$p_{D,cr}(t_D) = \frac{2}{(k_f w_f)_D}\sqrt{\pi\eta_{fD}t_D}, \quad \text{(B.41)}$$

Which is the short term approximation of pressure near the wellbore for a finite conductivity vertical fracture. Eq. B.41 will produce fracture linear flow response as described by Cinco and Samaniego (1981). This response is of little value, as fracture linear flow occurs at such short times it is masked by short time wellbore storage and skin effects and if near-never observed in practice.

The long time approximation follows a similar methodology as the short time approximation. Returning to Eq. B.37, at long times in the real domain, the Laplace variable will approach zero. Therefore, the full solution,

$$\bar{p}_{D,cr}(u) = \frac{\pi}{(k_f w_f)_D} \frac{1}{u\left[\frac{u}{\eta_{fD}} + \frac{2\sqrt{u}}{(k_f w_f)_D}\right]^{1/2}}, \quad \text{(B.37)}$$

Simplifies to,

$$\bar{p}_{D,cr}(u) = \frac{\pi}{(k_f w_f)_D} \frac{1}{u\left[\frac{2\sqrt{u}}{(k_f w_f)_D}\right]^{1/2}}. \quad \text{(B.42)}$$

Arraying:

$$\bar{p}_{D,cr}(u) = \frac{\pi}{\sqrt{2}(k_f w_f)_D} \frac{\sqrt{(k_f w_f)_D}}{u\sqrt[4]{u}}, \quad \text{(B.43)}$$

Simplifying further yields:

$$\bar{p}_{D,cr}(u) = \frac{\pi}{\sqrt{2(k_f w_f)_D}} \frac{1}{u^{5/4}}, \quad \text{(B.44)}$$

The long term pressure behavior in the Laplace domain. Utilizing the work of Roberts and Kaufman (1966) we apply the following two identities

Table 2 — Laplace Inversion Lookup Table for Long Time Pressure Solution

$g(u)$	$f(t)$	Location
$\frac{1}{u^{\nu}}$	$\frac{t^{\nu-1}}{\Gamma(\nu)}$	Pg. 206, Eq. 4
$ag(u)$	$af(t)$	Pg. 169, Eq. 1

Utilizing **Table 2**, we assume the general shape of Eq. B.44 is of the form $ag(u)$. Taking the Laplace inversion of $g(u)$ results in:

$$p_{D,cr}(t_D) = \frac{\pi}{\sqrt{2(k_f w_f)_D}} \frac{t_D^{\frac{5}{4}-1}}{\Gamma\left(\frac{5}{4}\right)}, \quad \text{(B.45)}$$

Arraying,

$$p_{D,cr}(t_D) = \frac{\pi}{\Gamma(5/4)\sqrt{2(k_f w_f)_D}} \sqrt[4]{t_D}, \quad \text{(B.46)}$$

Which is the final long term pressure behavior measured at the wellbore for a finite conductivity vertical fracture. In accordance with Cinco and Samaniego's (1981) work, this agrees with the bilinear flow regime that is expected at long times.

APPENDIX C

GENERALIZED CONSTANT PRESSURE SOLUTION IN THE LAPLACE DOMAIN

This appendix provides the derivation of the generalized constant pressure solution in the Laplace domain. Developed from a mass balance approach with a control volume around the wellbore with a sand-face inlet and well-head outlet, this equation is of primary use in this work upon which all other theories are applied. We begin with the dimensionless rate relation, demonstrated as:

$$q_{D,WBS}(t_D) = 1 - C_D\left[\frac{dp_{wD}}{dt_D} - \frac{dp_{tD}}{dt_D}\right] \quad \text{(C.1)}$$

Defining dimensionless terms:

$$q_{D,WBS} = \frac{q_f}{q} \quad \text{(C.2)}$$

$$C_D = 0.0372\frac{24\,C_s}{\phi h c_t x_f{}^2} \quad \text{(C.3)}$$

$$p_{wD} = \frac{kh}{141.2qB\mu}[p_i - p_w] \quad \text{(C.4)}$$

$$p_{tD} = \frac{kh}{141.2qB\mu}[p_i - p_t] \quad \text{(C.5)}$$

where all values are in field units. Assuming that the tubing pressure remains constant, we take Eq. C.1 into the Laplace domain, following the theory presented by Blasingame (PETE 620 Notes, 1994), we have:

$$\bar{q}_D(u) = \frac{1}{u} - C_D\left[u\bar{p}_{wD}(u) - p_{wD}(t_D = 0)\right]. \quad \text{(C.6)}$$

Knowing that the dimensionless wellbore pressure, at initial dimensionless time is zero, we can rewrite Eq. C.6 as:

$$\bar{q}_D(u) = \frac{1}{u} - C_D u\,\bar{p}_{wD}(u). \quad \text{(C.6)}$$

Examining the convolution integral for a continuously changing flowrate (i.e. applicable for any case), displayed below for reference:

$$p_{wD}(t_D) = \int_0^{t_D} q'_D(\tau) p_{sD}(t_D - \tau) d\tau \quad \text{(C.7)}$$

Where

$$p_{sD}(t_D) = p_D(t_D) + s \quad \text{(C.8)}$$

Taking the Laplace transform of Eq. C.7:

$$\bar{p}_{wD}(u) = [u\, q_D(u) - q_D(t_D = 0)]\bar{p}_{sD}(u) \quad \text{(C.9)}$$

The flowrate at initial time is zero, therefore, Eq. C.10 condenses to:

$$\bar{p}_{wD}(u) = u\, q_D(u)\bar{p}_{sD}(u) \quad \text{(C.10)}$$

Substituting Eq. C.6 into Eq. C.10 yields:

$$\bar{p}_{wD}(u) = u\left[\frac{1}{u} - C_D u \bar{p}_{wD}(u)\right]\bar{p}_{sD}(u) \quad \text{(C.11)}$$

Multiplying through by the Laplace parameter yields:

$$\bar{p}_{wD}(u) = [1 - C_D u^2 \bar{p}_{wD}(u)]\bar{p}_{sD}(u) \quad \text{(C.12)}$$

Solving for the dimensionless wellbore pressure, we multiply through by $1/\bar{p}_{wD}(u)$ and $1/\bar{p}_{sD}(u)$ yielding:

$$\frac{1}{\bar{p}_{sD}(u)} = \frac{1}{\bar{p}_{wD}(u)} - C_D u^2 \quad \text{(C.13)}$$

Solving for the dimensionless wellbore storage pressure yields:

$$\bar{p}_{wD}(u) = \frac{1}{\frac{1}{\bar{p}_{sD}(u)} + C_D u^2} \quad \text{(C.14)}$$

From Van Everdingen and Hurst (1949) we recall the convolution integral relating the constant pressure solution to the constant rate solution, defined, in Laplace space, as:

$$\bar{q}_{D,cp}(u)\, \bar{p}_{wD,cr}(u) = \frac{1}{u^2} \quad \text{(C.15)}$$

Solving for the constant pressure solution, we assume that Eq. C.14 is a constant rate case, rather than applicable in all situations. Substituting Eq. C.14 into Eq. C.15 yields:

$$\bar{q}_{D,cp}(u) = \frac{1}{u^2} \frac{1}{\frac{1}{\frac{1}{\bar{p}_{sD,cr}(u)} + C_D u^2}} \quad \text{.....(C.16)}$$

Simplifying the right hand side of Eq. C.16:

$$\bar{q}_{D,cp}(u) = \frac{1}{u^2}\left[\frac{1}{\bar{p}_{sD,cr}(u)} + C_D u^2\right] \quad \text{.....(C.17)}$$

Multiplying through by u^2 yields:

$$\bar{q}_{D,cp}(u) = \frac{1}{u^2} \frac{1}{\bar{p}_{sD,cr}(u)} + C_D \cdot \quad \text{.....(C.18)}$$

Consulting Roberts and Kaufman (1966, pg. 202, Eq.172) demonstrate that the Laplace inversion of a constant is the Dirac delta, δ(t), an impulse function where the result is zero for all values other than at time equals zero, where it results in infinity. As Laplace inversion is additive, therefore, we know that the inversion of the wellbore storage constant will result in zero. For this reason, we can rewrite Eq. C.18 as:

$$\bar{q}_{D,cp}(u) = \frac{1}{u^2} \frac{1}{\bar{p}_{sD,cr}(u)}, \quad \text{.....(C.19)}$$

which is the generalized constant pressure solution.

APPENDIX D

CONSTANT PRESSURE SOLUTION WITH TIME-DEPENDENT CHOKED FRACTURE SKIN

This appendix examines the constant pressure behavior, derived in Appendix C, with the addition of a variable choked fracture skin pressure constraint. Larsen et al. (1990) initially proposed a hyperbolic relation for variable skin in order to describe the effects of the early-time pressure transient response due to fracture cleanup. This work examines the hyperbolic relation proposed by Larsen et al. for the constant pressure solution, along with an exponential and cumulative exponential time dependent skin. This work is performed in the Laplace domain with numerical inversion of the constant pressure solution.

Hyperbolic Model

Larsen et al. (1990) proposed a hyperbolic time dependent skin function to account for variations in production seen during cleanup, as shown by:

$$s = \frac{a}{b+t} + c \quad \text{.....(D.1)}$$

Where the parameters a, b and c are unique to the well being examined.

Loosely basing our model upon the original work of Larsen, we present Eq. D.2 proposed based on empirical field evidence:

$$s(t_D) = s_\infty + [s_0 - s_\infty]\frac{1}{\left[1+\frac{\tau}{t_D}\right]^\lambda} \quad \text{.....(D.2)}$$

Knowing that skin is an additive function to wellbore pressure in the real domain, and assuming a time dependent skin factor demonstrated as:

$$p_{sD,cr}(t_D) = p_{D,cr}(t_D) + s(t_D) \quad \text{.....(D.3)}$$

Substituting in Eq. D.2 into Eq. D.3, assuming that the skin factor term is variable with time, we arrive at:

$$p_{sD,cr}(t_D) = p_{D,cr}(t_D) + s_\infty + [s_0 - s_\infty]\frac{1}{\left[1+\frac{\tau}{t_D}\right]^\lambda} \quad \text{.....(D.4)}$$

In an effort to obtain the constant pressure solution, we will take advantage of the convolution integral, presented in Laplace space. Utilizing the *Mathematica* "LaplaceTransform" function to bring Eq. D.4 into Laplace space, yielding:

$$\bar{p}_{sD,cr}(u) = \bar{p}_{D,cr}(u) + \frac{s_\infty}{u} + \frac{\Gamma(1+\lambda)U(\lambda,0,u\tau)[s_0 - s_\infty]}{u} \quad \text{.....(D.5)}$$

where $\Gamma(x)$ is the gamma function, and $U(a,b,z)$ is the hypergeometric function. Application of the convolution integral in Laplace space, the constant pressure solution is expressed as a relation of the constant rate solution, provided below for reference:

$$\bar{q}_{D,cp}(u) = \frac{1}{u^2}\frac{1}{\bar{p}_{sD,cr}(u)} \quad \text{.....(D.6)}$$

We substitute the wellbore pressure including skin, Eq. D.5, into Eq. D.6 yielding:

$$\bar{q}_{D,cp}(u) = \frac{1}{u^2}\frac{1}{\bar{p}_{D,cr}(u) + \frac{s_\infty}{u} + \frac{\Gamma(1+\lambda)U(\lambda,0,u\tau)[s_0 - s_\infty]}{u}} \quad \text{.....(D.7)}$$

In order to solve the invert Eq. D.7 into the real domain, we must incorporate a dimensionless wellbore flowing pressure. Linear and bilinear flow relations have been derived in **Appendix A and B** (provided below for reference). We further introduce a third general "power-law" flow regime (capable of describing any potential flow pattern) also described as follows:

$$p_{D,cr}(t_D) = c_1 t_D{}^{\nu} \qquad \text{(power-law flow)} \quad \text{.....(D.8a)}$$

$$p_{D,cr}(t_D) = \sqrt{\pi}\sqrt{t_D} \qquad \text{(linear flow)} \quad \text{.....(D.8b)}$$

$$p_{D,cr}(t_D)\frac{\pi}{\Gamma(5/4)\sqrt{2(k_f w_f)_D}}\sqrt[4]{t_D} \qquad \text{(bilinear flow)} \quad \text{.....(D.8c)}$$

Transforming the dimensionless wellbore pressure solutions into the Laplace domain, yields:

$$\bar{p}_{D,cr}(u) = c_1\frac{\Gamma(1+\nu)}{u^{1+\nu}} \qquad \text{(power-law flow)} \quad \text{.....(D.9a)}$$

$$\bar{p}_{D,cr}(u) = \sqrt{\pi}\frac{\Gamma(3/2)}{u^{3/2}} \qquad \text{(linear flow)} \quad \text{.....(D.9b)}$$

$$\bar{p}_{D,cr}(u) = \frac{\pi\exp[5/4]}{\sqrt{2(k_f w_f)_D}}\frac{\Gamma(5/4)}{u^{5/4}} \qquad \text{(bilinear flow)} \quad \text{.....(D.9c)}$$

Substituting the dimensionless wellbore pressures (Eq. 9) into Eq. D.7, we arrive at the constant pressure solution, assuming a skin with a hyperbolic relation with time, in Laplace space shown as:

$$\bar{q}_{D,cp}(u) = \frac{1}{u^2}\frac{1}{c_1\dfrac{\Gamma(1+\nu)}{u^{1+\nu}} + \dfrac{s_\infty}{u} + \dfrac{\Gamma(1+\lambda)U(\lambda,0,u\tau)[s_0 - s_\infty]}{u}} \quad \text{(power-law flow)....(D.10a)}$$

$$\bar{q}_{D,cp}(u) = \frac{1}{u^2}\frac{1}{\sqrt{\pi}\dfrac{\Gamma(3/2)}{u^{3/2}} + \dfrac{s_\infty}{u} + \dfrac{\Gamma(1+\lambda)U(\lambda,0,u\tau)[s_0 - s_\infty]}{u}} \quad \text{(linear flow).....(D.10b)}$$

$$\bar{q}_{D,cp}(u) = \frac{1}{u^2}\frac{1}{\dfrac{\pi\exp[5/4]}{\sqrt{2(k_f w_f)_D}}\dfrac{\Gamma(5/4)}{u^{5/4}} + \dfrac{s_\infty}{u} + \dfrac{\Gamma(1+\lambda)U(\lambda,0,u\tau)[s_0 - s_\infty]}{u}} \quad \text{(bilinear flow) .....(D.10c)}$$

Multiplying Eq. D.10 through by the Laplace parameter squared:

$$\bar{q}_{D,cp}(u) = \frac{1}{c_1 u^{1-\nu}\Gamma(1-\nu) + us_\infty + u\Gamma(1+\lambda)U(\lambda,0,u\tau)[s_0 - s_\infty]} \quad \text{(power-law flow)....(D.11a)}$$

$$\bar{q}_{D,cp}(u) = \frac{1}{\sqrt{\pi}\sqrt{u}\Gamma(3/2) + us_\infty + u\Gamma(1+\lambda)U(\lambda,0,u\tau)[s_0 - s_\infty]} \quad \text{(linear flow).....(D.11b)}$$

$$\bar{q}_{D,cp}(u) = \frac{1}{\dfrac{\pi\exp[5/4]}{\sqrt{2(k_f w_f)_D}}\dfrac{\Gamma(5/4)}{u^{5/4}} + us_\infty + u\,\Gamma(1+\lambda)U(\lambda,0,u\tau)[s_0 - s_\infty]} \quad \text{(bilinear flow) .....(D.11c)}$$

Eq. D.11 are the constant pressure solution, in Laplace space, for linear, bilinear and a general power-law flow regime, which include a hyperbolic time dependent skin, and no wellbore storage. Numerical inversion through the Stehfest algorithm is employed to return the solution to the real domain.

Exponential Decay Model:

Continuing the efforts of Larsen et al. (1980), we propose an additional time dependent skin model following an exponential decay model. The following "exponential decay" model is proposed for a time-dependent skin factor:

$$s(t_D) = s_\infty + s_0 \exp[-t_D/\tau] \quad \text{.....(D.12)}$$

Substitution of Eq. D.19 into Eq. D.11, the wellbore pressure, including wellbore skin, in the real domain yields:

$$p_{sD,cr}(t_D) = p_{D,cr}(t_D) + s_\infty + s_0 \exp[-t_D/\tau] \quad \text{.....(D.13)}$$

In the Laplace domain, Eq. D.13 is:

$$\bar{p}_{sD,cr}(t_D) = \bar{p}_{D,cr}(t_D) + \frac{s_\infty}{u} + \frac{s_0}{u+1/\tau} \quad \text{.....(D.14)}$$

We substitute the wellbore pressure including an exponential model for time dependent skin, Eq. D.14, into Eq. D.6 yielding:

$$\bar{q}_{D,cp}(u) = \frac{1}{u^2} \frac{1}{\bar{p}_{D,cr}(t_D) + \frac{s_\infty}{u} + \frac{s_0}{u+1/\tau}} \quad \text{.....(D.15)}$$

Substituting in Eq. D.9, the three flow regimes examined in this work, into Eq. D.15, yields:

$$\bar{q}_{D,cp}(u) = \frac{1}{u^2} \frac{1}{c_1 \frac{\Gamma(1+\nu)}{u^{1+\nu}} + \frac{s_\infty}{u} + \frac{s_0}{u+1/\tau}} \quad \text{(power-law flow) .....(D.16a)}$$

$$\bar{q}_{D,cp}(u) = \frac{1}{u^2} \frac{1}{\sqrt{\pi} \frac{\Gamma(3/2)}{u^{3/2}} + \frac{s_\infty}{u} + \frac{s_0}{u+1/\tau}} \quad \text{(linear flow) .....(D.16b)}$$

$$\bar{q}_{D,cp}(u) = \frac{1}{u^2} \frac{1}{\frac{\pi \exp[5/4]}{\sqrt{2(k_f w_f)_D}} \frac{\Gamma(5/4)}{u^{5/4}} + \frac{s_\infty}{u} + \frac{s_0}{u+1/\tau}} \quad \text{(bilinear flow) .....(D.16c)}$$

Multiplying Eq. D.16 through by the Laplace parameter squared:

$$\bar{q}_{D,cp}(u) = \frac{1}{c_1 u^{(1-\nu)}\Gamma(1+\nu) + us_\infty + \frac{u^2 s_0}{u+1/\tau}} \quad \text{(power-law flow)} \quad \text{(D.17a)}$$

$$\bar{q}_{D,cp}(u) = \frac{1}{\sqrt{\pi}\sqrt{u}\Gamma(3/2) + us_\infty + \frac{u^2 s_0}{u+1/\tau}} \quad \text{(linear flow)} \quad \text{(D.17b)}$$

$$\bar{q}_{D,cp}(u) = \frac{1}{\frac{\pi \exp[5/4]}{\sqrt{2(k_f w_f)_D}}\frac{\Gamma(5/4)}{u^{3/4}} + us_\infty + \frac{u^2 s_0}{u+1/\tau}} \quad \text{(bilinear flow)} \quad \text{(D.17c)}$$

Eq. D.17 is the constant pressure solution for a vertical fracture assuming time-dependent exponential skin effects and no wellbore storage. The Stehfest algorithm provides accurate and rapid numerical inversion of this equation.

Cumulative Exponential Model:

A third "cumulative exponential" model is explored to describe time dependent skin behavior for the constant pressure solution. The cumulative exponential model is described as:

$$s(t_D) = s_\infty + [s_0 - s_\infty][1 - \exp[-(\tau/t_D)^\lambda]] \quad \text{(D.18)}$$

Substitution of Eq. D.18 into Eq. D.11, the wellbore pressure in the real domain yields:

$$p_{sD,cr}(t_D) = p_{D,cr}(t_D) + s_\infty + [s_0 - s_\infty][1 - \exp[-(\tau/t_D)^\lambda]] \quad \text{(D.19)}$$

Utilizing the *Mathematica* "LaplaceTransform" function to bring Eq. D.19 into Laplace space yielding:

$$\bar{p}_{sD,cr}(t_D) = \bar{p}_{D,cr}(t_D) + \frac{s_0}{u} - \frac{2K_1\left[\frac{2}{\sqrt{1/u\lambda\tau}}\right][s_0 - s_\infty]}{\sqrt{u/\lambda\tau}} \quad \text{(D.20)}$$

We substitute the wellbore pressure including cumulative exponential time dependent skin, Eq. D.20, into Eq. D.6 yielding:

$$\bar{q}_{D,cp}(u) = \frac{1}{u^2}\frac{1}{\bar{p}_{D,cr}(t_D) + \frac{s_0}{u} - \frac{2K_1\left[\frac{2}{\sqrt{1/u\lambda\tau}}\right][s_0 - s_\infty]}{\sqrt{u/\lambda\tau}}} \quad \text{(D.21)}$$

Substituting in Eq. D.9, the three flow regimes examined in this work, into Eq. D.21, yields:

$$\bar{q}_{D,cp}(u) = \frac{1}{u^2} \frac{1}{c_1 \dfrac{\Gamma(1+\nu)}{u^{1+\nu}} + \dfrac{s_0}{u} - \dfrac{2K_1\left[\dfrac{2}{\sqrt{1/u\lambda\tau}}\right][s_0 - s_\infty]}{\sqrt{u/\lambda\tau}}} \quad \text{(power-law flow)} \ldots\ldots \text{(D.22a)}$$

$$\bar{q}_{D,cp}(u) = \frac{1}{u^2} \frac{1}{\sqrt{\pi}\dfrac{\Gamma(3/2)}{u^{3/2}} + \dfrac{s_0}{u} - \dfrac{2K_1\left[\dfrac{2}{\sqrt{1/u\lambda\tau}}\right][s_0 - s_\infty]}{\sqrt{u/\lambda\tau}}} \quad \text{(linear flow)} \ldots\ldots\ldots\ldots \text{(D.22b)}$$

$$\bar{q}_{D,cp}(u) = \frac{1}{u^2} \frac{1}{\dfrac{\pi \exp[5/4]}{\sqrt{2(k_f w_f)_D}} \dfrac{\Gamma(5/4)}{u^{5/4}} + \dfrac{s_0}{u} - \dfrac{2K_1\left[\dfrac{2}{\sqrt{1/u\lambda\tau}}\right][s_0 - s_\infty]}{\sqrt{u/\lambda\tau}}} \quad \text{(bilinear flow)} \ldots\ldots\ldots \text{(D.22c)}$$

Multiplying Eq. D.22 through by the Laplace parameter squared:

$$\bar{q}_{D,cp}(u) = \frac{1}{c_1 u^{(1-\nu)}\Gamma(1+\nu) + us_0 - \dfrac{2u^2 K_1\left[\dfrac{2}{\sqrt{1/u\lambda\tau}}\right][s_0 - s_\infty]}{\sqrt{u/\lambda\tau}}} \quad \text{(power-law flow)} \ldots\ldots \text{(D.23a)}$$

$$\bar{q}_{D,cp}(u) = \frac{1}{\sqrt{\pi}\sqrt{u}\Gamma(3/2) + us_0 - \dfrac{2u^2 K_1\left[\dfrac{2}{\sqrt{1/u\lambda\tau}}\right][s_0 - s_\infty]}{\sqrt{u/\lambda\tau}}} \quad \text{(linear flow)} \ldots\ldots\ldots\ldots \text{(D.23b)}$$

$$\bar{q}_{D,cp}(u) = \frac{1}{\dfrac{\pi \exp[5/4]}{\sqrt{2(k_f w_f)_D}} \dfrac{\Gamma(5/4)}{u^{3/4}} + us_0 - \dfrac{2u^2 K_1\left[\dfrac{2}{\sqrt{1/u\lambda\tau}}\right][s_0 - s_\infty]}{\sqrt{u/\lambda\tau}}} \quad \text{(bilinear flow)} \ldots\ldots\ldots \text{(D.23c)}$$

We arrive at the constant pressure solution, assuming a cumulative-exponential time-dependent skin factor, in Laplace space. The Stehfest algorithm provides accurate and rapid numerical inversion.

APPENDIX E

CONSTANT PRESSURE SOLUTION INCLUDING WELLBORE PHASE REDISTRIBUTION

This appendix examines the constant pressure behavior, derived in Appendix C, with the addition of a wellbore phase redistribution parameter. Fair (1981) examined a variation of the wellbore storage effect, incorporating the result into the diffusivity equation for a constant rate, radial system. This work examines the exponential pressure distribution proposed by Fair (1981) for the constant pressure case in a vertically fractured well. This work in performed in Laplace space with numerical inversion of the constant pressure solution.

Fair (1981) proposed that the pressure response due to wellbore phase redistribution is an additive function to the traditional wellbore storage examined in classical theory. Eq. E.1 was proposed by Fair (1981) to examine the changing sand face flowrate due to changing wellbore pressure and wellbore phase redistribution.

$$q_D(t_D) = 1 - C_D\left[\frac{dp_{wD}}{d_{tD}} - \frac{dp_{\phi D}}{d_{tD}}\right] \quad \text{(E.1)}$$

Defining dimensionless terms:

$$q_{D,WBS} = \frac{q_f}{q} \quad \text{(E.2)}$$

$$C_D = 0.0372\,\frac{24\,C_s}{\phi h c_t x_f{}^2} \quad \text{(E.3)}$$

$$p_{wD} = \frac{kh}{141.2qB\mu}[p_i - p_w] \quad \text{(E.4)}$$

$$p_{\phi D} = \frac{kh}{141.2qB\mu}[p_i - p_\phi] \quad \text{(E.5)}$$

Taking Eq. E.1 into the Laplace domain, following the theory presented by Blasingame (PETE 620 Notes, 1994), we have:

$$\bar{q}_D(u) = \frac{1}{u} - C_D\Big[[u\bar{p}_{wD}(u) - p_{wD}(t_D = 0)] - [u\bar{p}_{\phi D}(u) - p_{\phi D}(t_D = 0)]\Big] \quad \text{(E.6)}$$

Assuming that the pressure of the wellbore is zero when dimensionless time equals zero, Eq. E.6 becomes:

$$\bar{q}_D(u) = \frac{1}{u} - C_D[u\bar{p}_{wD}(u) - u\bar{p}_{\phi D}(u)] \quad \text{(E.7)}$$

Recalling the convolution integral for a *continuously changing flowrate*:

$$p_{wD}(t_D) = \int_0^{t_D} q_D'(\tau) p_{sD}(t_D - \tau)\, d\tau \,. \quad \text{(E.8)}$$

Where

$$p_{sD}(t_D) = p_D(t_D) = s \quad \text{(E.9)}$$

Taking the Laplace transform of Eq. E.8:

$$\bar{p}_{wD}(u) = [u\bar{q}_D(u) - \bar{q}_D(t_D = 0)]\bar{p}_{sD}(u) \quad \text{(E.10)}$$

The flowrate at initial time is zero, therefore, Eq. E.9 condenses to:

$$\bar{p}_{wD}(u) = u\bar{q}_D(u)\bar{p}_{sD}(u) \quad \text{(E.11)}$$

Substituting Eq. E.7 into Eq. E.11 we arrive at:

$$\bar{p}_{wD}(u) = u\left[\frac{1}{u} - C_D u[\bar{p}_{wD}(u) - \bar{p}_{\phi D}(u)]\right]\bar{p}_{sD}(u) \quad \text{(E.12)}$$

Multiplying through by the Laplace parameter:

$$\bar{p}_{wD}(u) = [1 - C_D u^2[\bar{p}_{wD}(u) - \bar{p}_{\phi D}(u)]]\bar{p}_{sD}(u) \quad \text{(E.13)}$$

Combining pressure terms in order to separate the wellbore flowing pressure:

$$\bar{p}_{wD}(u)[1 + C_D u^2 \bar{p}_{sD}(u)] = [1 + C_D u^2 \bar{p}_{\phi D}(u)]\bar{p}_{sD}(u) \quad \text{(E.14)}$$

Solving for the flowing wellbore pressure

$$\bar{p}_{wD}(u) = \frac{[1 + C_D u^2 \bar{p}_{\phi D}(u)]\bar{p}_{sD}(u)}{1 + C_D u^2 \bar{p}_{sD}(u)} \,. \quad \text{(E.15)}$$

According to Fair (1981), the phase redistribution pressure $p_{\phi D}$ has an exponential relationship based on theoretical reasoning and unpublished laboratory data, demonstrated by the following relationship:

$$p_{\phi D}(t_D) = C_{\phi D}(1 - e^{-t_D/\alpha_D}) \,, \quad \text{(E.16)}$$

where dimensionless parameters are defined by:

$$C_{\phi D} = \frac{khC_{\phi}}{141.2qB\mu} \quad \text{(E.17)}$$

$$t_D = \frac{2.637x10^{-4}kt}{\phi\mu c_t {x_f}^2} \quad \text{(E.18)}$$

$$\alpha_D = \frac{2.637x10^{-4}k\alpha}{\phi\mu c_t {x_f}^2} \quad \text{(E.19)}$$

where constants are in field units. The wellbore phase redistribution constant, $C_{\phi D}$, is a logarithmic average between the surface and bottomhole flowing pressure, and α is dependent on two phase fluid flow properties such as gas bubble or slug rise time in the well (Fair 1981). Assuming a constant skin factor (i.e. one that does not vary with time), and that the reservoir is operating at a constant rate, we can take the Laplace transform of Eq. E.9 and E.16:

$$\bar{p}_{sD,cr} = \bar{p}_{D,cr} + \frac{s}{u} \quad \text{(E.20)}$$

$$\bar{p}_{\phi D,cr}(u) = \frac{C_{\phi D}}{u} - \frac{C_{\phi D}}{u + 1/\alpha_D} \quad \text{(E.21)}$$

Substituting Eq. E.20 and Eq. E.21 into Eq. E.15:

$$\bar{p}_{wD,cr}(u) = \frac{\left[1 + C_D u^2\left[\frac{C_{\phi D}}{u} - \frac{C_{\phi D}}{u + 1/\alpha_D}\right]\right]\left[\bar{p}_{D,cr} + \frac{s}{u}\right]}{\left[1 + C_D u^2\left[\bar{p}_{D,cr} + \frac{s}{u}\right]\right]} \quad \text{(E.22)}$$

Expanding all terms, we arrive at a generalized wellbore storage relationship, which includes the effects of wellbore phase redistribution:

$$\bar{p}_{wD,cr}(u) = \frac{\left[1 + C_{\phi D}C_D u - \frac{C_{\phi D}C_D u^2}{u + 1/\alpha_D}\right]\left[\bar{p}_{D,cr} + \frac{s}{u}\right]}{1 + u^2 C_D \bar{p}_{D,cr} + usC_D} \quad \text{(E.23)}$$

In order to find a constant pressure solution, we return to the convolution integral in Laplace domain for a constant flowrate defined as:

$$\bar{q}_{D,cp}(u)\bar{p}_{wD,cr}(u) = \frac{1}{u^2} \quad \text{(E.24)}$$

Substituting Eq. E.23 into Eq. E.24 we arrive at a constant pressure solution:

$$\bar{q}_{D,cp}(u)=\frac{1}{u^2}\frac{1+u^2C_D\bar{p}_{D,cr}+usC_D}{\left[1+C_{\phi D}C_Du-\dfrac{C_{\phi D}C_Du^2}{u+1/\alpha_D}\right]\left[\bar{p}_D+\dfrac{s}{u}\right]} \quad \text{.....(E.20)}$$

Recalling that, in the Laplace domain, our pressure solutions are defined by Eq. E.21:

$$\bar{p}_{D,cr}(u)=c_1\frac{\Gamma(1+\nu)}{u^{1+\nu}} \quad \text{(power-law flow).. (E.21a)}$$

$$\bar{p}_{D,cr}(u)=\sqrt{\pi}\frac{\Gamma(3/2)}{u^{3/2}} \quad \text{(linear flow)..... (E.21b)}$$

$$\bar{p}_{D,cr}(u)=\frac{\pi\exp[5/4]}{\sqrt{2(k_fw_f)_D}}\frac{\Gamma(5/4)}{u^{5/4}} \quad \text{(bilinear flow)..... (E.21c)}$$

Returning E.21 into E.20, we arrive at the final constant pressure solution which includes wellbore phase redistribution and a constant skin effect:

$$\bar{q}_{D,cp}(u)=\frac{1}{u^2}\frac{1+u^2C_Dc_1\dfrac{\Gamma(1+\nu)}{u^{1+\nu}}+usC_D}{\left[1+C_{\phi D}C_Du-\dfrac{C_{\phi D}C_Du^2}{u+1/\alpha_D}\right]\left[c_1\dfrac{\Gamma(1+\nu)}{u^{1+\nu}}+\dfrac{s}{u}\right]} \quad \text{(power-law flow).. (E.22a)}$$

$$\bar{q}_{D,cp}(u)=\frac{1}{u^2}\frac{1+u^2C_D\sqrt{\pi}\dfrac{\Gamma(3/2)}{u^{3/2}}+usC_D}{\left[1+C_{\phi D}C_Du-\dfrac{C_{\phi D}C_Du^2}{u+1/\alpha_D}\right]\left[\sqrt{\pi}\dfrac{\Gamma(3/2)}{u^{3/2}}+\dfrac{s}{u}\right]} \quad \text{(linear flow)..... (E.22b)}$$

$$\bar{q}_{D,cp}(u)=\frac{1}{u^2}\frac{1+u^2C_D\dfrac{\pi\exp[5/4]}{\sqrt{2(k_fw_f)_D}}\dfrac{\Gamma(5/4)}{u^{5/4}}+usC_D}{\left[1+C_{\phi D}C_Du-\dfrac{C_{\phi D}C_Du^2}{u+1/\alpha_D}\right]\left[\dfrac{\pi\exp[5/4]}{\sqrt{2(k_fw_f)_D}}\dfrac{\Gamma(5/4)}{u^{5/4}}+\dfrac{s}{u}\right]} \quad \text{(bilinear flow)..... (E.22c)}$$

Eq. E.22 is the constant pressure solution for a vertically fractured well with time-dependent wellbore storage, a constant skin factor producing from linear, bilinear or a general power-law flow relation.